2009-11-30

Performance of a Full-Scale Lateral Foundation with Fine and Coarse Gravel Backfills Subjected to Static, Cyclic, and Dynamic Lateral Loads

Joshua M. Pruett
Brigham Young University - Provo

Performance of a Full-Scale Foundation with Fine and Coarse Gravel Backfills Subjected to Static, Cyclic, and Dynamic Lateral Loads

Joshua M. Pruett

A thesis submitted to the faculty of
Brigham Young University
in partial fulfillment of the requirements for the degree of

Master of Science

Travis M. Gerber, Chair
Kyle M. Rollins
Norman L. Jones

Department of Civil and Environmental Engineering

Brigham Young University

December 2009

ABSTRACT

Performance of a Full-Scale Foundation with Fine and Coarse Gravel Backfills Subjected to Static, Cyclic, and Dynamic Lateral Loads

Joshua M. Pruett

Department of Civil and Environmental Engineering

Master of Science

Full-scale lateral load tests were performed on a pile cap with five backfill conditions: no backfill, densely compacted fine gravel, loosely compacted fine gravel, densely compacted coarse gravel, and loosely compacted coarse gravel. Static loads, applied by hydraulic load actuators, were followed by low-frequency, actuator-driven cyclic loads as well as higher frequency dynamic loads from an eccentric mass shaker.

Passive resistance from the backfill significantly increased the lateral capacity of the pile cap. Densely compacted backfill materials contributed about 70% of the total system resistance, whereas loosely compacted backfill materials contributed about 40%. The mobilized passive resistance occurred at displacement-to-height ratios of about 0.04 for the densely compacted gravels, whereas passive resistance in the loosely compacted materials does not fully mobilize until greater displacements are reached.

Three methods were used to model the passive resistance of the backfill. Comparisons between calculated and measured responses for the densely compacted backfills indicate that in-situ shear strength test parameters provide reasonable agreement when a log-spiral method is used. Reasonable agreement for the loosely compacted backfills was obtained by either significantly reducing the interface friction angle to near zero or reducing the soil's frictional strength by a factor ranging from 0.65 to 0.85. Cracking, elevation changes, and horizontal strains in the backfill indicate that the looser materials fail differently than their densely compacted counterparts.

Under both low frequency cyclic loading and higher frequency shaker loading, the backfill significantly increased the stiffness of the system. Loosely compacted soils approximately doubled the stiffness of the pile cap without backfill and densely compacted materials roughly quadrupled the stiffness of the pile cap. The backfill also affected the damping of the system in both the cyclic and the dynamic cases, with a typical damping ratio of at least 15% being observed for the foundation system.

ACKNOWLEDGMENTS

I owe my heartfelt thanks to Dr. Travis M. Gerber, my graduate advisor, for his tutelage and advisement, and for keeping me employed for the duration of my graduate studies. His help and mentorship have helped me progress in my education. To the other members of my committee, Kyle M. Rollins and Norman L. Jones: thank you for your insightful instruction and help throughout my education. Fellow student Colin Cummins contributed significantly to the analysis of certain portions of this research study and fellow student Richard Christensen helped produce some of the figures in this document. I appreciate their contributions. I also appreciate the students and staff members whose labor made this research possible.

I am deeply grateful to Wayne E. Lee and to the Brigham Young University Civil Engineering Scholarship Society for assisting me financially during my graduate education; without their help I could not have made it this far. I would especially like to thank my wife, Amanda, whose support has been a boon throughout my Master's candidacy. The support of my parents and siblings has also been greatly appreciated.

The research presented in this thesis was supported by the National Science Foundation under Award Number CMS-0421312 and the George E. Brown, Jr. Network for Earthquake Engineering Simulation (NEES), which operates under NSF Award Number CMS-0402490. Additional support was provided via a pooled-fund study led by

the Utah Department of Transportation (UDOT) under Contract No. 069148 “Dynamic Passive Pressure of Abutments and Pile Caps” with participation from the Departments of Transportation of California, Montana, New York, Oregon, and Utah. Daniel Hsiao was the project manager for UDOT. I gratefully acknowledge this crucial support.

The views, interpretations, and recommendations expressed in this thesis are those of the author and do not necessarily reflect those of the research sponsors.

TABLE OF CONTENTS

LIST OF TABLES

LIST OF FIGURES

1 Introduction

1.1 Background

Building and bridge structures are often founded upon pile groups connected with a concrete cap, an arrangement which increases resistance to lateral loads and overturning moments and decrease lateral displacements. Lateral loadings and displacements, along with accompanying overturning moments, can be induced by wind or earthquakes. The interaction between the soil and the piles, as well as the passive earth pressure provided by the backfill material on the sides of the pile cap, provide the lateral resistance of a pile cap foundation.

Rankine, Coulomb, and log-spiral theories provide a means to calculate the ultimate passive pressure of backfill materials surrounding pile foundations for static loading conditions. The relationship between the development of passive pressure and foundation displacement into the soil, however, is not as well defined. Some approaches employ a simple linear-elastic relationship while others specify non-linear (often hyperbolic) relationships. Unfortunately, very few of the relationships that have been developed account for cyclic and dynamic behavior. Seismic loading conditions are accompanied by dynamic and cyclic effects which alter the load-displacement behavior of the soil. While both loading types accompany seismic events, cyclic and dynamic

loadings have different effects on the resistance of a soil. Cyclic effects tend to have a "softening" effect on a soil, while dynamic effects can appear to produce an increase in soil resistance due to damping and other factors. Due to a lack of well-defined load-displacement relationships addressing both cyclic and dynamic loading effects, the engineering community has often used static load-displacement relationships in seismic design.

1.2 Objective of Research and Scope of Thesis

In May and June of 2007, a series of lateral load tests were performed on a full-scale pile cap in which cyclic and dynamic loadings were superimposed on static loading conditions. The object of this research was to help quantify the effects of cyclic and dynamic loadings, and develop appropriate load-displacement relationships, for different backfill soils. The research consisted of two major parts: field testing, and analysis and interpretation of test results.

During field testing, the six-pile pile cap was laterally loaded with various different backfill conditions. The full range of backfill conditions tested consisted of: 1) no backfill present (free response condition); 2) loosely compacted clean sand; 3) densely compacted clean sand; 4) loosely compacted fine gravel; 5) densely compacted fine gravel; 6) loosely compacted coarse gravel; 7) densely compacted coarse gravel; 8) densely compacted clean sand with MSE walls; 9) 0.91-m wide zone of densely compacted coarse gravel between the cap and loosely compacted clean sand; and 10) 1.83-m wide zone of densely compacted coarse gravel between the cap and loosely compacted clean sand. This document focuses on the full width fine and coarse gravel

backfill conditions as well as the no backfill condition. Cummins (2009) evaluated the densely and loosely compacted clean sand.

The lateral loading of the pile cap was effectuated by a combination of hydraulic load actuators and an eccentric mass shaker. Using the actuators, the pile cap was slowly pushed (statically loaded) to incrementally higher target displacement levels. At each target displacement, the pile cap was cyclically displaced a small distance by the actuators at about 0.75 Hz, after which the shaker was used to superimpose higher frequency dynamic loading on top of the static force from the actuators. During the dynamic loading, the actuators between the test and reaction foundations were fixed in length to prevent the pile cap from unloading and displacing back towards its original location.

The analysis and interpretation of the data collected during testing produced various results associated with static, cyclic, and dynamic loadings. The results include lateral load versus displacement relationships for the pile cap with the aforementioned backfill conditions and earth pressure distributions along the pile cap face. Comparisons between measured and theoretically-based or calculated values are also among the results. Descriptions of vertical displacement, horizontal displacement and cracking of the backfill also resulted from the field testing. The stiffness and damping for both cyclic and dynamic loading conditions were also determined for the pile cap with the various backfill conditions.

1.3 Organization of Thesis

This document is organized as follows. A review of relevant literature is presented in the next chapter. Following the literature review, a description of the testing methods, including the test setup and the site and backfill characteristics, is given. Subsequently, the particular methods used to analyze the test data are discussed, including the methods of data reduction as well as the use of models to estimate passive resistance for comparison with the measured data. Chapters following the presentation of data analysis methods describe the results from each of the five backfill conditions examined for this study, namely no backfill present (the baseline response), densely compacted fine gravel, loosely compacted fine gravel, densely compacted coarse gravel, and loosely compacted coarse gravel. The final chapter presents conclusions and recommendations regarding the results of testing.

2 Literature Review

A review of the available literature indicates that studies involving laterally loaded full-scale pile caps under cyclic and dynamic loading are limited. Full-scale testing of pile caps is expensive and time consuming, so relatively few tests have been conducted on them. A brief summary of some of these tests, along with an overview of some of the analysis and testing issues will be presented here.

2.1 Full-Scale Lateral Load Tests

The following contains literature relevant to the lateral resistance of pile cap foundations under non-static loading conditions.

Cummins (2009)

Cummins (2009) studied the effects of lateral cyclic and dynamic loadings on a full-scale pile cap backfilled with clean sand in both loosely compacted and a densely compacted states. The work reported by Cummins and the author of this thesis was part of the same, larger research effort conducted at the Salt Lake City International Airport. A test with no backfill in place behind the cap was performed to isolate the load response of the pile group and cap. Displacement-controlled static loading was applied by a hydraulic load actuator to the foundation system to push the cap into the backfill soil in incrementally larger target displacements. After each of the targets was reached small

displacement load cycles were applied to the foundation in order to simulate the effects of seismic loading. These loads were applied alternately by the actuator, at low frequencies, and by an eccentric mass shaker, at higher frequencies; for some displacement intervals, the shaker was the first loading mechanism used, and for others, the actuator cycles came first. As this is the same method of loading applied in the current study, more will be discussed in subsequent chapters.

Changes in the backfill surface were monitored visually after each displacement interval for cracks, as well as surveyed with an optical level before the pile cap was displaced and after the maximum displacement level (but before the load was released) in order to quantify changes in the elevation of the backfill. Pressure cells were used to monitor the development of passive pressure with depth along the face of the pile cap. Pressure distributions were used to derive a passive earth load against the pile cap and compared to actuator-based loads obtained by subtracting the baseline response (i.e., the load response of the pile cap foundation with no backfill) from the total resistance of the pile cap with backfill. The changes to the backfill surface were used to infer failure mechanisms and to verify the assumed failure surface used in analysis with the elevation change profile and stress cracks.

Cummins found that the passive resistance due to the sand backfill was a significant portion of the total lateral resistance, with the loosely compacted sand contributing far less resistance than the densely compacted sand, emphasizing the importance of proper compaction in the backfill of building foundations and bridge abutments. Cummins also observed that the presence of backfill significantly increases the lateral stiffness of the foundation under cyclic and dynamic loads, and that damping

varied widely according to the shaking frequency. At similar displacement intervals, similarities between the damping for different frequency ranges indicate that higher frequency dynamic loading does not appreciably increase the resistance of the foundation system relative to low frequency cyclic loading.

Runnels (2007) and Valentine (2007)

Runnels (2007) and Valentine (2007) report full-scale static and dynamic load and displacement testing on a twelve pile group with loosely compacted silty sand and densely compacted silty sand backfill, respectively, at the FHWA testbed site located at I-15/South Temple in Salt Lake City, UT. The test foundation they used had been previously employed in research reported in Cole (2003). The tests on loose and dense silty sand investigated by the authors were part of a group of tests performed on the same pile cap with varying backfill conditions, including a pile cap baseline response condition where no backfill material was placed against the pile cap. The backfill materials were laterally loaded with a hydraulic load actuator to incrementally larger target displacements. After the target displacement was reached, the cap was cycled using small displacements at low frequency using the hydraulic actuator and at high frequency using an eccentric mass shaker placed on top of the pile cap. The results of the no backfill material (baseline) test were used to isolate the passive earth response due to both static and dynamic loading. The methods employed by Runnels (2007) and Valentine (2007) closely resemble those used in the testing presented in this thesis.

Runnels observed that passive earth resistance is largely neglected in design due to lack of full-scale testing. His tests on loose silty sand show that over 20 percent of the total system resistance to lateral loading come from passive resistance in the backfill.

Moreover, his dynamic testing shows that the dynamic stiffness of the system is nearly doubled by the presence of the backfill material. The backfill also appears to mitigate the loss in stiffness that occurs with increased forcing frequency in the baseline response of the system. The dynamic damping of the system is higher than that expected of a structural system in both the backfill and baseline cases, but is typical of soil-structure interactions.

Runnels used four different computational methods to estimate the peak load on the pile cap from the backfill. Two of these methods, Coulomb and Log Spiral, gave estimates within ten percent of the measured value. The Rankine method significantly underestimated the load, and the CALTRANS method significantly overestimated the load. Computations using the hyperbolic method recommended by Duncan and Mokwa provided the best match of the load-deflection curves measured during testing.

Valentine shows that over half of the static resistance provided by the pile cap system with dense silty sand backfill is due to passive resistance. He notes that the backfill loses resistance, or "relaxes", when it is held at a given displacement level over time and that further loss in resistance occurs after dynamic cycling. He observed that the natural frequency of the pile cap-backfill system increased with increasing pile cap displacement, as does damping. The load resistance decreased with increasing dynamic displacement amplitude and frequency, which suggests either non-linearity in the behavior of the soil or that cyclic degradation effects are larger than rate loading effects in the backfill.

Valentine also monitored passive pressure with tactile pressure grids and pressure cells. Loads derived from the tactile pressure sensors were consistent with the overall

load-displacement measurements, but required a multiplier of nearly 2 to obtain a match with the measured loads. On top of this discrepancy, the tactile sensors were not as robust as the pressure cells, being far more susceptible to point loadings on a given grid cell and overall damage. The passive pressure distribution observed with the pressure cells was nonlinear and concentrated near the base of the pile cap.

Valentine found that the Rankine, Coulomb, and log-spiral methods all underestimated the passive earth response by at least 30%, but a hyperbolic load-displacement model provided a reasonable match to the development of the passive pressure with pile cap displacement. He also observed that the reloading stiffness of the pile cap system with dense silty sand was 3 to 4 times higher than the resistance of the pile cap system with no backfill, more than twice what Runnels observed with the loose silty sand backfill. The presence of the dense silty sand backfill doubled the damping of the system under dynamic loading. The backfill itself exhibited reloading stiffness and damping values within the expected range for soils of its type.

Cole (2003) Cole and Rollins (2006) and Rollins and Cole (2006)

The research was originally presented in Cole (2003), a doctoral dissertation evaluating the contribution of passive earth pressures to total lateral resistance and the effect of load cycling on the lateral load capacity of a foundation. The pile cap used was the 12 pile group identified previously in the work of Runnels (2007) and Valentine (2007). Four backfill materials were examined under both static and cyclic loading with hydraulic jacks. Four commonly used methods of estimating peak passive resistance and displacement were used and compared to the measured results. The log spiral method proposed by Duncan and Mokwa (2001) using the Ovesen Brinch-Hansen correction for

3D effects was found to be the best predictor of the ultimate passive pressure. The hyperbolic load-displacement model proposed by Duncan and Mokwa (2001) was also found to best describe the load versus deflection relationship for monotonically applied loads. Cyclic loading requires extra consideration. Cole (2003) and Cole and Rollins (2006) propose a simple bilinear model, combined with the hyperbolic model from Duncan and Mokwa (2001), to adjust load versus deflection estimates for cyclic effects. Two normalized relationships are considered: one describing soil movement and the other describing the reduction of the stiffness as a function of the previous maximum deflection of the pile cap. The proposed model gives reasonable results when compared to observed behavior. The model is limited to cases involving between 10 and 15 cycles, one-way loading of the backfill material and cohesion effects particular to the case at hand.

Rollins et al. (2000) and Rollins and Sparks (2002)

Lateral load tests on a nine-pile group connected by a concrete pile cap were performed at the Salt Lake City International Airport. The tests were conducted first with no backfill, and then with a densely compacted sandy gravel backfill. A 14.2 MN capacity statnamic device mounted on a sled for horizontal loading was used to apply a dynamic load in both backfill conditions. Rollins et al. (2000) found that the maximum load due to statnamic testing did not coincide with the maximum displacement, but that the pile cap continued to displace after the peak had been reached. The addition of the gravel backfill increased the resistance to statnamic loading by 134% over the foundation response without backfill. A static lateral load test was performed to determine the nonlinear load-displacement curve. Gaps between the piles and the soil surrounding

them had developed during statnamic testing; a fact that was evident in the significant capacity increase at displacements larger than those achieved during the statnamic tests. It was determined that the dynamic resistance of the foundation was typically about 125% higher than the static resistance at similar displacement levels; moreover, the dynamic stiffness was generally 2.5 times higher than the static stiffness.

Rollins and Sparks (2002) reported specifically on the static portion of the testing sequence. The static tests were only performed in the backfilled case for this round of testing, resulting in a need to calculate the static baseline response by some means other than measuring a tested response. The total resistance was broken into three components, namely the friction between the base of the pile cap and the granular fill underneath it, the pile-soil-pile interaction, and the static passive resistance. These components were summed to find the total resistance and then compared to the measured resistance, as shown in Figure 2-1. The 25 mm gap between the piles and the surrounding soil had to be accounted for in the calculations to obtain a match between the computed and measured resistance.

The results of the static test indicate that passive resistance on a pile cap makes up a significant portion of the total lateral resistance; in fact, passive resistance from the gravel backfill contributed 40% of the total lateral resistance. Estimates of the passive resistance were computed using Rankine, Coulomb, log-spiral, and GROUP methods; the log-spiral method provided the best agreement with the measured resistance. The first part of Figure 2-2 gives a range of normalized load-displacement relationships from the literature. The second part of Figure 2-2 compares estimates of the load-displacement relationship with the measured result. The displacement required to mobilize the full

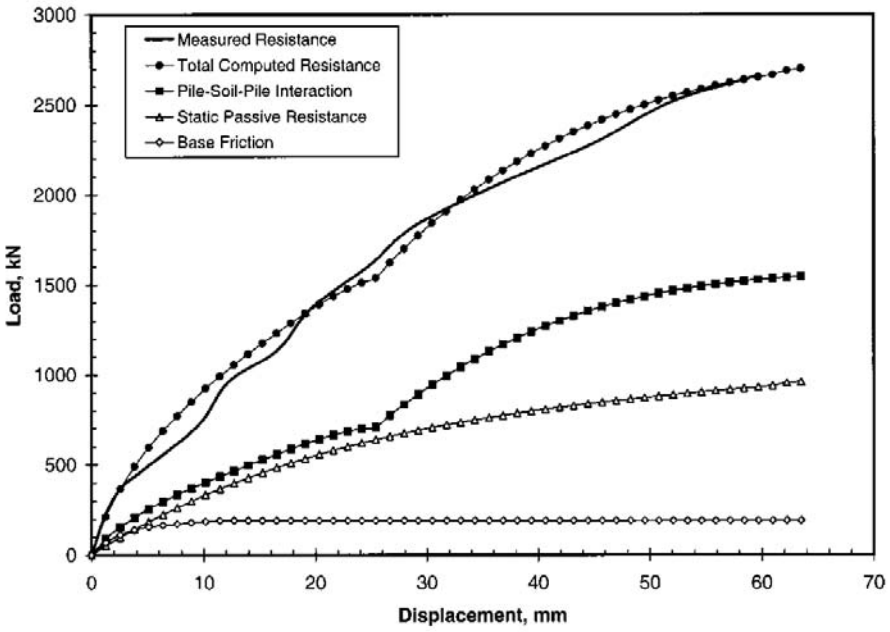

Figure 2-1 Contribution of various components to the total lateral resistance of a pile cap with sandy gravel backfill

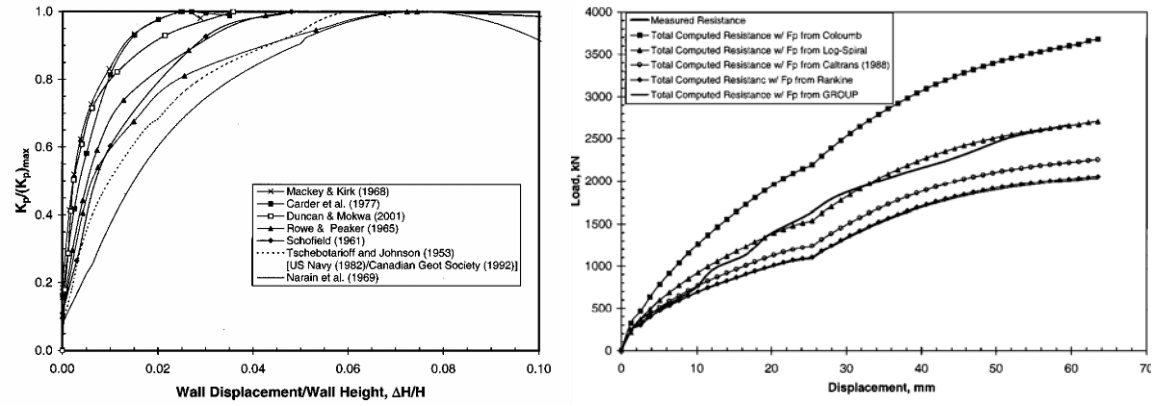

(a) (b)

Figure 2-2 (a) Comparison of normalized load-displacement curves from various authors; (b) comparison of various passive resistance estimation procedures with measured resistance

passive resistance of the gravel backfill is at the high end of the range of typical values. The authors conclude that this "soft" backfill response is likely due to the influence of the weak base layer below the compacted backfill.

Maroney (1994), Romstad et al. (1996), and CALTRANS SDC (2004)

In a joint research effort between the California Department of Transportation (CALTRANS) and the University of California at Davis, large-scale abutment systems were constructed and tested under static and cyclic loading conditions. This test was originally reported in Maroney (1994), and then reported again in Romstad et al. (1996). The structure backfill and embankment conditions were selected to be representative of "typical" bridge abutments in California. Two loading configurations were examined: longitudinal and transverse. In the longitudinal configuration, an abutment back-wall founded on three piles with a dense sand structure backfill and a clayey silt embankment fill was reacted against an abutment founded on four piles with dense sand structure backfill and a sand embankment until it failed. Load and pressure cells were used to monitor the development of passive resistance, with the pressure cells indicating a shifting pressure distribution based on the rotation of the abutment wall and the failure state of the soil. In the transverse configuration, the abutment with sand backfill and embankment was loaded from the side, with the jacks pushing against the wing-wall. Pressure and load cells also monitored the development of resistance in the abutment system and backfill. The researchers discovered that, with their loading configuration and wall system, the piles bore the brunt of the transverse loading and were quickly damaged, resulting in a dramatic decrease in the stiffness of the system.

The results of the longitudinal loading configuration were used to develop a method for estimating the strength and stiffness of the backfill, as well as the load-displacement relationship of the abutment system based on physical phenomena. Maroney and Romstad et al. suggest using a modified Mohr-Coulomb model based on their observations towards the end of the longitudinal testing when the abutment was near its ultimate strength. A linear failure surface and plane-strain conditions can then be used to obtain the ultimate strength. Dimensionless strength and stiffness versus displacement charts are provided to simplify application of the method. Maroney warns, however, that "if the limits of the soil regions within an abutment are significantly different than those tested, results…may vary and should be evaluated with due consideration". In light of the fact that the research presented in this thesis is based on simple a pile cap and not an abutment with wing-walls, and given that the backfill soils are notably different than those presented by Maroney (1994) and Romstad et al. (1996), their complete methods are not likely comparable, and will not be presented in the analysis portion of this thesis. However, the bilinear method presented by CALTRANS in its Seismic Design Criteria is based on the ultimate static force from the tests presented by Maroney, and the CALTRANS bilinear method will be presented in the analysis portion of this thesis.

2.2 Small-Scale Lateral Load Tests

Gadre and Dobry (1998)

A series of cyclic lateral load centrifuge test involving seven different soil-foundation contact configurations were performed to evaluate the contributions and interactions of base shear, active and passive forces, side shear, and normal load to the

lateral response of an embedded pile cap foundation. The results of these tests were presented by Gadre and Dobry (1998). Horizontal displacements were applied by a servocontrolled hydraulic actuator in six incrementally larger cycles to capture the response of the soil at a full range of behaviors; the cycling was too slow to incur dynamic effects. The researchers found that, of the seven configurations tested, the configuration modeling the passive contribution to the total load resistance was the most substantial single factor in the total lateral resistance of the system.

Fang et al. (1994)

Fang et al. (1994) reported on a small scale test to monitor the development of passive earth pressures as a vertical, rigid wall displaced into a mass of dry sand in a variety of wall-movement modes. Each mode of movement was monitored in an effort to provide a comprehensive and reliable basis for evaluating the validity of theories and procedures that have been developed to compute passive earth pressures. The model used to achieve this basis consisted of a one-meter wide, 0.55-m tall, 120-mm thick steel plate in a soil bin with transparent sides through which the behavior of the backfill could be observed. Three main types of wall movement were examined: translational, rotation about the top, and rotation about the bottom. In the translational movement test, the passive state was mobilized nearly simultaneously at different depths; of the methods to evaluate the mobilized passive force it was determined that a log-spiral based composite failure wedge provided the best match to the observed behavior. Friction of the soil against the side wall of the soil bin made a difference in the total load resistance of the backfill. As the wall rotated about its top, the backfill near the top of the wall did not yield sufficiently to cause a passive state. In the case of the wall rotating about its base, a

non-linear passive pressure distribution developed, with lower pressure at the bottom of the wall than at the mid-height of the wall when the center of rotation was close to the wall. In the cases where the wall experienced rotation, Fang et al. report that the influence of the type of wall movement became less important as the center of rotation moved away from the wall and the movement became increasingly similar to simple translation.

2.3 Full-Scale Lateral Load Tests on Pile Groups without a Pile Cap

Snyder (2004), Walsh (2005), Christensen (2006), Taylor (2006), and Rollins et al. (2005)

Lateral load tests were performed on uncapped pile groups, single piles, and drilled shafts at the Salt Lake City International Airport test site. The resistance developed by a pile or pile group under lateral loading is due primarily to the interaction of the pile with the soil in the top 5 to 10 pile diameters. Several pile-to-pile spacing arrangements were tested in both clay and sand to develop p-multipliers and p-y curves to improve general understanding about lateral pile and pile group resistance in different soil groups and present the effects of cyclic loading on pile-soil and pile-soil-pile lateral resistance, as reported in Snyder (2004), Walsh (2005), Christensen (2006), and Taylor (2006). It was observed that while group effects were not significant at low displacement levels, they quickly became so as the pile group was displaced. Cyclic loading typically reduces the lateral resistance capacity on the order of 20-30% by the 15th load cycle for a given displacement. About half of the capacity reduction due to cyclic loading occurs between the first and second load cycle. Taylor (2006) presents a comparison of 1.2-m diameter drilled shafts to 0.324-m diameter steel pipe piles to illustrate the effect of pile

diameter on the lateral resistance of a pile. Subsurface and drilled shaft construction details are described at length. The drilled shafts presented by Taylor were used as part of the reaction foundation in the research presented in this thesis.

Along with the static and cyclic component of his research, Snyder (2004) also presents the results of dynamic tests on the test foundation. The dynamic test was performed after the last static load cyclic of a given displacement interval as an extra cycle for the first four static displacement intervals and then the first and final cycle of the last displacement interval. The dynamic load was applied by means of a statnamic sled, and resulted in higher stiffness values and resistance capacities than the static loading. Snyder (2004) did not draw any conclusions from the dynamic tests due to various gaps in the available information, but Rollins et al. (2005), upon examination of the tests investigated by Snyder (2004), concluded that the increase in resistance during dynamic loading was due to damping.

2.4 Observations of Structure Performance and Experimental Results

Performance of a Highway Bridge and Abutment Subjected to Earthquake Loading

The response of an overpass bridge to seismic loading was monitored for feedback on the current state of practice for seismic bridge and abutment design, the result of which was reported in Goel and Chopra (1997). The structure evaluated was a short bridge with a monolithic abutment-superstructure connection on one end; the other abutment-superstructure abutment was fitted with a neoprene bearing strip to allow for thermal expansion in the bridge deck. The bridge had been equipped at construction with sufficient instrumentation to record ground and structural motions during an earthquake.

Goel and Chopra examine two earthquakes in particular: one representing the design level event and the other representing a service level event. Hysteresis loops were derived using calculated abutment forces plotted against computed deformations; these yielded the abutment stiffness. Abutment stiffness exhibits a tendency to be stiff at small deformations, to decrease as deformation increases under stronger shaking, and to recover to some degree, albeit only partially and slowly, at the end of an event as the shaking intensity declines.

The forces, stiffnesses, and other parameters obtained from the motion of the structure were compared to parameters from current design procedures. Goel and Chopra found that the longitudinal capacity estimated by the design procedures were twice the observed capacity due to the overestimation of the contribution of passive pressure in the design method. Results from the design method concerning the transverse direction agreed with the observed data as long as the deformations were similar.

Review of Passive Pressure Experiments and Theory to Affect Policy Change

Wood (2009) conducted a review of more than ten experimental and theoretical studies of soil-structure interaction in order to encourage wider use of monolithic abutment connections to bridge superstructure in New Zealand. Figure 2-3 contains a summary of the experimental passive force-displacement responses of wall and cap structures moving laterally into a soil backfill. A review of these studies confirms that that the log-spiral method is the best at estimating the passive force. Using the collected test results, the methods presented by Duncan and Mokwa (2001) and Shamsabadi et al. (2007) to compute the resistance using a log-spiral failure surface were examined and compared. Wood concludes that information obtained from experimental and analytical

research can be used to reliably estimate the passive resistance at bridge abutments and recommends that this resistance be included in the assessment and design analysis of bridges.

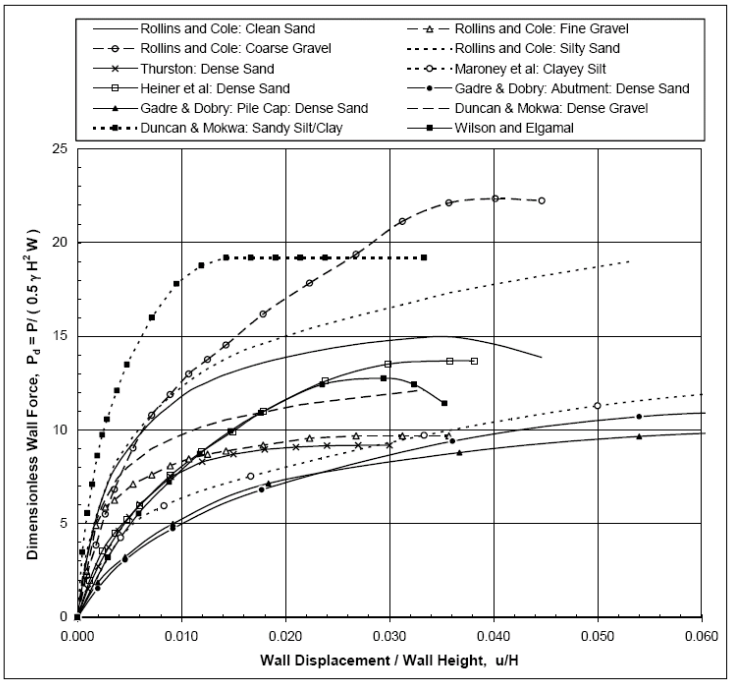

Figure 2-3 Experimental passive force-displacement curves for translation of wall structures from various authors (Wood, 2009)

2.5 Analysis Method Considerations and Testing Issues

Development of PYCAP

In order to quantify the effects of different backfill, loading, pile depth, and embedment conditions on the lateral resistance of pile cap foundations, Mokwa and Duncan (2001) established a pile cap testing facility and performed lateral load tests on various arrangements of pile and pile cap foundations. Five backfill conditions were tested: a relatively undisturbed native soil, which was a overconsolidated, desiccated

clay; dense Newcastle Sand, a relatively clean, poorly graded sand; loose Newcastle sand; dense crusher-run gravel; and no backfill. The authors found a direct relationship between the strength of the backfill and the lateral load behavior. Two primary factors determine the lateral resistance of a pile-cap foundation: the stiffness and strength of the soil in contact with the face of the cap, and the depth of pile cap. A total of 31 tests were performed, the results of which were used as a database for a passive pressure development model based on log spiral failure surfaces with differing cap heights and cap embedment depths. The resulting model is discussed in the following paragraph.

There are three main earth pressure theories typically used in geotechnical engineering: Rankine, Coulomb, and logarithmic spiral. Of these, Rankine and Coulomb are more widely used due to the complexity of applying log spiral theory. There are three methods to apply log spiral theory: tables and charts, graphical methods, and numerical methods. Duncan and Mokwa (2001) developed an Excel spreadsheet called PYCAP to reduce the effort involved in a numerical application of log spiral theory. PYCAP incorporates soil parameters and soil-structure interaction details. At certain minimum parameter values, numerical difficulties are encountered and other methods are applied to achieve a solution. The Ovesen-Brinch-Hansen correction for three dimensional effects is included to account for the shape of the structure, but limited to a maximum value of two. The change in passive earth resistance with structural movement is approximated by a hyperbolic relationship. In Duncan and Mokwa (2001), the resistance and deflection parameters from two full-scale lateral load tests were entered into PYCAP and the computed results were compared with the measured test results. Passive resistances were computed using Rankine, Coulomb, and log-spiral theories without the Ovesen-Brinch-

Hansen correction for three-dimensional effects, and log-spiral theory with the correction for three-dimensional effects. Duncan and Mokwa found that log-spiral-based passive force with the Ovesen-Brinch-Hansen correction factor provided the most accurate result. If used appropriately, PYCAP provides reasonably accurate estimates of passive resistance.

Development of the LSH Method

In light of recent changes to the seismic design procedure, which do not include the contribution of the backwall and abutment foundation in the lateral resistance of a bridge to seismic loading, Shamsabadi et al. (2005) developed a procedure to predict the passive response of the backfill which is included in the design procedure. A limit-equilibrium, method of slices approach based on a log-spiral failure surface is used to determine the mobilized passive pressure behind a given abutment wall. The indeterminate nature of the interslice forces in a method of slices approach is resolved as part of the solution process instead of making assumptions which may alter the evaluation of the soil response. The authors' objective was to develop failure surfaces base on strains, which start at the top of the wall and spread toward the base. The concepts of stress level (SL), a dimensionless ratio of the stress at some point in the loading of the soil over the fully mobilized stress, and the strain at which half of the fully mobilized passive stress is developed (ε_{50}), along with a stress-strain relationship based on triaxial test response, were developed from a series of triaxial tests performed by Ashour et al. (1998). According to the authors, the combination of the limit equilibrium method of slices with the log spiral and realistic interslice forces "provides a unique opportunity to evaluate the nonlinear force-displacement capacity of bridge abutments for

seismic design". As a result, a method for determining the load-displacement relationship, along with the changes in geometry of the failure surface during loading, was developed.

The mobilization of passive earth response and load-displacement relationship developed in this method were validated with a number of cases where the method was used on a variety of modeling types, including finite element, small-scale, centrifuge, and full-scale models. In these case studies, the method generally predicated the result of the lateral load test within 10% of the measured or otherwise calculated value. The flowchart shown in Figure 2-4 gives the calculation process for the method. The method was later modified and used for several additional case studies as presented in Shamsabadi et al. (2007).

In order to provide better estimates for bridge design, Shamsabadi et al. (2007) presents newly revised models to estimate mobilized lateral abutment backfill resistance and a relationship between the mobilized resistance and the deflection required to mobilize it. The model is based on log spiral failure theory coupled with a modified hyperbolic soil structure stress-strain behavior relationship, also known as the LSH method (for log-spiral with hyperbolic load-displacement model). The procedure for using the LSH method is outlined in Figure 2-5. A hyperbolic force-displacement relationship was also developed to be used by structural engineers. It incorporates the average abutment stiffness, the maximum mobilized backfill capacity, and the maximum displacement required to mobilize that capacity in a single tool to approximate loads and deflections in performance based designs. These two tools were used in several case studies to compare computed results with measured data and resulted in very good

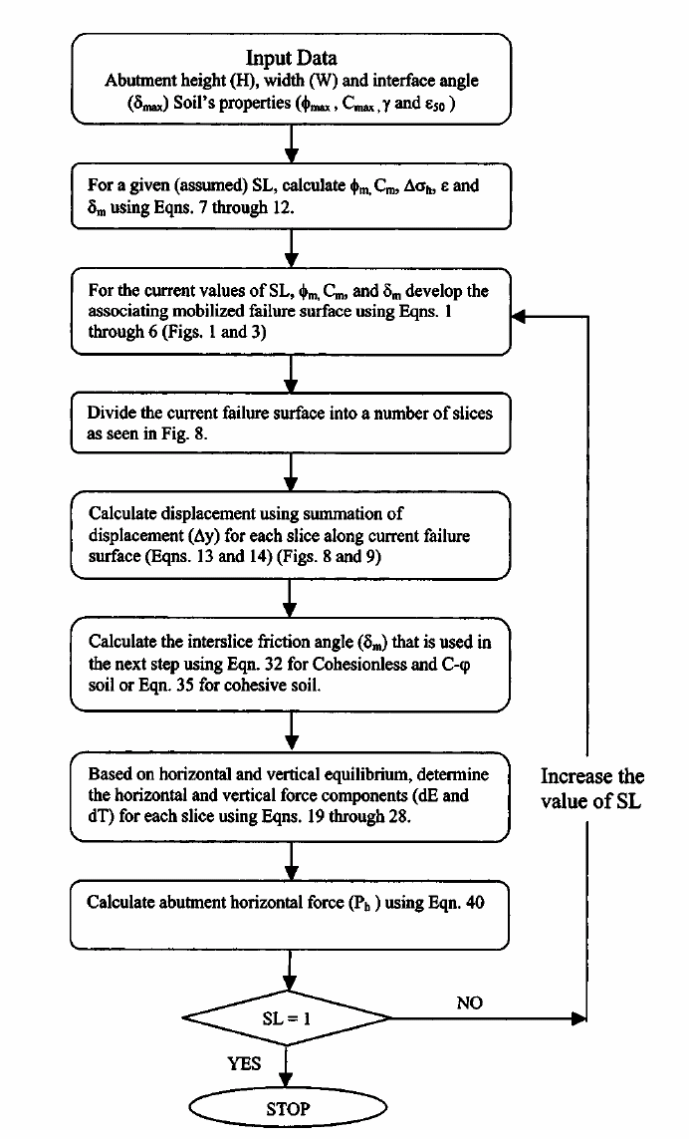

Figure 2-4 Method developed in Shamsabadi et al. (2005) to compute the passive resistance of a backfill soil

matches with the observed loads and displacements. The LSH model can be applied to nonlinear seismic soil-abutment interaction analyses for use in performance-based bridge design. Shamsabadi et al. (2007) find that the two models presented are practical and versatile tools that can be used for the seismic design of bridges.

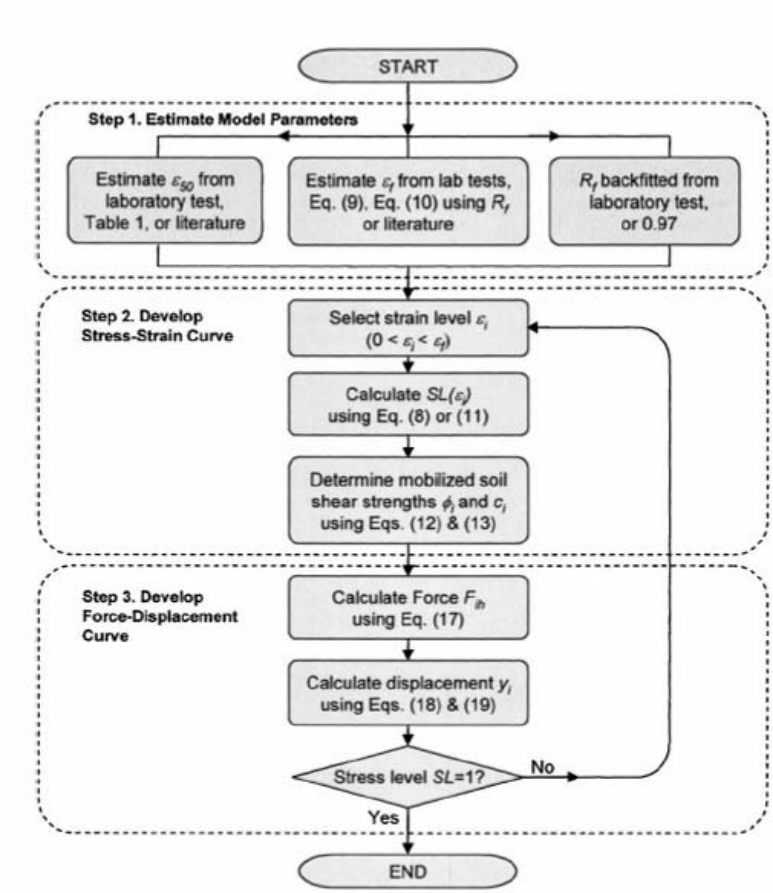

Figure 2-5 Flowchart for the LSH (Shamsabadi et al., 2007) method of predicting lateral passive resistance of an abutment backfill soil

Development of a Three-Dimensional Passive Pressure Model

Soubra and Regenass (2000) developed a "kinematically admissible" method of examining the three-dimensional nature of the passive earth pressure developed in soils behind rigid retaining walls which focuses on three different failure mechanisms. In this procedure, the Soubra and Regenass employ the upper-bound method of the limit analysis theory (for simplicity) and examine the effect of soil weight, cohesion, and surcharge loading. The increase in passive pressure due to decreasing wall breadth is also of interest to the authors. The first mechanism in the procedure is an extension of

the two-dimensional Coulomb mechanism into three dimensions, where the three-dimensional failure block is modeled as a single rigid block. The second mechanism is a multiblock approach, in which a given number of blocks are used to represent the failure zone. The profile of the multiblock approach appears curved, similar to a log-spiral failure surface. This mechanism yields better predictions than the single block mechanism, but geometrically misrepresents the failure zone in the plan view. This shortcoming is remedied by the third mechanism, which uses the multiblock approach but truncates the corners of the failure zone into a conical shape, giving a curved outline in plan to better represent experimental observations. The truncated multiblock mechanism yields the best predictions of the three methods. The three mechanisms are shown in Figure 2-6. In order to avoid redundancy, the profile of the truncated multiblock mechanism, which is identical to that of the multiblock mechanism, is not included in the figure.

The interfaces between the blocks, along the soil-wall interface, and along the failure surface are regions where energy is dissipated. Using the work equation, one can equate the total rate of external work to the total rate of energy dissipation along the above-mentioned interfaces, thereby obtaining an expression for the passive earth force, as shown in Equation 2-1:

$$P_p = K_{p\gamma} \cdot \gamma \cdot \frac{h^2}{2} \cdot b + K_{pc} \cdot c \cdot h \cdot b + K_{pq} \cdot q \cdot h \cdot b \qquad \textbf{(2-1)}$$

where $K_{p\gamma}$, K_{pc}, and K_{pq} are the passive earth coefficients due to soil weight, cohesion, and surcharge load, respectively, h is the height of the wall, and b is the wall width.

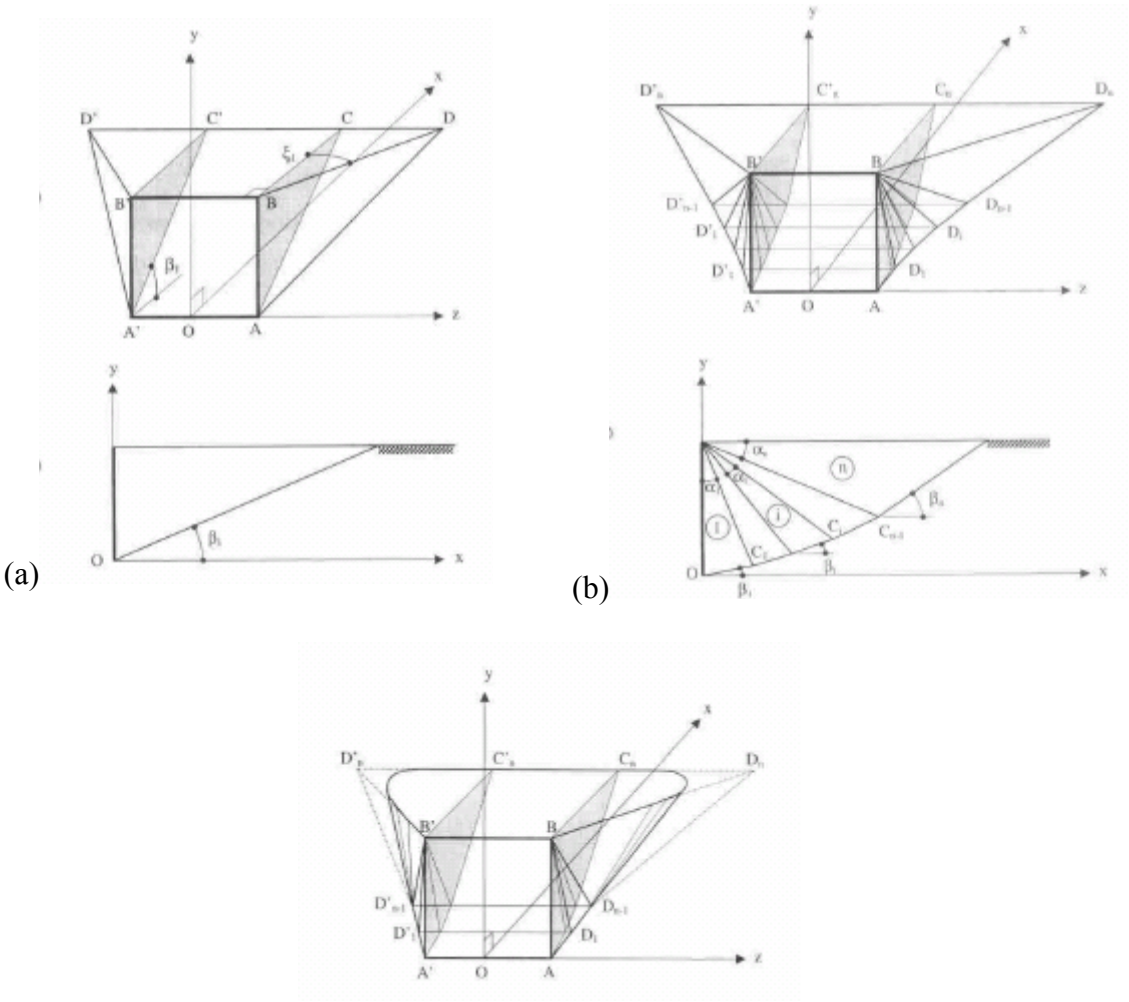

Figure 2-6 Diagrams of different failure mechanisms in Soubra and Regenass (2000)

In the numerical analysis of the truncated multiblock mechanism, Soubra and Regenass observed that for interface friction angles less than two-thirds of the internal friction angle and for internal friction angles lower than 40°, a single block truncated mechanism is sufficient to provide an accurate computation of passive resistance. As internal and interface friction angels increase, so does the number of blocks required to

accurately model the development of passive pressure. A five-block truncated method was found to produce consistently reasonable results for internal and interface friction angles greater than the above mentioned threshold values. While this method inherently accounts for three-dimensional effects in the computation of the passive resistance of backfill, it is not as readily applied as PYCAP and the LSH method; hence, it will not be used in the analysis of backfill response in this thesis.

Embedded Pressure Cell Issues

An examination of the possible causes of the drift and scatter commonly observed in pressure cell readings was carried out in an instrumented retaining wall facility at the Virginia Polytechnic Institute. Several authors in the literature have proposed temperature changes and change in backfill height as reasons for the observed drift; however, these phenomena do not completely account for the magnitude and variety of the many of the observed cases of drift. Tests were performed with two backfill types: moist silty sand and dry clean sand. Filz and Duncan (1993) observed that virtually no drift occurred in the dry sand, whereas considerable drift occurred in the moist sand material. Tests to evaluate the influence of moisture infiltration on pressure cell readings showed that this was a major source of pressure cell drift and methods to prevent moisture ingress were evaluated. Filz and Duncan concluded that many occurrences of drift are cause by concrete volume change around the cells as water migrates into the concrete face, distorting the pressure cell and reducing the fluid pressure inside the cell. They recommend sealing the concrete against moisture ingress to reduce drift and suggest isolating the pressure cell from the concrete around it to help eliminate drift altogether. Scatter in the pressure cell readings is due largely to local variations in soil stresses and

can be remedied by increasing the number of cells or measuring over a large area to obtain representative readings.

Filz and Brandon (1994) evaluated the capacity of embedded pressure cells to measure static and dynamic pressures. The cells used in their study were small, with a total width of 55 mm and a height of 15.6 mm, and the dynamic pressures measured were induced by compaction devices, nevertheless there are a few lessons that seem pertinent to the present study. The tests involved in the literature were performed at the retaining wall facility mentioned above, and involved small earth pressure cells placed at the bottom of a six inch lift of soil to measure the static and dynamic pressures induced by vibrating compactors. Filz and Brandon observed that reflection of seismic waves at the backfill boundaries can create a standing wave at the pressure cell, interfering with the measurement. Other factors that influence the pressure cell readings include the presence of clods in the backfill and variations in cell placement conditions (e.g., departures from flush). Higher than average readings can be drawn from protruding cells, while deeply embedded cells will produce lower than average readings.

3 Testing Methods

Details regarding the testing conducted for this research effort are contained in this chapter. A description of the site surface conditions, history, and subsurface conditions are provided prior to discussing the test methods in order to give a complete picture of the testing program. The testing layout, equipment, and testing procedure are also described with particular focus on descriptions of the backfill materials used, including field and laboratory tests performed to ascertain the strength characteristics of the soil.

3.1 Site Description

Testing for the research presented in this thesis occurred in May and June of 2007 at a site located approximately 300 m north of the control tower at the Salt Lake City International Airport, in Salt Lake City, Utah. Several research projects have previously been conducted at this site, including testing of single piles, pile groups, and drilled shafts (for examples, see Johnson (2003), Rollins et al. (2005a, 2005b), and Taylor (2006)). An aerial photograph of the test site and the surrounding area is shown in Figure 3-1.

Previous testing at the site has provided a large amount of data pertaining to the subsurface conditions. Imported clayey to silty sand and gravel fill generally cover the top 1.5 m of the test site. Deeper in the soil profile the soils consist of alternating silt and

clay layers with an occasional interbedded sand layer. The imported fill previously described was excavated around the test and reaction foundations and a 1.68-m high pile cap was constructed over the piles such that its top face matched the elevation of the surrounding ground surface. The soils adjacent to the cap were excavated away so that only the north face of the pile cap was in contact with the backfill soil. The water table during testing was located from zero to about 50 mm above the base of the pile cap.

Figure 3-1 Aerial photograph of test site (adapted from Google Maps/Earth)

3.2 Subsurface Characteristics

As previously mentioned, the test site has been used in several full-scale pile and drilled shaft tests which have provided substantial subsurface soil information. The first extensive subsurface investigation of the site was conducted in 1995, as presented by Peterson (1996). A variety of in-situ tests (such as SPT and CPT) and extensive laboratory shear strength and index property tests have been performed. Figure 3-2 shows locations of subsurface tests in relation to the previously existing pile groups and drilled shafts. The pile cap used in this research was constructed on the 9-pile group on the north end of the test site. The middle row of piles was removed to facilitate a broad range of movement and reduce the overall force needed to displace the cap. The research presented in this thesis focuses on the interplay between the pile cap and the backfill near the surface; as such, complete data from all previous subsurface investigations focusing on deep foundations will not be presented here. If the reader would like to know the particulars of the subsurface characteristics, Peterson (1996), Rollins et al. (2005a, 2005b), Christensen (2006), and Taylor (2006) explore that topic in considerable detail. Figure 3-3 shows a simplified subsurface profile (largely based on Peterson and presented by Christensen), along with results of a CPT conducted near the test pile cap foundation. The clean sand layer near the ground surface (which replaced previously imported materials) was excavated out and the piles truncated in order to construct the pile cap below the ground surface. Soils beneath the cap down to a depth of about 10 m consist of different layers of lean clay and sandy silt with two 1.5 to 2 m thick silty sand and poorly graded sand layers. Deeper soils consist of interbedded sandy silts and silty sands, with the end of the piles resting in a silty sand layer, as shown in Figure 3-3.

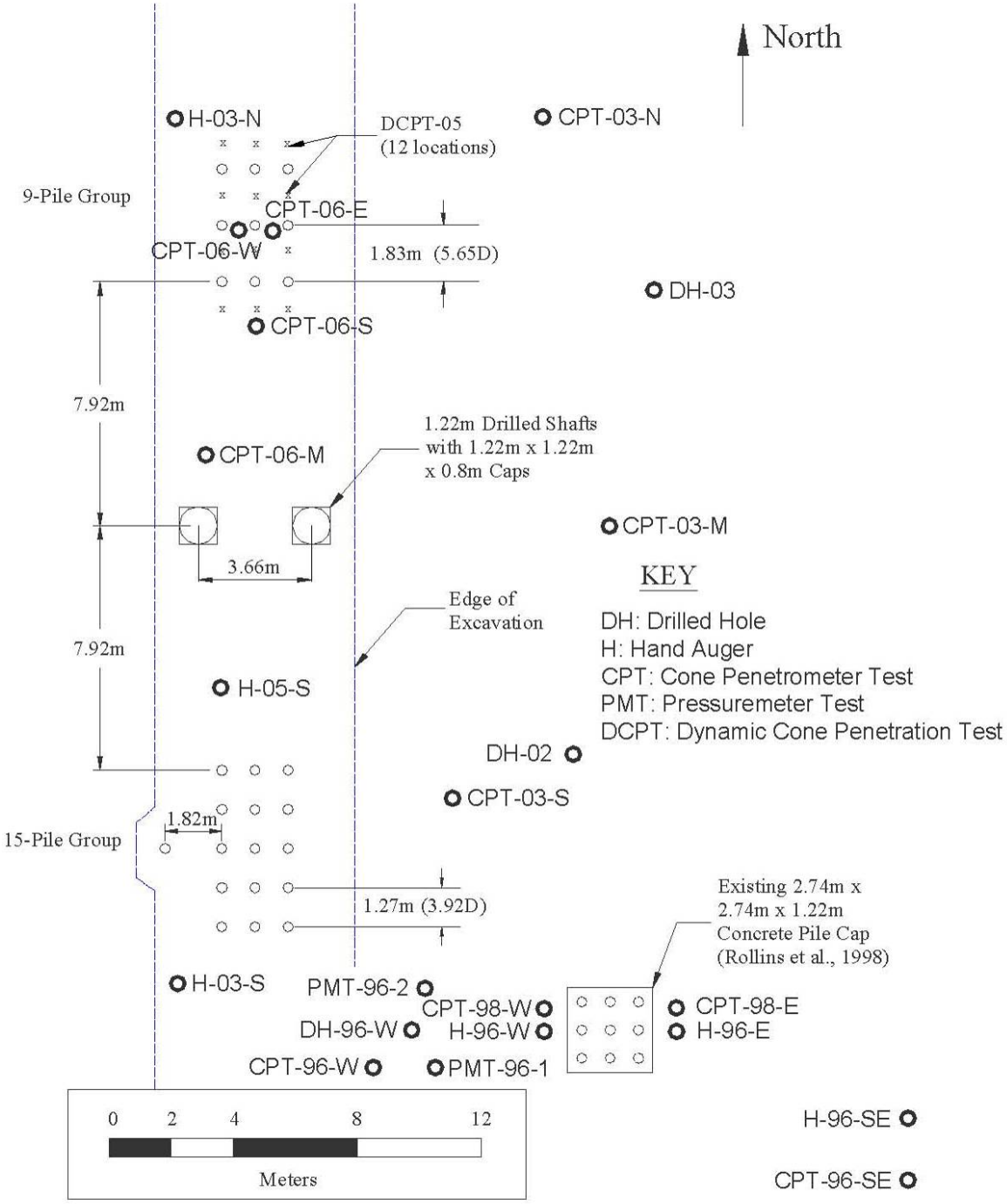

Figure 3-2 Entire test site with locations of subsurface tests (Christensen, 2006)

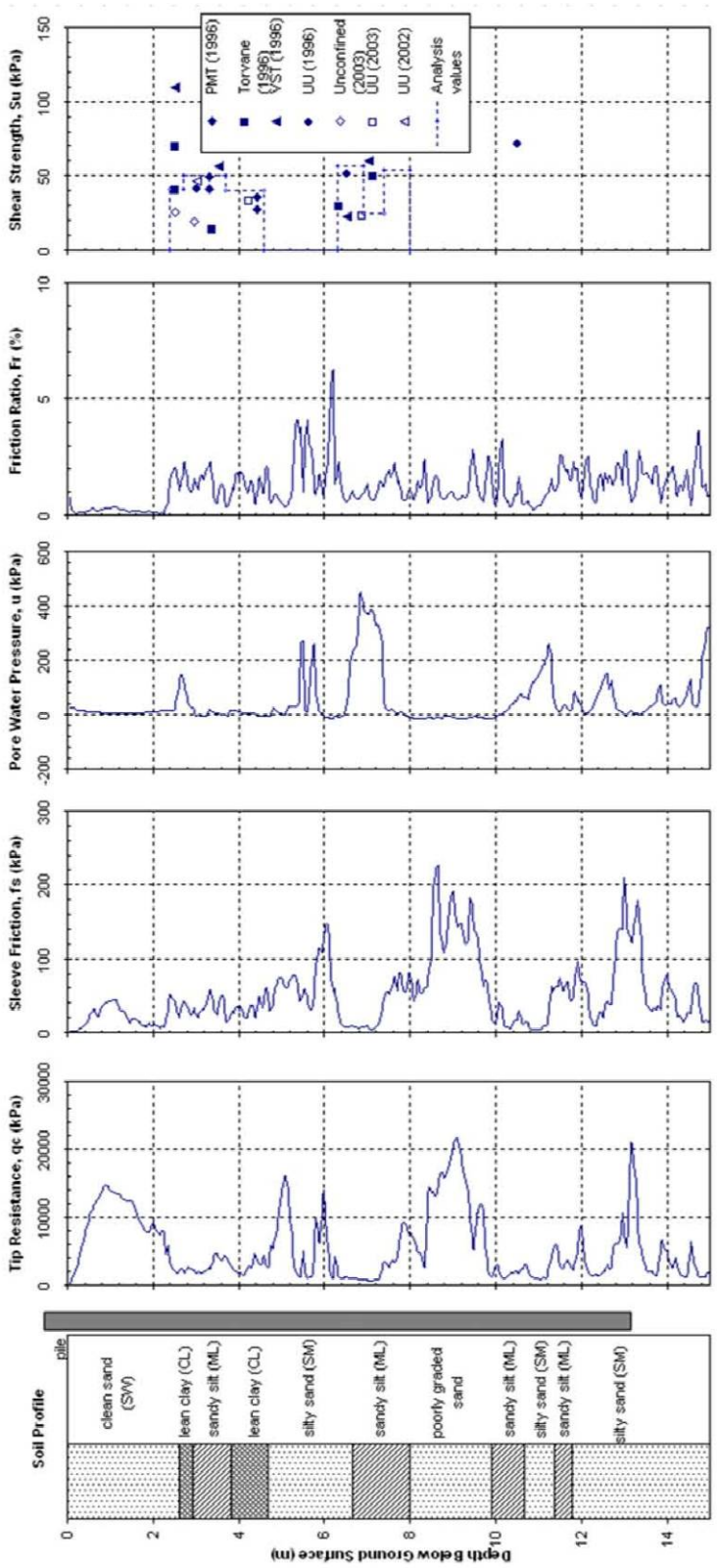

Figure 3-3 Idealized soil profile with CPT data (Christensen, 2006)

3.3 Testing Layout, Equipment, and Procedure

3.3.1 General

The primary elements of the test layout consist of a reaction foundation, a test pile cap, and the backfill soil zone. Figure 3-4 shows a plan and profile view of the test site and equipment. Additional views of the testing setup are provided in the photos presented in Figure 3-5. Characterization of the backfill materials is provided in Section 3.4.

3.3.2 Reaction Foundation

The reaction foundation consisted of the two existing 1.2-m diameter drilled shafts, spaced 3.66 m center-to-center, buttressed with a sheet pile wall and two reinforced steel I-beams. The 1.2-m square caps on the top 0.61-m of the drilled shafts were constructed to facilitate loadings during previous testing. The west and east shafts extend to depths of 16.8 m and 21.3 m, respectively. Shaft reinforcement consists of eighteen #36 vertical bars extending to a depth of 10.67 m below ground. A #16 spiral pitched at 75 mm wraps the vertical reinforcement and a 120-mm clear cover of concrete covers the steel. Half of the vertical bars extend beyond 10.67 to 16.76 m wrapped in a spiral pitched at 300 mm. The average compressive strength of the concrete in the shafts is 41 MPa.

To increase the lateral capacity of the reaction foundation, a sheet pile wall was installed on the north side of the drilled shafts. The AZ-18 sheet piling, constructed of ASTM A-572, Grade 50 steel, used was selected from sections readily available in the local area. Installation depth was controlled by the 12.2 m length of the available stock.

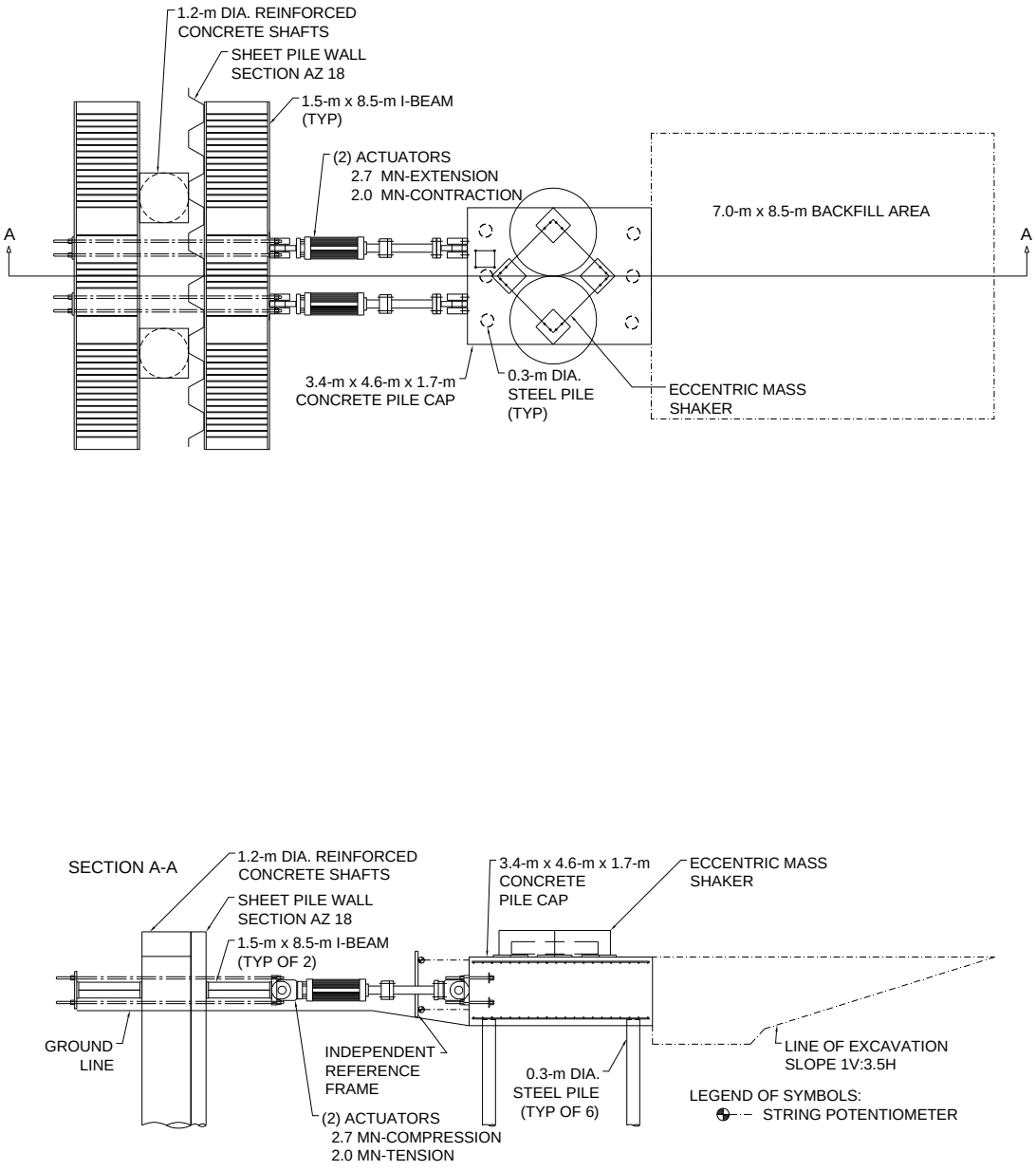

Figure 3-4 Plan and profile view of test setup

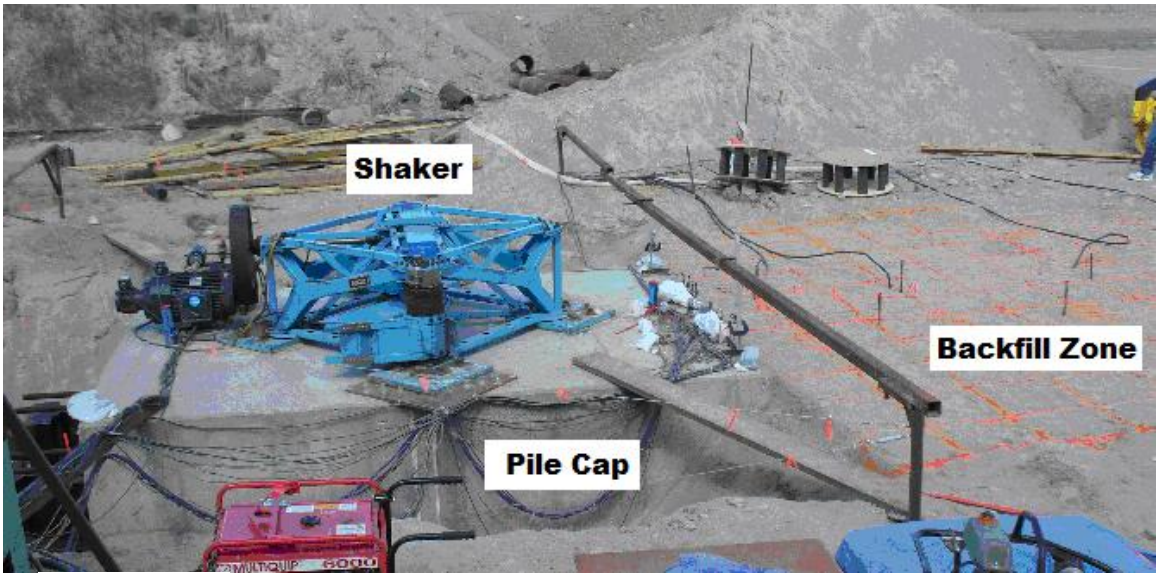

Load
Actuators

Figure 3-5 Photos of test site and equipment setup

The sheet pile wall was installed using a vibratory hammer, and the sheet piling was kept as vertical and flush with the faces of the shafts as possible. The piling, as built, extended to depths of 10.24 to 10.85 m below the excavated ground surface.

To help ensure composite behavior and proper load distribution, two 8.53-m long, 1626- by 406-mm I-beams with numerous stiffeners were placed with the web horizontal on either side of the shafts and sheet piling as shown in Figure 3-4. The reaction foundation was tied together with eight 64-mm diameter high-strength threaded bars that were post-tensioned to 45 kN. These threaded bars were also used to tie the loading system to the load frame.

3.3.3 Piles and Pile cap

The group of test piles used in the present study were used in previous lateral-load studies including those reported by (Snyder 2004). The piles are made of ASTM A252 Grade 3 (i.e., 310 MPa minimum yield strength) steel pipe, with an outside diameter and wall thickness of 324 and 9.5 mm, respectively. They were driven closed ended to a depth of about 13 m below the ground surface. After the removal of three (the middle row) of the original nine piles the remaining piles were spaced 3.66-m center to center in the direction of loading. This spacing is more than 11 pile diameters, which should eliminate group interaction effects in the test foundation. The tops of the piles were cut off, leaving approximately 150 mm for embedment into the future cap. The piles were filled with 41-MPa concrete and attached to the cap with a rebar cage consisting of six #25 vertical bars and a #13 spiral at a 152-mm pitch. The 5.49-m long cages extend above the pile approximately 1.47 m into the cap to support the upper mat of horizontal

reinforcement. Inclinometer tubes and shape array tubes were placed in the north center and south center piles.

The final cap dimensions are 4.57-m long by 3.35 m wide by 1.68 m tall. The concrete used in the cap has a compressive strength of 41 MPa. The primary reinforcement in the cap consists of a mat of transverse and longitudinal reinforcing bars placed in both the top and the bottom of the cap. Each mat is a grid of #19 bars spaced at 203 mm on-center in each direction. Threaded bars were set into place during construction to provide an integral connection to the pile cap. These bars were placed to serve as connectors for the eccentric mass shaker and the hydraulic load actuators.

3.3.4 Loading Equipment

Two 2.7-MN capacity hydraulic actuators were used to apply a northward horizontal force to the southern face of the pile cap. Each actuator was attached to the reaction foundation using the threaded bars that were used to tie the I-beams together. The actuators were attached to the test pile cap using threaded bars (four for each actuator) embedded in the cap during construction. Both ends of the actuators have free-swiveling heads to provide moment-free loading conditions. A 227 l/min pumping unit was used to provide hydraulic pressure to the actuators. The actuator-driven load was applied at the mid-height of the cap, approximately 0.84 m below the backfilled ground surface. The actuators were modified with 1.22-m long extensions to span the distance between the test pile cap and the reaction foundation.

An eccentric mass shaker on loan from the Network for Earthquake Engineering Simulation (NEES) equipment site at UCLA was used to provide dynamic loading to the pile cap. The shaker was oriented on the top of the pile cap so that the maximum force

vector was perpendicular to the reaction frame and parallel to the actuator load. The magnitude of force generated by the shaker is based on Equation 3-1.

$$F = 0.04016 \times (WR) \times f^2 \quad \textbf{(3-1)}$$

where F is force (kN), WR is the weight-distance (i.e., moment) of the shaker basket (kN-cm), and f is the shaker frequency (Hz). The weight and eccentricity of the shaker baskets can be adjusted by changing the number of 0.08 kN steel blocks in the baskets. These blocks can be positioned in various arrangements within the baskets. Equation 3-1 is empirical; unit conversions are covered in the first term of the equation. With the steel block configuration used during this study, the WR parameter was equal to 110.97 kN-cm, resulting in a shaker capacity of 446 kN at a maximum frequency of 10 Hz.

3.3.5 Instrumentation

An independent reference frame located between the pile cap and the reaction foundation was used to provide a stationary datum from which to measure the movement of the test pile cap. The frame was embedded in the ground with concrete, and steel guide cables were used to reduce movement within its long span.

Four string potentiometers were mounted to the primary frame and attached to the southern pile cap face near the four corners (the face to which the actuators were attached), with two near the top (740 mm above the load point) and two close to the bottom (480 mm below the load point) of the cap. Seven additional string potentiometers were mounted to the top of the pile cap near the backfilled face and attached to metal stakes driven into the surface of the backfill at various distances from the face of the cap.

In this way, a measure of relative displacement between the cap and points within the backfill was obtainable.

Triaxial accelerometers were mounted to each corner of the top pile cap surface, and an additional accelerometer was mounted to the top of the cap near the center of the backfilled face of the cap. Data from the string potentiometers was unreliable during shaking because the reference frame was mounted to the ground and responded dynamically when the shaker was used. The accelerometer data was double integrated to find pile cap displacements during shaker operation due to the unreliability of the string potentiometer readings during that time. Data was processed using a forward and backward FIR filter to eliminate phase distortion. A data recording frequency of 200 samples per second (sps) was used to capture the pile cap response up to 10 Hz.

The amount of resistance provided by the soil backfill can be determined in two ways. In the first way, the pile cap is laterally loaded both with and without backfill in place, and the difference between the two responses can be assumed to be the load-displacement response of the backfill. The second way consists of using pressure cells to measure the earth pressure directly, then multiplying by the contributory areas of the pile cap face that corresponded to the individual pressure cells to determine the force placed on the cap by the backfill soil. The pressure cells have the obvious advantage of also providing a pressure distribution along the cap face. Six pressure cells were used, spaced at depths of 0.14, 0.42, 0.70, 0.98, 1.26, and 1.54 m in the center portion of the pile cap. These stainless steel pressure cells were designed with a reinforced backplate to reduce point loading effects when directly mounting the cell to a concrete or steel structure, and the cells employ a semi-conductor pressure transducer rather than a vibrating wire

transducer to more accurately measure rapidly changing pressures. The cells were cast integrally with the pile cap so their top surfaces were flush with the concrete face.

To further document changes in the backfill during testing, a square grid, with lines spaced at 0.61-m, was painted on the backfill. After cyclic and dynamic testing at each displacement interval, cracking on the backfill surface was mapped by visual inspection with the aid of the grid. Vertical displacements were measured at grid nodes with traditional surveying equipment before the first load for a given backfill material and after the last load was applied.

3.3.6 General Testing Procedures

The following procedure was generally used to perform load testing of the pile cap. After placing and compacting any backfill materials, the pile cap was loaded by the hydraulic load actuators to displace it to its initial target displacement level, which was typically 6.3 mm. A brief pause to manually record verification data was followed by the actuator-driven application of 15 small displacement cycles (a single cycle typically had a displacement amplitude of about 2 mm at 0.75 Hz). The actuators were then returned to their pre-cycling positions and the actuator lengths were fixed to make each actuator act as a strut between the reaction foundation and test cap, whereupon the shaker was activated to apply a dynamic step-ramped loading. The shaker loading consisted of rotating at a specific frequency for 15 cycles, then quickly ramping to the next target "dwell" frequency. The range of dwell frequencies in this testing went from 1 to 10 Hz, in 0.5 Hz increments. Afterwards, the shaker was allowed to ramp back down to a stationary position. The operation of the shaker typically lasted about 3½ minutes, including the ramp up and the ramp down to the stopped position.

After some data processing and inspection of the backfill and testing equipment, the actuators were extended again to push the pile cap to the next displacement level. Upon reaching the target displacement level, rather than having the actuators cycle first as was performed previously, the shaker was used with the actuator lengths fixed. After the shaker loading was completed, the actuators applied their cyclic loading. In this way, the use of cyclic actuator loads and dynamic shaker loads was generally alternated between each target displacement level throughout the testing program until the maximum target displacement was reached.

In general, target displacement levels occurred in 6.3 mm increments, ranging up to 87 mm of displacement (actual maximum displacements depended on the load capacity of the actuators, the behavior of the reaction foundation, and the working condition of all the other equipment). The movements of both the reaction foundation and the test foundation influenced the displacement control of the actuators; as such, establishing an appropriate displacement in the actuator control program for each loading increment depended on the relative stiffnesses of both the test and the reaction foundations. The stiffnesses of the two foundation systems over the entire range of displacement were not precisely known prior to testing. As such, the displacements attained for each loading increment vary somewhat from the target displacement levels. Inspection of the load-displacement curve at the time of testing occasionally suggested (particularly with those tests involving loosely compacted backfills) that the incremental displacement for a given load increment was insufficient to cause the load-displacement curve to attain the static backbone curve (i.e., the curve that would have been produced had the loading been applied monotonically rather than in a stepped fashion). For such displacement levels the

pile cap was pushed to the next target displacement level without cyclic and dynamic loading to make the load path approach the backbone curve. The evidence of proximity to the backbone curve is seen in the data as an initially steep reloading path during the early portion of the loading increment followed by a flattening of the load path.

Data was acquired during testing using a sampling rate of 200 samples per second (sps). Data files were filtered to 1 sps to facilitate data screening and to use in analyses for portions of the tests involving relatively static loading conditions.

During the tests that involved backfill soil, any observed cracking of the backfill soil was mapped with the aid of the grid painted on the ground surface to capture the progression of cracking with increasing pile cap displacement. Before initially loading the cap, the vertical elevations of the grid nodes were surveyed and inclinometer readings were taken for the center piles in the front and back rows of the pile cap. These measurements were repeated when the cap was held at the maximum displacement level. Elevation surveys and inclinometer readings were not taken at intermediate displacement levels because of time constraints. Shape array data was collected throughout the test; however, it will not be presented in this document.

3.3.7 Summary of Tests

During the 2007 testing program, a total of 12 individual tests were conducted. The backfill conditions for each test are shown in Table 3-1. This thesis focuses on tests #7, 8, 10, 11, and 12 -- the fine and coarse gravel materials and the no backfill test representing the "baseline" response of the test foundation.

3.4 Backfill Soil Characterization

The two backfill soil types from the testing that are presented in this document are referred to as fine gravel and coarse gravel. This nomenclature is consistent with the terminology used by Rollins and Cole (2006) and Cole and Rollins (2006) in describing

Table 3-1 Summary of tests conducted

Test Number	Test Date	Backfill Condition
1	18-May-07	Free Response (Condition Cap)
2	25-May-07	Densely Compacted Clean Sand
3	29-May-07	Loosely Compacted Clean Sand
4	1-Jun-07	0.91-m wide Gravel Zone with Loosely Compacted Clean Sand
5	1-Jun-07	No Backfill (Free Response)
6	4-Jun-07	1.83-m wide Gravel Zone with Loosely Compacted Clean Sand
7	6-Jun-07	Loosely Compacted Fine Gravel
8	11-Jun-07	Densely Compacted Fine Gravel
9	18-Jun-07	Mechanically Stabilized Earth (MSE) Wall with Dense Clean Sand
10	21-Jun-07	Loosely Compacted Coarse Gravel
11	21-Jun-07	No Backfill (Free Response)
12	26-Jun-07	Densely Compacted Coarse Gravel

similar materials for tests conducted at the I-15 Test Bed site at South Temple in Salt Lake City, Utah. These soils were placed and tested in both loosely and densely compacted states in order to represent a modest compactive effort (about 90 to 95% of standard Proctor) and a good compactive effort (about 96% of modified Proctor), respectively.

3.4.1 Fine Gravel Backfill

According to the USCS, the fine gravel classifies as a well graded sand with gravel (SW). The AASHTO classification of the fine gravel material is A-1-a. The name

"fine gravel" appears to be a misnomer on the basis of the USCS; however, since AASHTO uses a #10 sieve rather than a #4 sieve to distinguish between gravel and sand, so this roadbase material would appropriately be identified as fine gravel in the AASHTO soil classification system. Figure 3-6 shows the particle distribution of the fine gravel backfill material. The gradation limits shown in the figure correspond to the gradation limits for locally used UDOT roadbase material. Table 3-2 provides an index property summary for the fine gravel backfill.

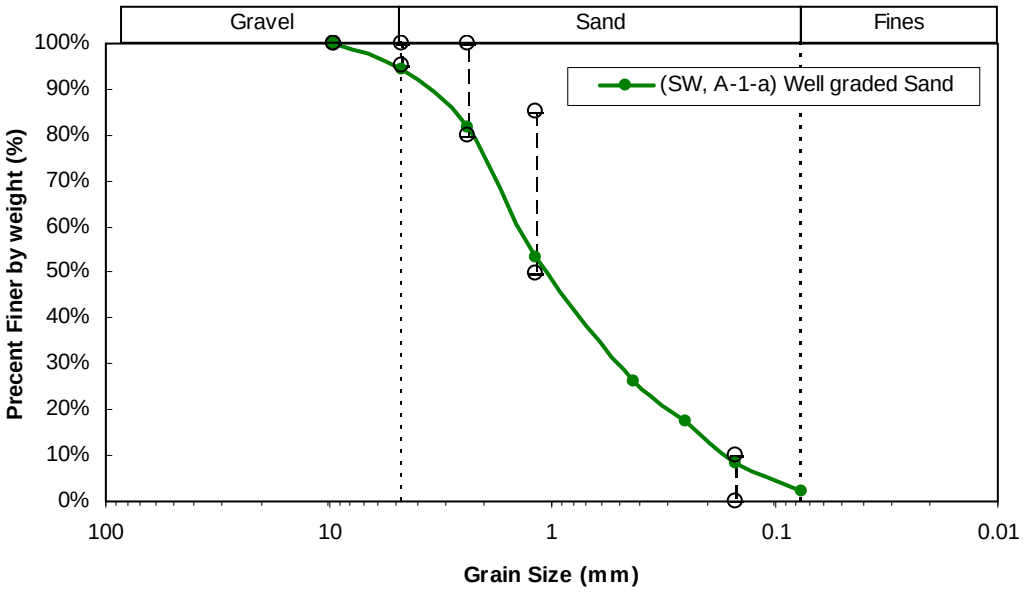

Figure 3-6 Particle distribution with gradation limits for fine gravel backfill

Table 3-2 Index properties for the fine gravel backfill material

Backfill Type	Gravel (%)	Sand (%)	Fines (%)	D_{60} (mm)	D_{50} (mm)	D_{30} (mm)	D_{10} (mm)	C_u	C_c
Fine Gravel	39	57	4	4.5	3	1.03	0.2	22.5	1.2

Table 3-3 shows the optimum moisture content and maximum dry density of the clean sand material using standard and modified effort, respectively. As stated previously, testing was performed on the material in two separate compaction states: loosely compacted and densely compacted. A jumping jack and a robust trench compactor were used to compact the soil to the desired density levels. Several nuclear density gauge readings were taken for each lift to verify the degree of compaction and moisture content. Histograms showing the density distribution of densely compacted fine gravel and loosely compacted fine gravel are shown in Figure 3-7 and Figure 3-8, respectively. Table 3-4 provides the average in-situ unit weight properties of the fine gravel backfill. The densely compacted fine gravel has an average dry density of about 95% of the modified Proctor maximum dry density, while the loosely compacted fine gravel has an average dry density of about 94% of standard Proctor maximum dry density or about 87% of modified Proctor density. Using the correlation developed by Lee and Singh (1971), relative density can be estimated from relative compaction (i.e. percentage of modified Proctor density). On this basis, the densely and loosely compacted fine gravel materials have estimated relative densities of approximately 74% and 35%, respectively.

Table 3-3 Density characteristics of the fine gravel backfill material

Backfill Type	USCS	Standard Effort		Modified Effort	
		w_{opt} (%)	γ_d (kN/m^3)	w_{opt} (%)	γ_d (kN/m^3)
Fine Gravel	SW	8	19.2	7	20.7

Table 3-4 Average in-situ unit weight properties for fine gravel backfill

Backfill Type	$\gamma_{d,avg}$ (kN/m^3)	w_{avg} (%)	$\gamma_{m,avg}$ (kN/m^3)	Relative Compaction
Densely Compacted Fine Gravel	19.6	9.7	21.7	94.8% of modified
Loosely Compacted Fine Gravel	18.0	6.6	19.2	93.9% of standard (87.0% of modified)

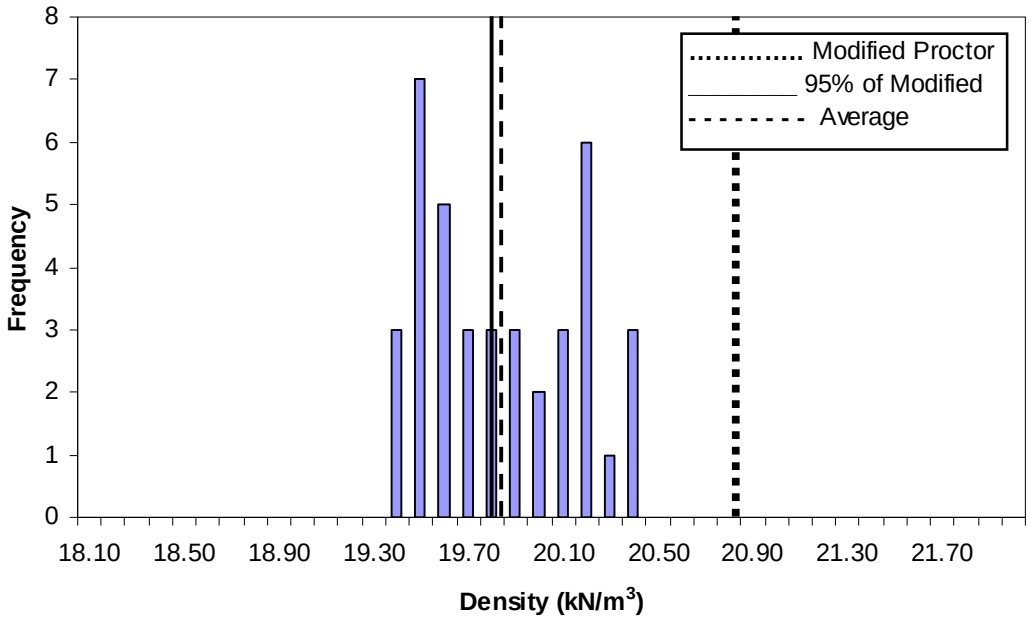

Figure 3-7 Density distribution of densely compacted fine gravel backfill

Direct shear tests were performed in the Brigham Young University soil mechanics laboratory to determine the shear characteristics of the fine gravel backfill material at both of the aforementioned compaction levels. The normal stress during these tests ranged from about 10 kPa to about 380 kPa. The shear strength envelopes for the densely and loosely compacted fine gravel backfill are shown in Figure 3-9. Failure

envelopes for both peak and ultimate values were evaluated. In-situ direct shear tests were also performed on the fine gravel material at the time of testing. In these tests, a 0.46-m square, 0.23-m high steel box is positioned over a progressively carved-out sample of the material and loaded horizontally with a hydraulic jack. Normal stresses during the in-situ tests ranged from about 10 kPa to about 30 kPa. The in-situ direct shear tests are staged (i.e., the specimen is sheared to the point of apparent failure under one normal stress, whereupon additional normal stress is added to the same specimen and the specimen is sheared again) so a single specimen can be used for all the points on the failure envelope. A summary of the engineering characteristics of the backfill soils based on the direct shear test results is presented in Table 3-5. The soil friction angle and cohesion intercepts for the laboratory and in-situ direct shear tests are different from each

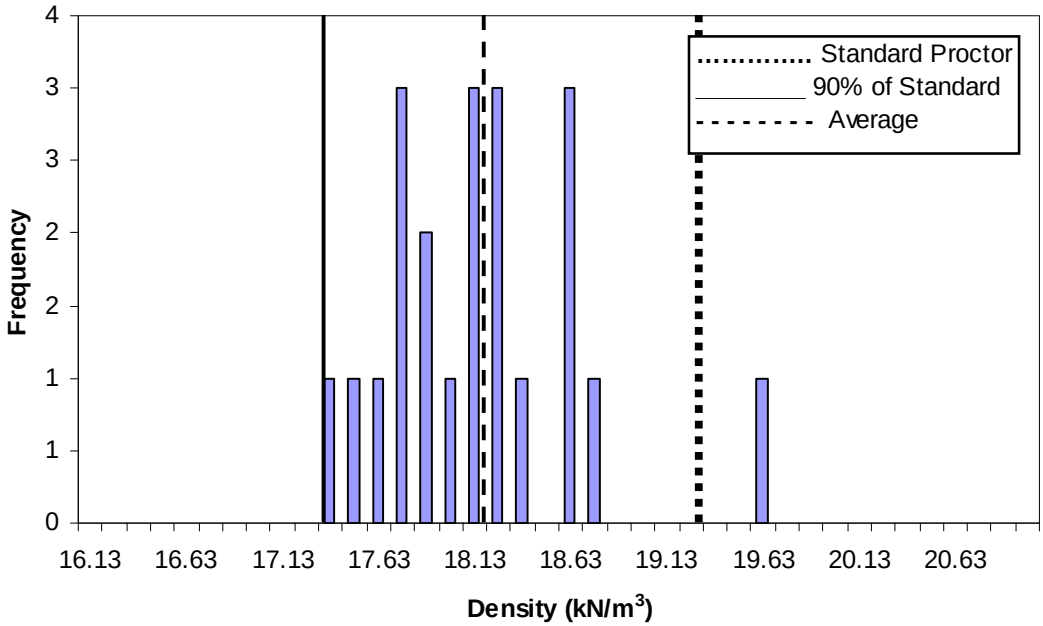

Figure 3-8 Density distribution of loosely compacted fine gravel backfill

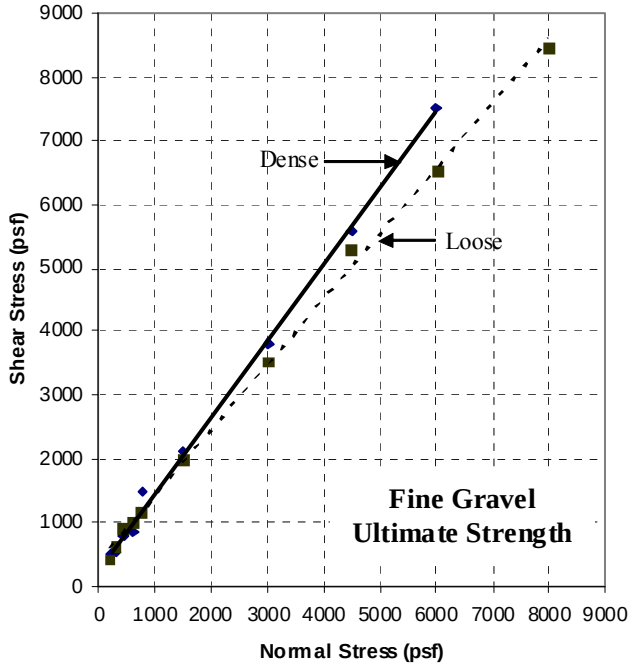

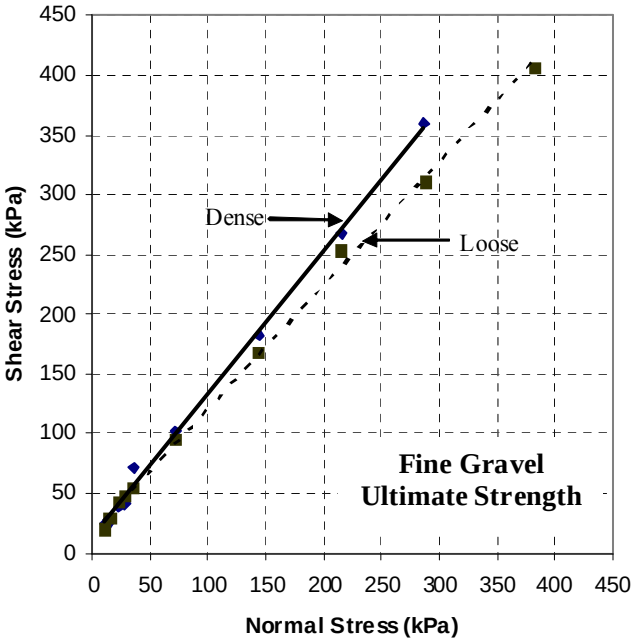

Ultimate Strength

0 to 287* kPa (0 to 6000 psf)

	Dense	Loose
φ' =	50.3°	45.8°
c' =	11 kPa	18 kPa
	(231 psf)	(375 psf)

72 to 287* kPa (1500 to 6000 psf)

	Dense	Loose
φ' =	50.0°	44.9°
c' =	13 kPa	27 kPa
	(275 psf)	(566 psf)

*383 kPa (8000 psf) for Loose Fine Gravel

Figure 3-9 Direct shear results for densely compacted and loosely compacted fine gravel backfill

other. Unfortunately, there are issues with both tests. In the lab direct shear test, the strength parameters may be artificially high due to the relatively large particle sizes present in the reconstituted specimen (the specimen as tested had a thickness-to-maximum-particle-size ratio of 3 rather than the normal 6 or more, while its diameter-to-maximum- particle-size ratio was just at the specified threshold of 10). Because these diameter ratios were not fully met, the lab-based test results should be somewhat discounted. Repeated loading of dilative soils (e.g. dense sands and gravels) during staged testing may lead to a reduction in resistance as the test progresses to higher stages. Hence, for in-situ direct shear tests, this may lead to lower friction parameters than if a fresh specimen was evaluated for each confining pressure.

Table 3-5 Direct shear summary for the fine gravel backfill material

Backfill Type	Laboratory Values				In-situ	
	Peak		Ultimate			
	ϕ (°)	c (kPa)	ϕ (°)	c (kPa)	ϕ (°)	c (kPa)
Densely Compacted Fine Gravel	52.0	13.0	50.0	13.1	44.3	19.7
Loosely Compacted Fine Gravel	45.8	17.7	44.9	27.1	43.0	4.8

Along with the normal direct shear tests, a series of modified laboratory direct shear tests were performed to quantify the interface friction angle (δ) between the concrete and fine gravel. The interface friction angle was determined by placing a concrete sample into the bottom half of the shear box, filling the top half of the box with fine gravel compacted to the appropriate density, and shearing the composite sample under the same normal stress range as the internal friction angle tests. The concrete sample used was very similar to, but slightly less rough than, the pile cap face, and may

have resulted in a slightly lower interface friction angle than was present in the field. This may have some effect on the accuracy of the passive pressure computations performed in the analysis presented later in this thesis. The interface friction angle determined from the ultimate stress points was 30.5 degrees for densely compacted fine gravel against concrete. The δ/φ ratio for the densely compacted fine gravel based on ultimate value results is 0.61 (as compared to a typically assumed value of 0.75).

3.4.2 Coarse Gravel Backfill

The USCS classification of the coarse gravel material is poorly graded gravel with sand (GP). AASHTO classifies the coarse gravel as an A-1-a soil. Figure 3-10 shows the particle distribution of the coarse gravel backfill material. The coarse gravel is currently used locally as P-154 material, as specified by the FAA, the gradation limits for which are shown alongside the particle size distribution in the figure below. Table 3-6 provides a summary of the grain size distribution and other properties for the coarse gravel backfill material.

Table 3-7 gives the optimum moisture content and maximum dry density of the coarse gravel material using standard and modified effort, respectively. Testing was performed on the material in two separate compaction states: loosely compacted and densely compacted. A jumping jack and a robust trench compactor were used to bring the coarse gravel backfill to the desired compaction levels. Nuclear density gauge readings were taken for each lift to verify the degree of compaction and moisture content.

The histograms in Figure 3-11 and Figure 3-12 demonstrate the density distribution of densely compacted coarse gravel and loosely compacted coarse gravel,

Table 3-6 Index properties for the coarse gravel backfill material

Backfill Type	Gravel (%)	Sand (%)	Fines (%)	D_{60} (mm)	D_{50} (mm)	D_{30} (mm)	D_{10} (mm)	C_u	C_c
Coarse Gravel	66	33	2	27	19	2.7	0.3	85	0.8

Table 3-7 Compaction characteristics of the coarse gravel backfill material

Backfill Type	USCS	Standard Effort		Modified Effort	
		w_{opt} (%)	γ_d (kN/m^3)	w_{opt} (%)	γ_d (kN/m^3)
Coarse Gravel	GP	8	20.8	6	22.0

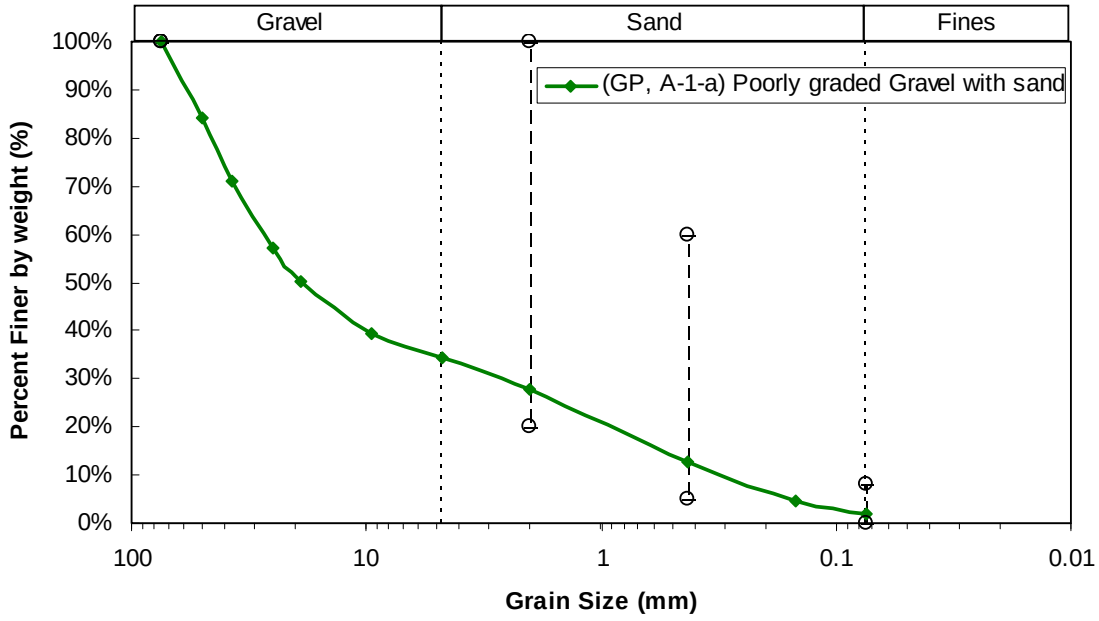

Figure 3-10 Particle distribution and P-154 qualifying limits for coarse gravel backfill

respectively. The densely compacted coarse gravel backfill material has an average dry density of about 96% of modified Proctor maximum density. The loosely compacted coarse gravel backfill has an average dry density of about 95% of standard Proctor maximum density or about 89.5% of modified Proctor density. Table 3-8 summarizes the in-situ compaction properties of the coarse gravel backfill.

Direct shear testing of the coarse gravel in the laboratory was not possible using conventionally sized testing equipment due the relatively large particle sizes. In order to obtain shear strength estimates, friction angles for the coarse gravel in both its loosely and densely compacted states were determined using relationships developed by Duncan (2004) based on a relatively large database of sand, gravel, and rockfill. Relative compaction (i.e., percent modified Proctor) was used as a proxy for relative density based on the correlation developed by Lee and Singh (1971). Relative density can be estimated using this correlation as 82% for the densely compacted coarse gravel and about 48% for the loosely compacted coarse gravel. Friction angles obtained for the fine gravel using these correlations were compared to direct shear test results, yielding good agreement between the two approaches, which helped confirm the appropriateness of using the Duncan (2004) relationships to estimate the friction angle of the coarse gravel.

In-situ direct shear tests were also performed on the coarse gravel material at both levels of compaction. In these tests, a 0.46-m square, 0.23-m high steel box encloses a sample of the material and is loaded from the side with a hydraulic jack. Because of the relative coarseness and poorly graded nature of the gravel, it was not possible to carve the box into place as is normally done; rather, a lift of soil was compacted in and around the box and then the outside soil was removed. Normal stresses during the in-situ tests

ranged from about 10 kPa to about 30 kPa. The in-situ direct shear tests are staged so a single sample can be used for all the points on the failure envelope. Repeated loading of dilative soils during staged testing may lead to lower resistance as the test progresses to higher stages. This may lead to lower friction parameters than if a fresh specimen was tested for each confining pressure. A summary of the engineering characteristics of the coarse gravel backfill material based on the correlation and the in-situ direct shear results is presented in Table 3-9.

An initial estimate of the interface friction angle for the coarse gravel backfill material against concrete was obtained by using the δ/φ ratio from testing the fine gravel material against concrete. For the correlated engineering properties, this ratio translates into an interface friction angle between 32 and 33 degrees for the densely compacted coarse gravel and about 30 degrees for the loosely compacted coarse gravel. Using the same ratio for the in-situ direct shear-based properties the interface friction angle is between 24 and 25 degrees for the densely compacted coarse gravel and about 24 degrees for the loosely compacted coarse gravel.

Table 3-8 Average in-situ unit weight properties for coarse gravel backfill

Backfill Type:	γd,avg (kN/m3)	wavg (%)	γm,avg (kN/m3)	Relative Compaction
Densely Compacted Coarse Gravel	21.2	2.9	21.8	96.4% of modified
Loosely Compacted Coarse Gravel	19.7	1.9	20.1	94.9% of standard (89.5% of modified)

Table 3-9 Direct shear summary for the coarse gravel backfill material

Backfill Type	Correlated		In-situ	
	φ (°)	c (kPa)	φ (°)	c (kPa)
Densely Compacted Coarse Gravel	54.0	0	40.6	13.7
Loosely Compacted Coarse Gravel	50.0	0	39.7	0

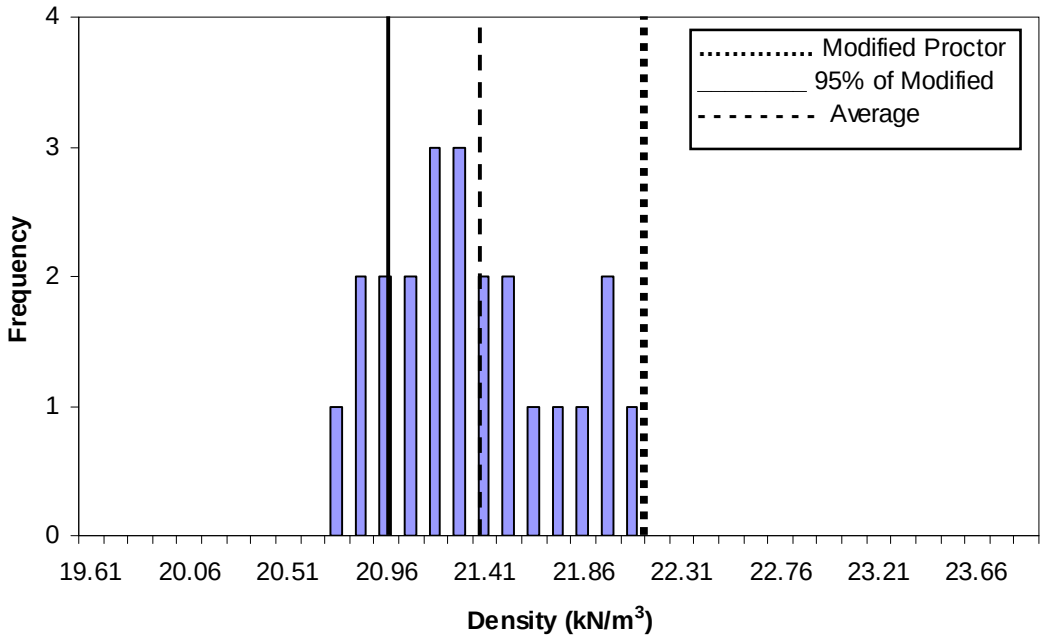

Figure 3-11 Density distribution of densely compacted coarse gravel backfill

3.4.3 Backfill Dimensions

The soil backfills were placed against the 3.35-m wide by 1.68-m high side of the pile cap, resulting in a loaded face with an aspect ratio of 2. As shown in the plan view portion of Figure 3-4, the backfill zone was approximately 7.0 m wide and 8.5 m long. The cross-sectional view in Figure 3-4 shows that the soil within the first 2.44 m from the

cap within the excavation extends to a depth of approximately 2.16 m, after which the base of the excavation slopes up to its exit point at the ground surface. The dimensions of the backfill zone were selected to minimize the amount of backfill soil needed while still enclosing the anticipated shape of a log-spiral failure plane in three dimensions.

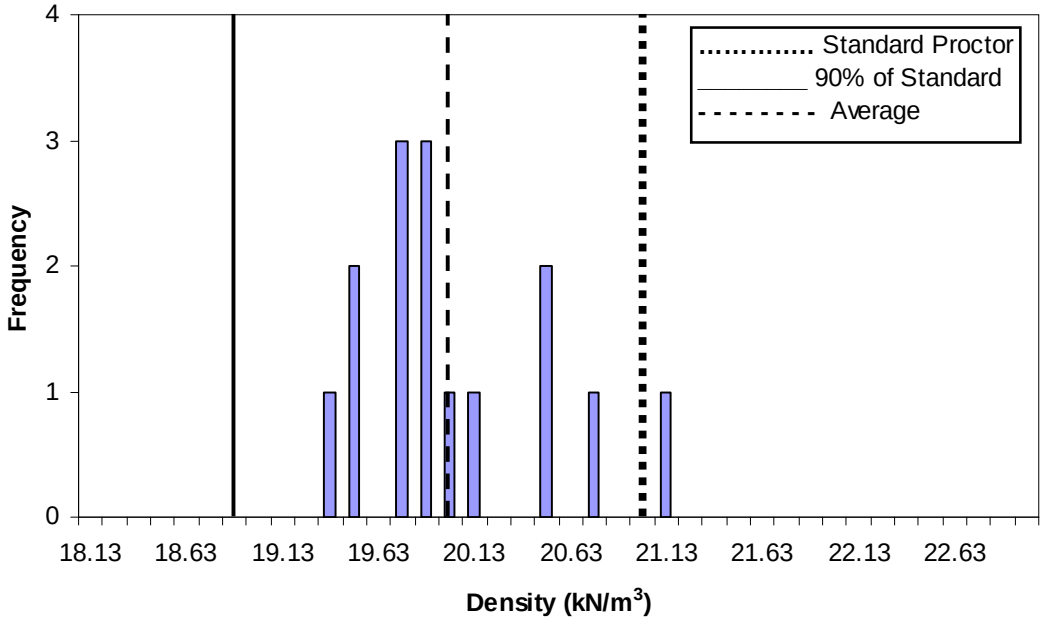

Figure 3-12 Density distribution of loosely compacted coarse gravel backfill

4 Data Analysis Methods

4.1 General

This chapter describes the methods used to analyze data collected during the pile cap load tests. Results derived from these methods will subsequently be presented for each respective backfill condition in its own chapter.

4.2 Load-Displacement Response and Passive Earth Force

The most basic relationships reduced from the test data were horizontal load versus displacement relationships for the pile cap with varying backfill conditions. Due to the actuator cycling and the rotations of the eccentric mass shaker, these relationships do not follow a smooth curve to describe the system response due to the loading and displacement of the pile. The load-displacement response of the system can be found by picking the peak load at the end of each static actuator push, before any cyclic or dynamic testing has begun, and finding the displacement that corresponds to each load. The series of points obtained from this process becomes the coordinates of the load-displacement response of the system for a given backfill condition.

The passive earth force from the backfill material can be determined by taking the load-displacement response of the pile cap with the backfill in place and subtracting the

response of the pile cap without any backfill (i.e., the "baseline" response of the pile cap). The baseline response reflects the pile cap resistance provided by pile-soil interaction. The pile cap response with no soil present is shown in Figure 4-1 and is based on the test conducted on June 21, 2007. As indicated in Table 3-1, there were two other tests conducted without backfill present; however, they were not used as the baseline for several reasons. The first test provided the initial loading of the test cap and would not be comparable to a reloading of the cap until the pile-to-cap connections had softened after the first few complete load-displacement cycles of up to 90 mm of displacement. In fact, this "conditioning" of the cap was the primary purpose of the first load test. Comparisons of the "unloading" slopes of the load-displacement curves during the retraction of the cap to its starting position at the end of each test later showed generally consistent values, suggesting that the cap was well conditioned and that the baseline response of the cap was relatively constant throughout testing. The test on June 1, 2007 did not have any dynamic effects in the load-displacement relationship because the shaker had malfunctioned; also, there were fewer intervals at which cyclic actuator loading were applied. The behavior of the cap during the June 21, 2007 test suggests that the baseline response is non-linear, a characteristic to which the cyclic and dynamic loadings contributed particularly to at lower displacement levels.

To quantify the non-linear baseline response, a fifth order polynomial curve was fitted to the peak points of the response (i.e., the maximum load and displacement before any cyclic loading was applied to the cap) and forced through zero. The fitted curve is shown in Figure 4-2 along with the measured response curve. The equation was used to quantify the baseline response at the peak points of other tests. Due to the high order of

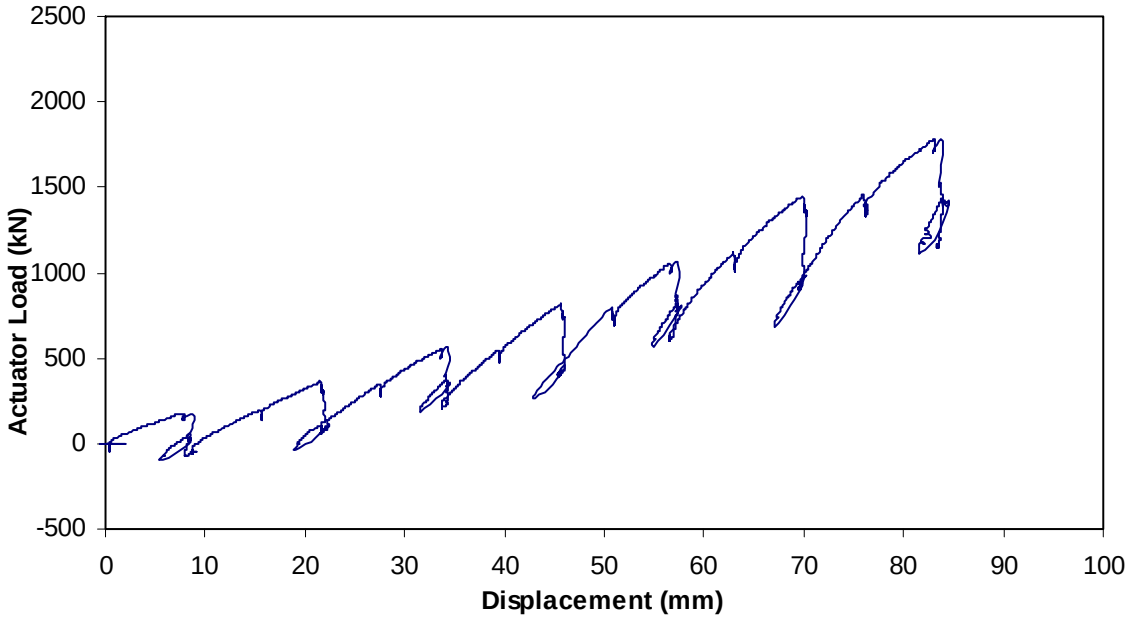

Figure 4-1 Load versus displacement relationship for pile cap with no backfill materials present (baseline test)

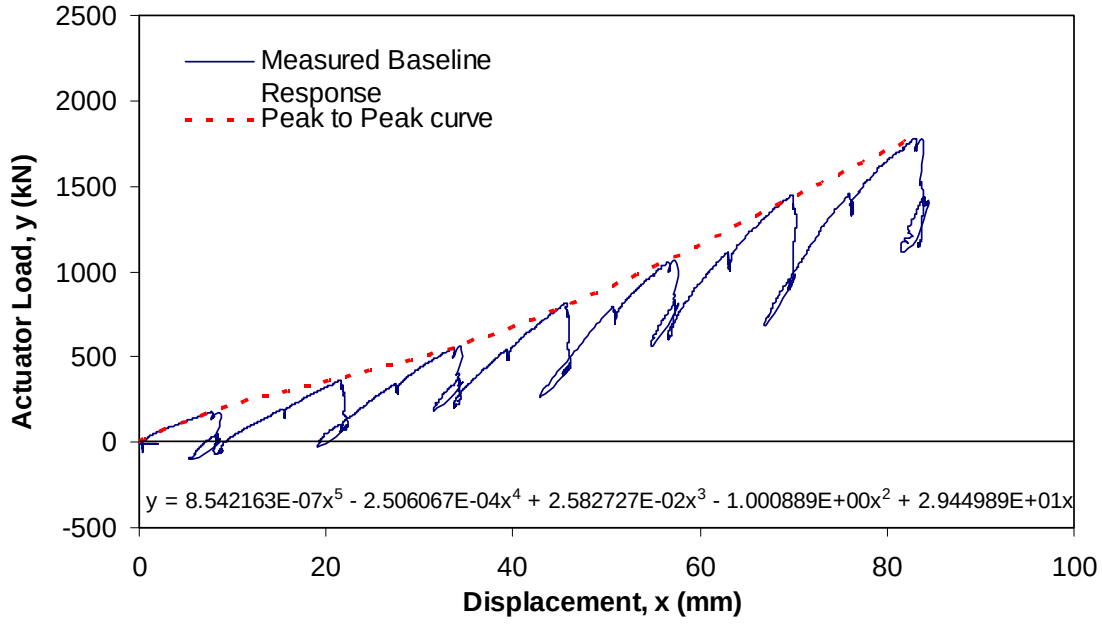

Figure 4-2 Measured baseline response with modeled baseline response

the polynomial, caution must be taken when extrapolating beyond the 83 mm maximum displacement from the baseline test.

Plots of the total response of the test foundation to static, cyclic, and dynamic loading with backfill in place are shown in subsequent chapters for each backfill condition. To facilitate understanding of these figures, the loading sequence (or loading path) has been color coded. Portions of the loading path which occur as the actuators are being used to slowly push the pile cap to the next target displacement level are shown in green. These portions are also referred to in this text as "static pushes." Portions of the loading path in which the actuators are being used to apply 15 cycles of small amplitude cyclic loading are shown in blue. Portions of the loading path in which the eccentric mass shaker is being used to apply a dynamic loading to the pile cap are shown in red. Because of the extremely large quantity of data otherwise involved, these plots are based on 1-sps datasets and hence do not fully reflect the cyclic and dynamic portions of the test. Also, the load shown in the figures is the combined load applied to the pile cap by the two actuators. The total load acting on the cap can be found by superimposing the shaker load, inertial load, and any backfill reaction; such a feat requires a detailed analysis of each dynamic loading loop. In order to provide an overall perspective of each test, the actuator loads alone have been used to produce these figures. More detailed analysis of the dynamic loading loops will be provided later in this document.

During the loading of the pile cap, a differential in cap displacement was observed between the east and west sides of the cap. The maximum differential during the first test with backfill, based on the top two string potentiometers, was 4.3 mm, with the west side leading. The differential displacement can be explained in part by the different stiffness

of the drilled shafts used in the reaction foundation. The west shaft is somewhat stiffer than the east shaft (see Taylor, 2006), causing the west side of the pile cap to move more than the east side. An attempt to mitigate this differential movement was made by applying uneven loads in the actuators, but some differential movement still occurred. The reported pile cap displacements are based on the median displacement measured by the string potentiometers mounted to the pile cap.

Plots of passive earth force versus displacement for the backfill soils developed by subtracting the baseline response of the pile cap from the measured pile cap response with backfill in place are shown in subsequent chapters for each backfill condition. The total measured response of the pile cap and the baseline response from which the passive earth force was developed are also shown in these figures. For simplicity, only the static load-displacement response was used in these figures.

4.3 Calculated Passive Earth Force

Several methods were used to calculate the passive force versus displacement relationship for the backfill soils. In this study, passive earth pressures were calculated using a modified version of the spreadsheet program PYCAP developed by Duncan and Mokwa (2001), which implements the classical log-spiral solution for passive force with a hyperbolic displacement curve; the computer program entitled ABUTMENT, which implements the Log Spiral Hyperbolic (LSH) approach presented by Shamsabadi et al. (2007); and the CALTRANS standard design method. Comparisons of these methods to the measured earth pressures will be shown in subsequent chapters.

4.3.1 PYCAP Methodology

Duncan and Mokwa (2001) presented a method in which the ultimate passive force (pressure) from a soil backfill is determined using the log-spiral method while the force versus displacement curve is based on a hyperbolic load-displacement relationship where initial loading stiffness (k_{max}) is based on the solution for a laterally loaded plate embedded in an elastic half-space (Douglas and Davis, 1964). The methodology has been implemented by Mokwa using an EXCEL spreadsheet entitled PYCAP.

Input parameters include soil properties such as soil friction angle (ϕ), cohesion (c), soil-foundation interface friction (δ), an adhesion factor (α), initial soil modulus (E_i), Poisson's ratio (ν), and in-situ unit weight (γ). The inputs describing the foundation geometry are the foundation height (H), width (b), embedment depth (z), surcharge (q) and failure displacement divided by cap height (Δ_{max}/H).

The soil friction angle and cohesion, as well as the interface friction angle, were generally determined from direct shear testing. Initial soil modulus was found using the stress-strain unloading/reloading curve of a one-dimensional consolidation test and confirmed by comparing with typical values. Values for Poisson's ratio were selected from typical values. Specific values for each parameter used in analyses will be presented subsequently. Three-dimensional loading effects are accounted for using the factor (R_{3D}) developed by Brinch-Hansen (1966). To accommodate the observation by Ovesen and Stromann (1972) that the Brinch-Hansen correction factor is incorrect, the correction factor is limited to a value of 2.

Along with a load-displacement curve of the passive earth pressure, PYCAP outputs include the soil loading stiffness (k_{max}); the hyperbolic failure ratio (R_f), which is

derived from Δ_{max}/H; and the coefficient of passive earth pressure (K_p) from the log-spiral method of calculating passive soil resistance.

The initial soil moduli used in the analysis of the gravel backfill soils in this study were determined from oedometer tests and correlations. The range of suggested values given in Duncan and Mokwa (2001) is presented in Table 4-1. A synopsis on how each modulus value used in analysis compares to these ranges will be given subsequently for each backfill condition in its respective chapter.

Table 4-1 Suggested initial tangent modulus for different densities of sands and gravels (from Duncan and Mokwa, 2001)

Density	D_r	N_{60}	Normally loaded	Preloaded or compacted
Loose	40%	3	E_i = 9600 - 19200 kPa	E_i = 19200 - 38300 kPa
Medium	60%	7	E_i = 14400 - 23900 kPa	E_i = 23900 - 47900 kPa
Dense	80%	15	E_i = 19200 - 28700 ksf	E_i = 28700 - 57500 ksf

4.3.2 ABUTMENT (LSH) Methodology

In this methodology, the ultimate pressure of the backfill is determined by dividing the backfill soil into slices and then satisfying force-based, limit-equilibrium equations for mobilized logarithmic-spiral failure surfaces. A modified hyperbolic stress-strain relationship is used to determine displacement. This methodology, referred to as the LSH method and developed by Shamsabadi et al. (2007), has been incorporated by Shamsabadi into the computer program ABUTMENT.

Input parameters for the LSH method are soil properties and foundation geometry. The soil properties needed are internal friction angle (ϕ), soil cohesion (c), soil-

foundation interface friction (δ), in-situ unit weight (γ), Poisson's ratio (ν), and strain at 50% strength (ε_{50}) (ideally determined from triaxial testing). An additional failure ratio (R_f) parameter must be defined which helps control the sharpness of the hyperbolic curve. Unlike the R_f values used in some hyperbolic soil models; this value typically ranges from 0.95 to 0.98. Output from the program includes the load-displacement curve and the passive horizontal earth pressure coefficient. The program charts the outputs at different levels of stress mobilization in a table. Most of the soil input parameters were selected in the same way that they were chosen for the analyses using PYCAP. The strain parameter is difficult to precisely define but was estimated using the stress-strain loading curve of a one-dimensional consolidation test and then compared with values shown for similar backfill materials in Shamsabadi et al. (2007). Within the computer program, the log-spiral force method of calculation was used with the "composite" option while the stresses and strains were calculated using the "modified hyperbolic" option. Three-dimensional end effects were accounted for using an effective foundation width determined using the modified Brinch-Hansen (1966) relationships used in the PYCAP-based analyses.

4.3.3 CALTRANS Methodology

Based on full scale abutment tests conducted at UC Davis (see Maroney, 1994), CALTRANS developed a method to determine the initial stiffness and ultimate passive resistance for abutment backfill to use in standard design work. The initial stiffness (K_{abut}) and ultimate force (P_{ult}) are determined using Equation 4-1 and Equation 4-2:

$$K_{abut} = 11.5 \frac{kN/mm}{m} * w_{abut} * \left(\frac{h}{1.7} \right) \quad \textbf{(4-1)}$$

$$P_{ult} = 239\, kPa * A_{abut} * \left(\frac{h}{1.7} \right) \quad \textbf{(4-2)}$$

where w_{abut} is the width of the abutment, h is the height of the abutment and A_{abut} is the area of the abutment (with dimensions of length expressed in terms of meters). The load-displacement relationship follows the initial stiffness and then flattens to a constant resistance when the ultimate pressure is exceeded. The method is based on an abutment with wingwalls with a dense sand structure backfill and a loamy soil embankment. Different abutment heights are assumed to scale linearly relative to the height of the abutment in the U.C. Davis tests and does not account for changes in backfill properties. In fact, soil properties are not explicitly addressed in the method. For the geometry of the test pile cap evaluated in this document, the initial stiffness based on this method is 39 kN/mm and the ultimate passive resistance is approximately 1360 kN.

4.4 Response to Cyclic Actuator and Dynamic Shaker Loadings

Slow, actuator-driven cyclic loadings and cyclically applied dynamic loadings from the eccentric mass shaker were applied to the pile cap during testing. The behavior of the pile cap under these loadings was analyzed by resolving the forces on the test cap during testing and isolating the pile cap from the response of the reaction foundation. The forces acting on the cap include the actuator force; the shaker force; the damping, stiffness, and inertial forces from the cap itself; and the damping, stiffness, and inertial

forces from the backfill. The actuator loads account for the net damping, stiffness, and inertial forces from the reaction foundation system.

Acceleration data from the accelerometers on the cap provided motion input to calculate the inertial force for the pile cap system during dynamic loading using a constant, single lumped-mass representation of the test cap, the shaker, the upper eight pile-diameters of the piles, one of the actuators, and the backfill (if any) assuming a log-spiral failure geometry. The total weight of the above-mentioned test components without any backfill was approximately 707 kN. The log-spiral shape of the failure mass computed using the modified version of the PYCAP program was used to determine the mass of the densely compacted backfill, which was then adjusted by the Brinch-Hansen three-dimensional factor to account for fanning of the failure wedge beyond the edges of the pile cap. The backfill weights used for densely and loosely compacted fine gravel were 1420 and 360 kN, respectively, whereas the weights used for densely and loosely compacted coarse gravel were 1690 and 420 kN, respectively. Inertial forces are negligible for the slowly applied actuator-based loadings.

In order to represent the combined internal stiffness and damping effects of the pile cap with the backfill (if any was present), force-displacement loops were created by combining the inertial force with the shaker and actuator forces. System stiffness and damping for the actuator-based cyclic testing were calculated using the median of the 15 loading loops. System stiffness and damping for the shaker-based dynamic loading were calculated from the median of the 15 loops from each dwell frequency mentioned in the discussion of the eccentric mass shaker loading in Section 3.3.6 (ranging from 1 to 10 Hz, at 0.5 Hz intervals).

The system stiffness, k, was calculated using the average slope from peak to peak of the force-displacement loops as shown in Figure 4-3 and Equation 4-3:

$$k = \frac{(P_{\max} - P_{\min})}{(u_{\max} - u_{\min})} = \frac{P_{amp}}{u_0} \quad \textbf{(4-3)}$$

where u_{max} is the maximum displacement, u_{min} is the minimum displacement, P_{max} and P_{min} are the loads associated with the maximum and minimum displacements (which are not necessarily the maximum and minimum loads during the loop), and P_{amp} is the load amplitude.

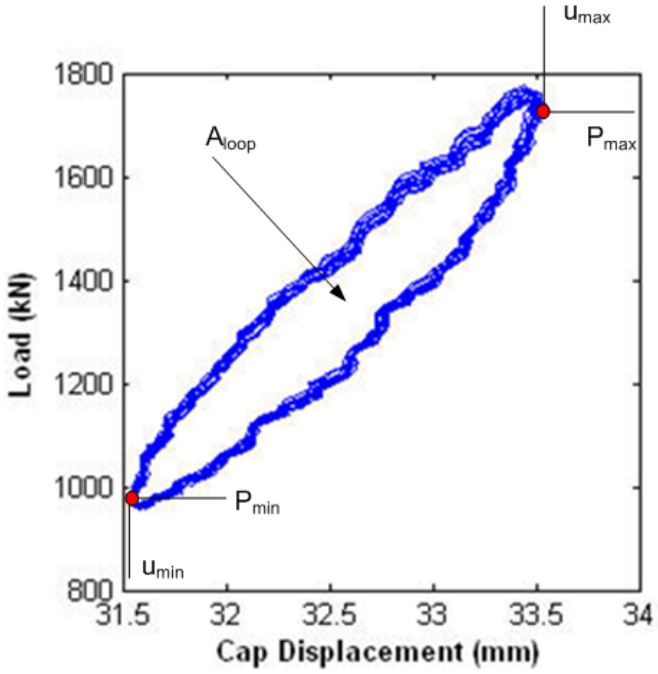

Figure 4-3 Example of actuator-based load-displacement loops

Due to the ramped manner in which the shaker force was applied, it is difficult to isolate the effects of the number of loading cycles. Additionally, due to the ramped nature of the loading, the calculated stiffness is due to reloading instead of being an initial loading stiffness.

For dynamic loading conditions, damping can be assessed with either the half-power bandwidth method or by using the area and slope of the force-displacement loops directly. The half-power bandwidth method requires a plot of the measured dynamic displacement versus the frequency ratio, ω/ω_n (ω is the circular frequency of the forcing function and ω_n is the natural circular frequency of the structure). Two frequencies, ω_1 and ω_2, on opposing sides of $\omega/\omega_n = 1$ whose displacement amplitudes correspond to $1/\sqrt{2}$ times the displacement amplitude at $\omega/\omega_n = 1$ are selected and used to determine the damping ratio, ξ, by satisfying Equation 4-4.

$$\left(\frac{\omega}{\omega_n}\right)^2 = \left(1-2\xi^2\right) \pm 2\xi\sqrt{1-\xi^2} \qquad \textbf{(4-4)}$$

This equation is often simplified to Equation 4-5 by assuming a small damping ratio:

$$\frac{\omega_b - \omega_a}{\omega_n} \cong 2\xi \qquad \textbf{(4-5)}$$

When damping is large (> 20% is the typically cited value) Equation 4-5 becomes unstable and should not be used. In cases where damping exceeds approximately 38%,

the spread between ω_1 and ω_2 increases, and ω_1 is forced to be less than zero, rendering Equation 4-4 invalid. Due to the load capacity of the eccentric mass shaker, the dynamic displacement amplitude versus frequency curves often did not extend to a high enough range to identify ω_2 .

Attempts to use the more rigorous solution with extrapolations of the measured response curve to estimate ω_2 revealed that the dynamic displacement amplitude versus frequency curves (where displacement amplitude was normalized by the net applied load from the shaker and actuator in order to establish a relatively stationary forcing function) exhibited an atypical shape in which ω_2 - ωn was greater than ω_n - ω_1, which prevented a solution to Equation 4-5 consistent with the measured data. The change of stiffness and damping with respect to shaker frequency due to material nonlinearity is a suspected cause of this behavior.

Damping during dynamic loading, ξ, was determined directly from the force-displacement loops using Equation 4-6:

$$\xi = \frac{1}{4\pi}\frac{A}{E_s} \qquad \textbf{(4-6)}$$

where A is the area of the force-displacement loop and E_s is the stored strain energy which equals 0.5 $k\ u_o^2$, in which k is the slope of the loop and u_o is the peak displacement amplitude of the loop.

Plots displaying displacement amplitude, stiffness, loop area, and damping as a function of frequency and pile cap displacement level due to static loading are presented

subsequently for each pile cap backfill condition in its respective chapter. At frequencies less than 4 Hz, shaker forces and resulting pile cap displacements are small, making it difficult to distinguish between the true response and instrumental noise. Hence, results are not presented for frequencies less than 4 Hz.

Stiffness and damping values from the cyclic actuator data generally exhibit a saw-tooth shaped trend. When the actuator cycles are performed before the shaker cycles the stiffness is higher due to softening of the soil during dynamic loading (i.e., when the actuator loading occurs after shaker loading, the dynamic loading from the shaker has already disturbed the backfill beyond the loading state at the end of the static push). This trend is similar to that observed in Figure 4-4, which shows typical load-displacement loops when the actuator cycles are initiated after shaker loading and prior to it, respectively. When the actuator cycles are performed first, the position of the cap drifts while the stiffness of the system remains relatively constant for each progressive loop. However, no drift is observed when the static cycles are performed after dynamic shaker loading. The drift is common to cyclic loading of soil and occurs as the soil softens, or relaxes, under cyclic loading.

Stiffness and damping fluctuate in terms of frequency and displacement amplitude as the pile cap is dynamically loaded by the eccentric mass shaker. As mentioned previously, the shaker was unable to produce large forces or displacements at low frequencies, which caused the load-displacement loops to be influenced by small differences. As the frequency increases to 4 Hz and beyond, the load-displacement loops become more distinct but their size and orientation change significantly with continuing increase in shaker frequency. The load-displacement loops also change significantly due

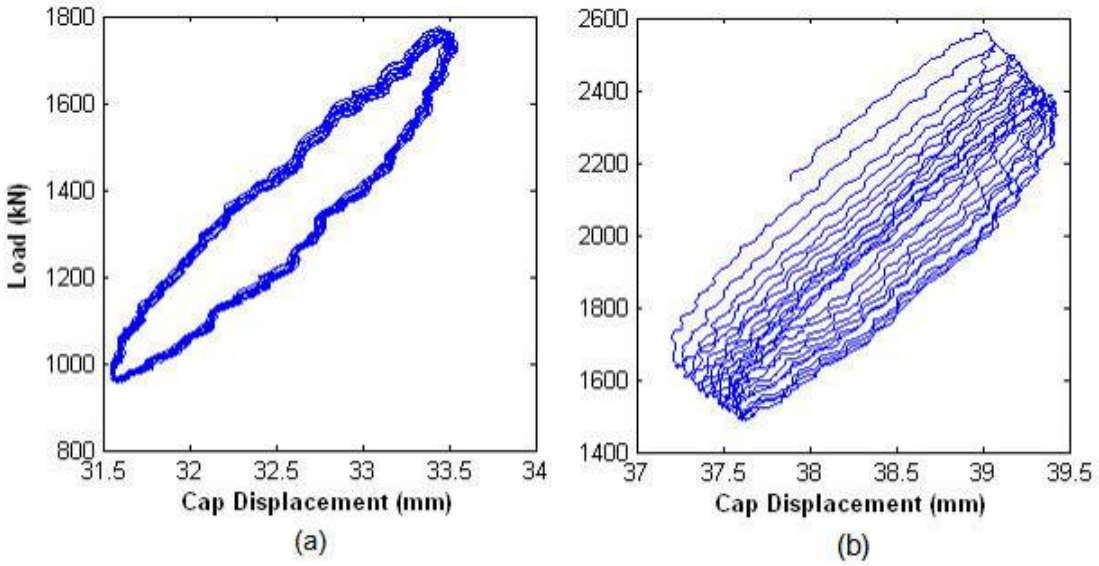

Figure 4-4 Typical actuator loops when actuator cycles are applied (a) second and (b) first

to the order of the shaker and actuator. Typical load-displacement loops from dynamic shaker loading can be seen in Figure 4-5. In order to keep the figure relatively uncluttered, many of the loading frequencies have been omitted.

4.5 Passive Earth Pressure Distributions

In addition to the load-displacement response data from the actuators, passive earth pressure from the backfill soil was measured directly with a vertical array of six earth pressure cells distributed evenly in the central portion of the pile cap face. Plots of earth pressures as a function of pile cap displacement for the different backfill soil conditions are shown for each backfill test in its respective chapter.

The lower-most pressure cell exhibited irregular behavior in relation to the other cells in the array in many of the tests. While this pressure cell does appear to measure increasing pressure for the first couple of displacement levels, subsequent pressure

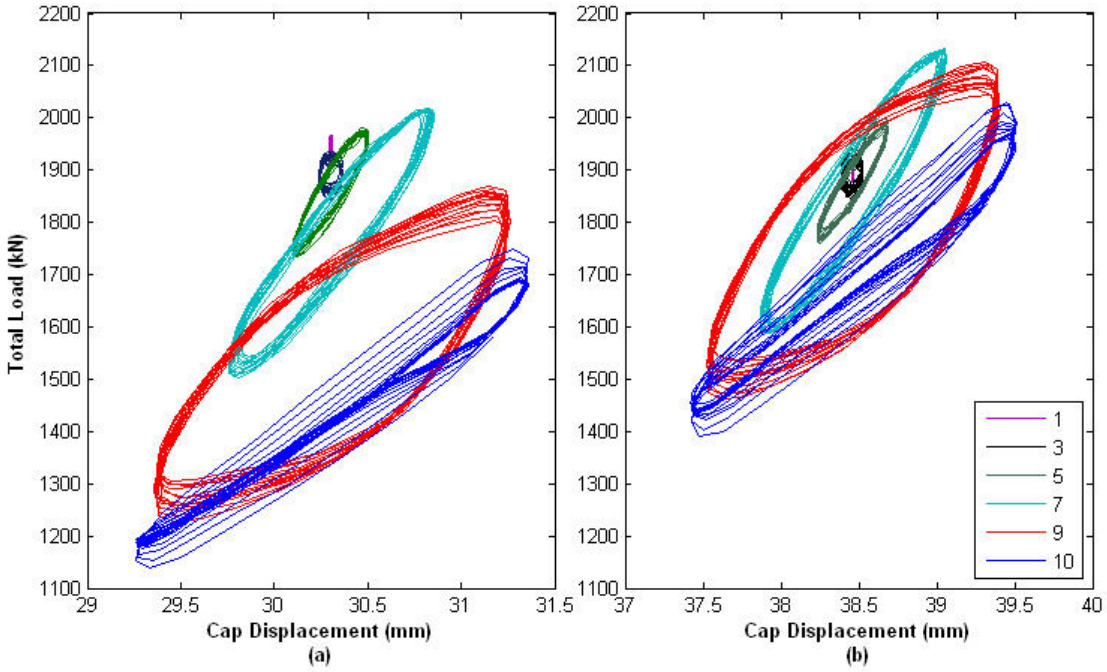

Figure 4-5 Typical load-displacement loops when shaker cycles are applied (a) second and (b) first

measurements tend to drop off, returning to relatively small values. This behavior may be indicative of pile cap rotation effects with the top of the cap rotating further out into the backfill soil, as the studies conducted by Fang et al. (1994) suggest. However, in comparing the relatively small amount of cap rotation that occurred during the test to that required to obtain such a pressure distribution based on an elastic pressure distribution acting on a vertically embedded plate as developed by Douglas and Davis (1964), the actual amount of cap rotation was considerably less than the rotation needed to produce a decrease in pressure at the bottom of the pile cap of the magnitude witness during many of the tests. As such, we believe it unlikely that the low pressures at the base of the cap are significantly caused by rotation effects. It is possible that the pressure cell was damaged in some way or that, given that the cell was placed in the vicinity of the point

where top of the center pile is embedded into the cap, an interaction between the end of the embedded pile and the concrete of the cap near the cell produced stress on the back side of the pressure cell, which led to inaccurate measurements.

By multiplying each pressure cell reading by the corresponding contributory area across the face of the pile cap and then summing the resulting forces, passive earth forces can be determined. These pressure cell-based forces can then be compared to passive earth forces derived from the load actuators, which were determined by subtracting the baseline response of the pile cap from the measured pile cap response with the backfill in place. Although the actual soil pressure distributions are generally irregular with depth, the plots of force calculated using these pressure cells have shapes which are consistently similar, albeit generally lower in magnitude, to the passive earth forces curves derived from the actuator-based measurements. Comparisons between pressure cell- and actuator-based passive earth forces are shown in subsequent chapters for each backfill test.

Differing pressure conditions outside the spatial coverage provided by the pressure cells may contribute to the differences between pressure cell- and actuator-based passive earth forces, particularly near the edges of the pile cap. In his analysis of a uniformly loaded strip foundation, Borowicka (1938) determined that the contact pressure near the foundation centerline could approach two-thirds of the net average pressure across the full width of a very rigid foundation. Elastic stress distributions (e.g., the distribution developed by Douglas and Davis (1964) for a vertically loaded plate embedded in an elastic half-space) show similar pressure distributions, with higher pressures near the edges of a foundation and lower pressures in the center.

An analysis was conducted using the pressure cell-based force and the actuator-based load response at the end of the static actuator push (before cyclic and dynamic loads are applied) for each displacement level for all of the backfill conditions in which the correlation between pressure cell-based and actuator-based forces was found to be approximately 0.6 (i.e., the pressure cell-based measurements are 60% of the force-based measurements). This correlation is illustrated in Figure 4-6. The correlation improves to approximately 0.7 if, as suspected, the lower-most pressure cell is frequently in error and is corrected to produce a resultant force which is consistent with an elastic stress distribution along the center of a vertical plate.

4.6 Cracking and Vertical Movement of Backfill

At each pile cap displacement level, after any cyclic and dynamic loadings, cracking within the backfill area was visually mapped using painted grid on the ground surface. Additionally, vertical surveys were performed at the beginning of each test and at the maximum displacement level in order to assess vertical changes in backfill elevation. The elevations were surveyed at the grid nodes to the nearest 3 mm; in reality, the tolerance is somewhat greater due to variations in making measurements along an irregular soil surface with varying particle sizes. Paired maps of backfill cracking and backfill elevation change contours for each of the backfill soil types are shown subsequently for each backfill test.

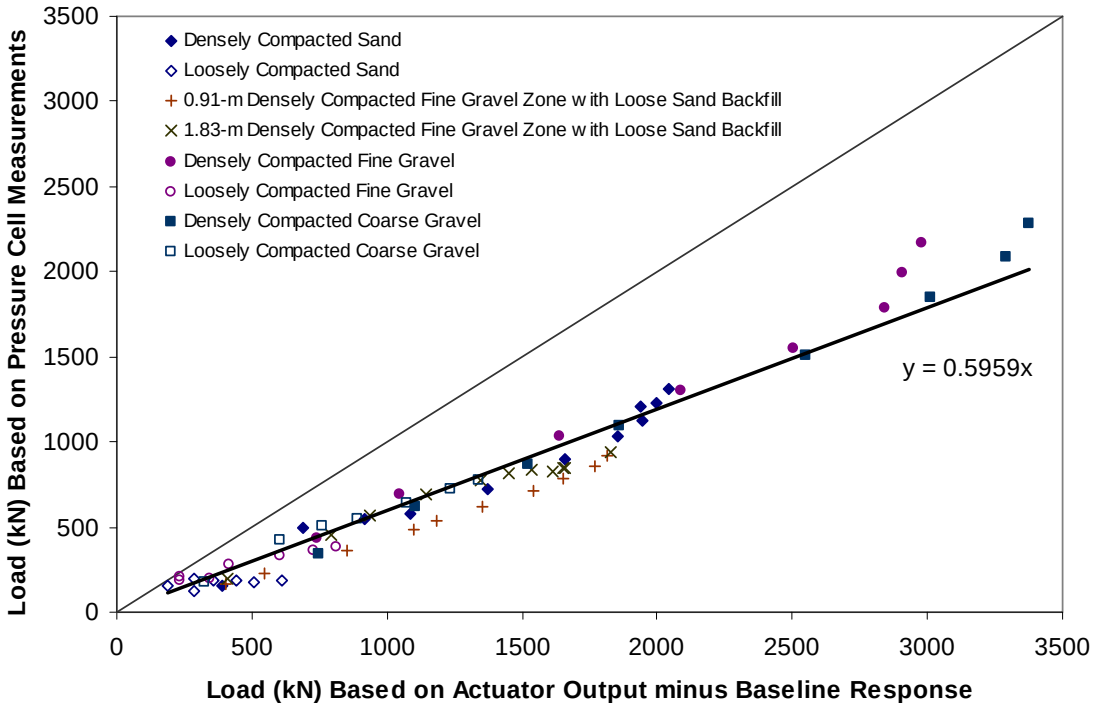

Figure 4-6 Passive earth loads based on pressure cells versus load actuators

4.7 Horizontal Movement of Backfill

String potentiometers mounted on the pile cap and attached to steel stakes installed at various points in the backfill material were used to measure relative movement along the top surface of the backfill throughout each test. These stakes were located at the following distances from the pile cap face: 0.61, 1.22, 1.83, 2.74, 3.66, 4.57, and 5.49 m. By knowing the relative movement between the cap face and the location of the stakes, as well as the absolute movement of the pile cap, absolute displacement of the backfill and strain in the backfill can be computed.

The changes in length recorded by the string potentiometers correspond to the total amount of compression between the cap face and the monitoring stakes. Negative change in length represented shortening of the string and positive change in length represented lengthening. Movement of the monitoring positions was calculated by subtracting the negative of the string potentiometer change in length from the displacement of the pile cap, effectively subtracting the magnitude of the backfill compression from the maximum total movement. When performed for each monitoring point, this method yielded the net movement of the stake. The data shown in subsequent plots are based on pile cap and stake positions at the end of each displacement interval (i.e., the time immediately after the pile cap had just been pushed to a new displacement level with the actuators).

To calculate the strain in the backfill material, the backfill was segmented into intervals bounded by the stakes. This segmentation produced seven intervals, one between the cap face and the first stake and the remaining between any two adjacent stakes. By normalizing the change in interval length by the initial interval length strains were calculated in each of the seven segments with positive values corresponding to compression.

In some cases, small negative displacements or strains (indicative of expansion) may be shown. These values likely result due to the limited precision with which the data could be collected and processed; any tilting of the steel monitoring stakes or differential movement between the far ends of the pile cap along which the different string potentiometers were mounted could result in small errors in the data. Also, in some instances, there were unexplained short-duration jumps in the string potentiometer

readings, and these readings were corrected manually by adjusting the affected data to match the data trend before and after the jumps.

Paired sets of plots showing the displacement of the backfill (as a function of distance away from the pile cap) and the calculated strains (as a function of pile cap displacement level) are shown in subsequent chapters for each backfill test.

5 Pile Cap with No Backfill Present (Baseline Response)

5.1 General

As shown previously in Table 3-1, three load tests were performed with no backfill in place. As explained in Section 4.2, the test performed on June 21, 2007 was used as the baseline response, the results of which are presented in this Chapter. Table 5-1 summarizes the test in terms of loads and displacements measured at the end of each "static push" with the actuators. The table also indicates the order in which actuator-driven cyclic loads and shaker-based dynamic loads were applied. This test followed the general test procedure without any significant deviations.

Table 5-1 Summary of test with no backfill (Test 11; June 21, 2007)

Displacement Interval	Displacement (mm)	Actuator Load (kN)	Actuator Cycles	Shaker Cycles
1	7.0	178	First	Second
2	16	189	None	None
3	21	365	Second	First
4	27	345	None	None
5	33	553	First	Second
6	39	548	None	None
7	45	815	Second	First
8	50	793	None	None
9	57	1066	First	Second
10	62	1119	None	None
11	69	1448	Second	First
12	75	1454	None	None
13	83	1782	First	Second

5.2 Load-Displacement Response

Figure 5-1 shows the entire actuator load verses pile cap displacement relationship for the test, with static pushes, actuator cycles and shaker cycles being represented by green, blue, and red data points, respectively. Section 4.2 provides some discussion relative to the interpretation of this data. No backfill was present in this test, so the horizontal load versus displacement relationship shown is the result of the resistance of the piles, the pile-soil interaction, and any friction due to contact of the base of the pile cap with the underlying soil.

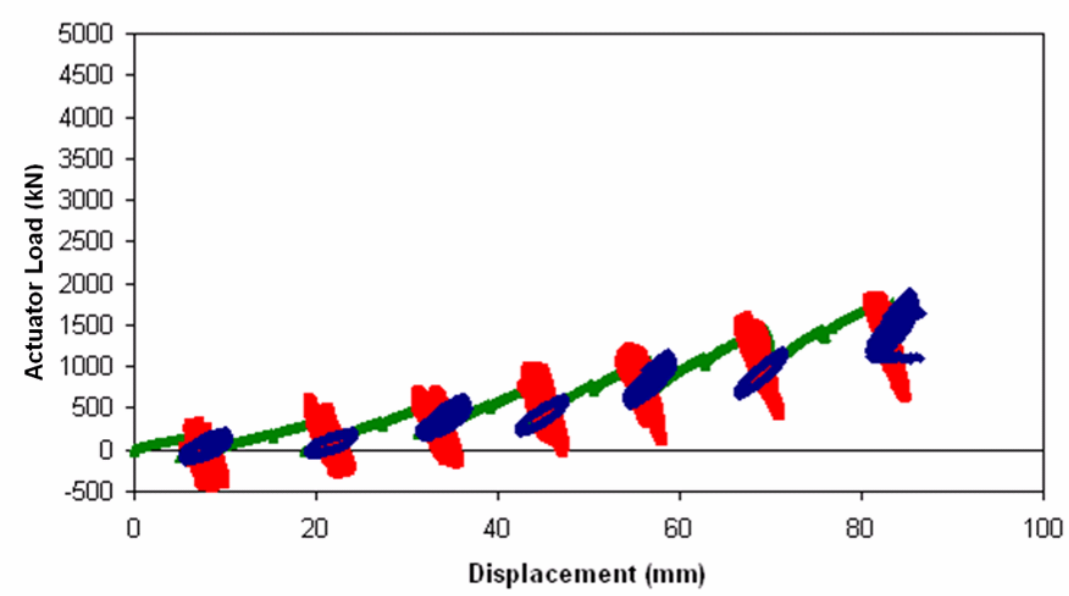

Figure 5-1 Actuator load versus pile cap displacement with no backfill (Test 11; June 21, 2007)

Figure 5-2 shows the equivalent monotonic response, or "backbone" curve, of the pile cap isolated from the data shown in Figure 5-1. As seen in Figure 5-2, the overall baseline response is somewhat non-linear, with stiffness increasing with each loading

interval as the pile cap is displaced. Slight decreases in load were observed between pushes while manual data points were being recorded. The decrease is attributable to relaxation of the soil acting on the piles and is not due to a decrease in pile cap displacement, which increases slightly during the same period. See Section 4.2 for further discussion of this load-displacement curve and its use as the baseline response for the pile cap.

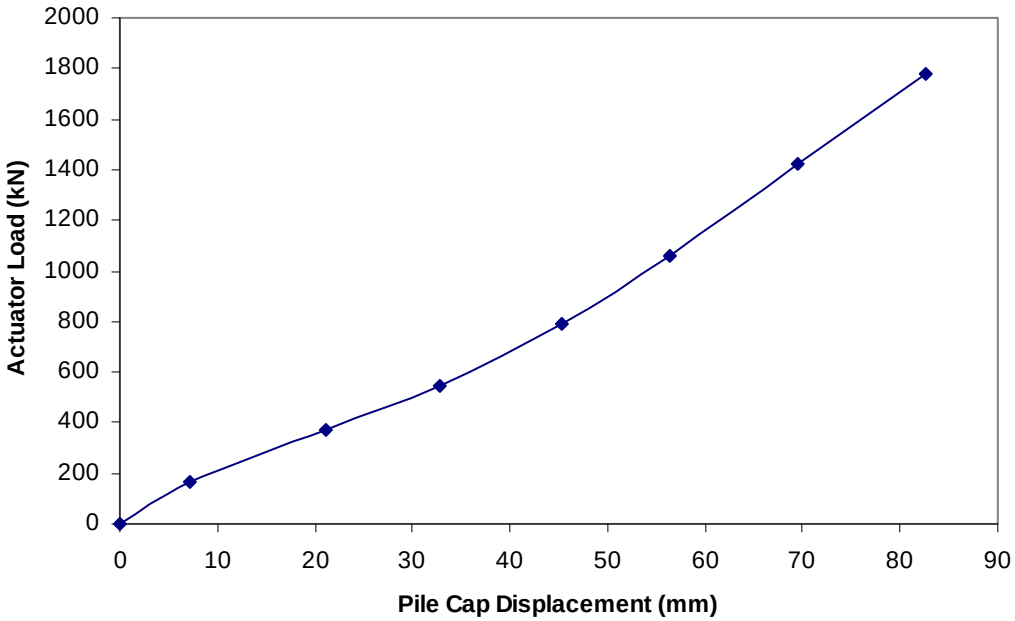

Figure 5-2 Total (and in this case, baseline) static response for pile cap with no backfill

5.3 Response to Cyclic Actuator Loading

After slowly pushing the pile cap to each target displacement, alternating combinations of cyclic actuator loads and dynamic shaker loads were applied to the test

foundation. The response of the pile cap to the small displacement amplitude load cycles from the actuator is presented and discussed in this section. Figure 5-3 shows the displacement amplitude, stiffness, loop area, and damping ratio for the pile cap without backfill as a function of cap displacement. Values are based on the median of the 15 small amplitude cycles performed at each displacement level. Displacement amplitude and loop area remain relatively constant throughout the test. However, as the pile cap displacement level increases, so does the stiffness, which causes the damping to decrease from approximately 40% to about 20%. An interesting attribute of the stiffness and damping data is the saw-tooth shape of the trend. This shape is caused by the order of the actuator and shaker cycles. The stiffness is higher when the actuator cycles are performed before the shaker cycles because of the softening of the soil surrounding the piles during dynamic loading (i.e., when the actuator cycles occur second, the soil has already experienced dynamic loading from the shaker).

5.4 Response to Dynamic Shaker Loading

After slowly pushing the pile cap to each target displacement, alternating combinations of small displacement cyclic actuator loads and dynamic shaker loads were applied to the test foundation. The first row of graphs in Figure 5-4 shows displacement amplitude as well as displacement amplitude normalized by the cyclic amplitude of net applied force from the shaker and actuators as functions of the forcing frequency and pile cap displacement level. The second and third rows of graphs show the calculated reloading stiffness and damping, respectively, of the pile cap system. The left column displays these parameters in terms of forcing frequency. If non-linear behavior is

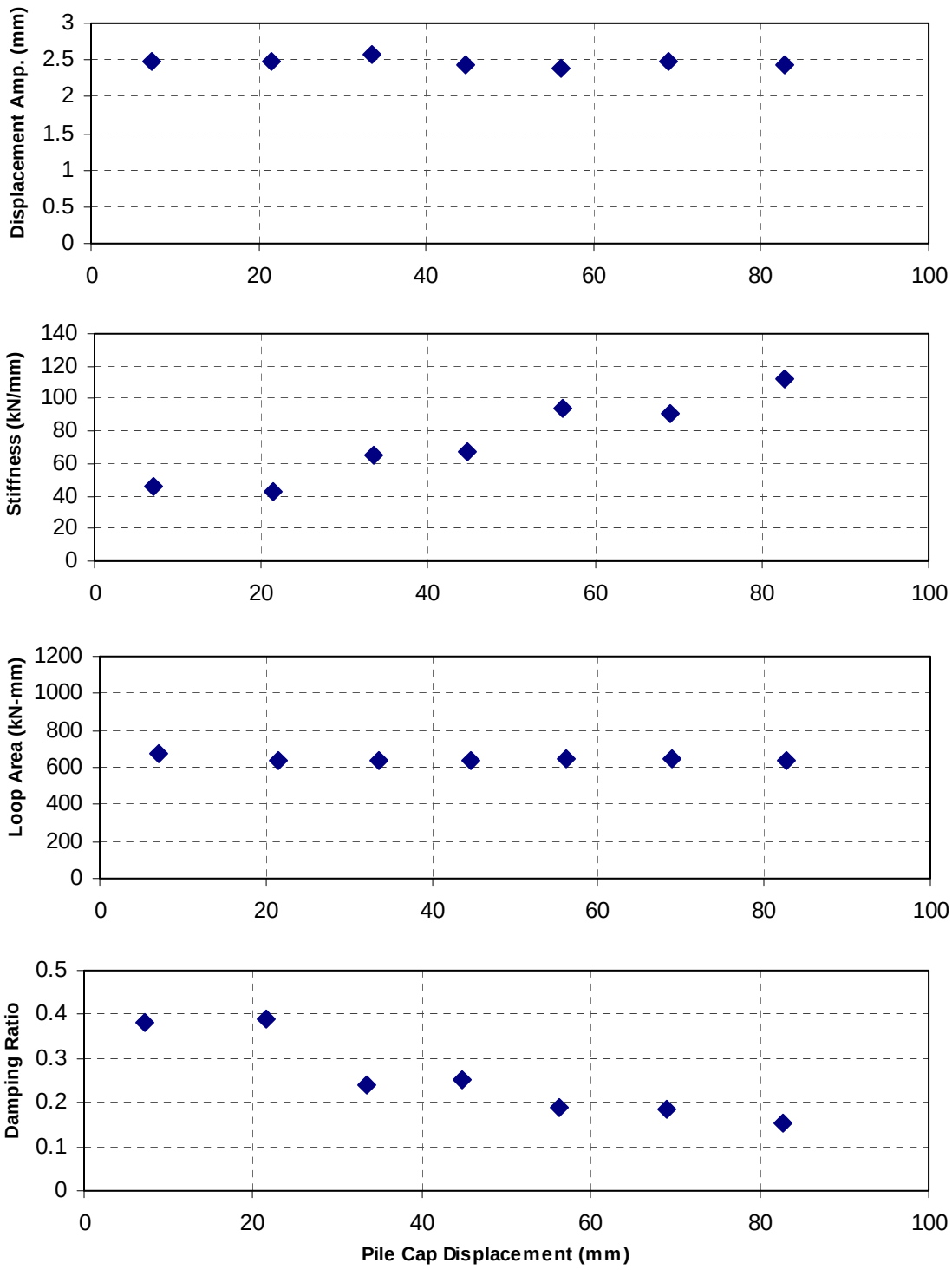

Figure 5-3 Summary of response to cyclic actuator loadings for pile cap without backfill (baseline test)

present, these properties will also depend on the displacement amplitude; thus, in the right column, these parameters are shown in terms of loop displacement amplitude. The data appear to suggest that both frequency and displacement amplitude must be considered when interpreting test results. The pile cap displacement levels shown in the figures correspond to cases in which the dynamic shaker cycles were applied before the actuator cycles.

The peaks in the normalized amplitude graph occur at the damped natural frequency of the system, which appears to increase with increasing pile cap static displacement level. This is consistent with the increasing stiffness with displacement level as also shown on the graph. The damped natural frequency of the pile cap appears to range from 5 to 6.5 Hz and stiffness generally ranges from between 100 and 200 kN/mm. The calculated damping ratios vary widely with both frequency and displacement amplitude, in a general range from 5 to 30% at intermediate frequencies and displacement levels. The variations in stiffness and damping with frequency are likely due to variations in phase between passive earth forces (whether acting on the piles or on the pile cap itself) and the inertial force from the foundation as suggested by Tokimatsu et al. (2004) in their work with large shaking table models of pile cap foundation systems. Some variation is also likely due to the simple lumped, constant, mass model used. Damping ratios increase to a range from about 35% to approximately 50% at higher frequencies and displacements. Using the half-power bandwidth approach to interpret the normalized displacement amplitudes yields damping ratios of 18, 17 and 8% for the three pile cap displacement levels shown in Figure 5-4.

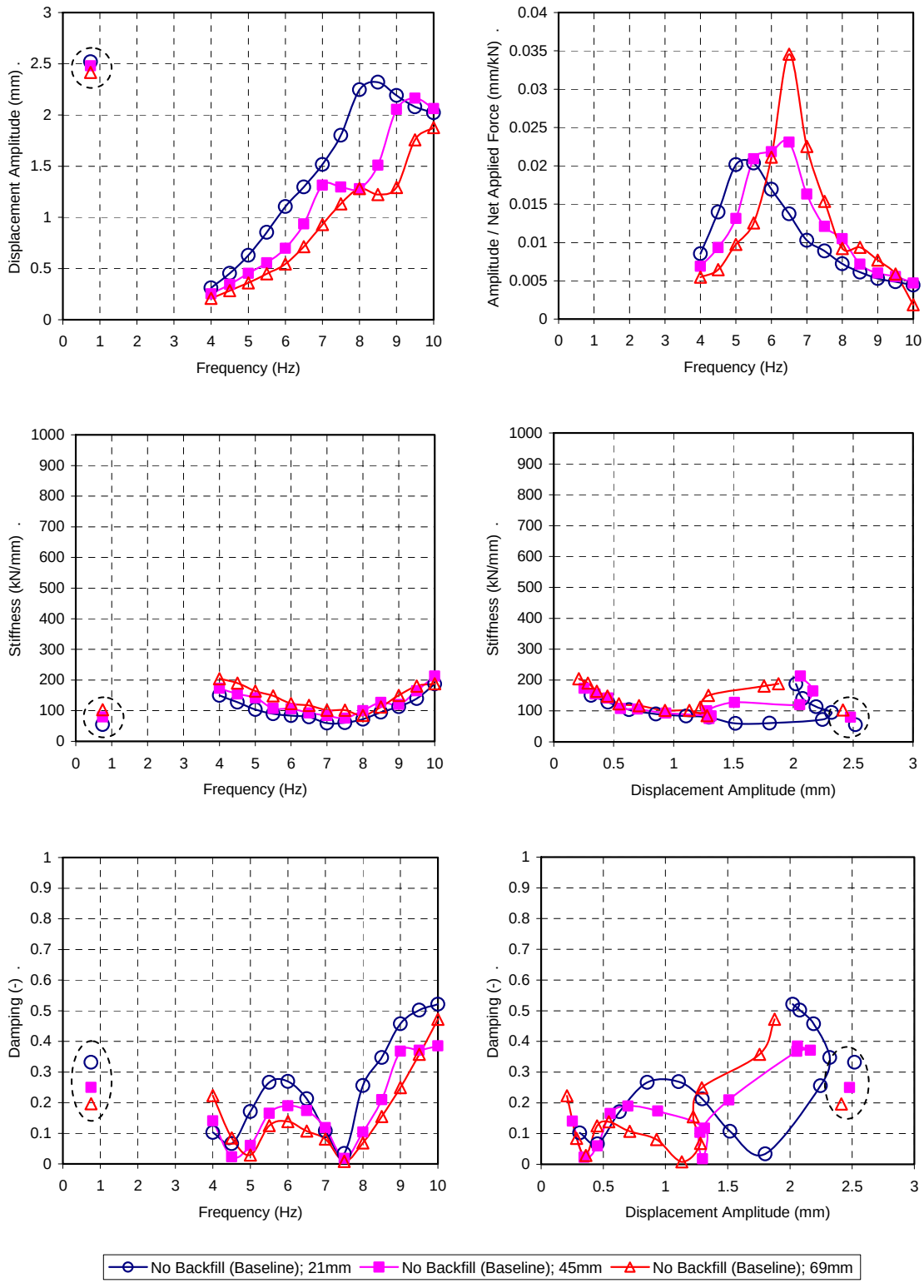

Figure 5-4 Summary of response to dynamic shaker loadings for pile cap without backfill (baseline condition)

6 Pile Cap with Densely Compacted Fine Gravel

6.1 General

The pile cap with densely compacted fine gravel backfill was tested on June 11, 2007. Table 6-1 summarizes the test in terms of loads and displacements measured at the end of each "static push" with the actuators. The table also indicates the order in which actuator-driven cyclic loads and shaker-based dynamic loads were applied. At certain displacement increments, cyclic and dynamic loadings were not applied in order to help assure that the test foundation displaced sufficiently into the backfill for the load path to return to the static-backbone loading curve. No significant deviations from the general test procedure occurred during this test.

6.2 Load-Displacement Response

Figure 6-1 shows the entire actuator load verses pile cap displacement relationship for the test, with static pushes, actuator cycles and shaker cycles being represented by green, blue, and red data points, respectively. Section 4.2 provides some discussion relative to the interpretation of this data.

Figure 6-2 shows three load-displacement response curves for the pile cap: one for the response with the backfill in place (the "total" response, which is the equivalent

Table 6-1 Summary of test with densely compacted fine gravel backfill

Displacement Interval	Displacement (mm)	Actuator Load (kN)	Actuator Cycles	Shaker Cycles
1	5.4	922	First	Second
2	13	1295	Second	First
3	19	1655	None	None
4	24	2047	First	Second
5	30	2208	None	None
6	35	2643	Second	First
7	41	2897	None	None
8	47	3299	First	Second
9	54	3569	None	None
10	61	3978	Second	First
11	68	4144	None	None
12	74	4445	First	Second
13	81	4571	None	None
14	87	4848	None	None

monotonic response, or "backbone" curve, derived from the data shown in Figure 6-1); one for the response with no backfill present (the "baseline" response); and one for the passive earth response of the backfill (obtained by subtracting the baseline response from the total response).

The curves show that total response and baseline response increase at different rates until approximately 62 mm of displacement. By this point, the backfill response levels off as the baseline and total responses increase at a similar rate. This leveling off is interpreted as the point when the backfill material is at failure. Hence, the ultimate passive resistance of the backfill, approximately 2860 kN, is developed at a cap displacement of about 62 mm, which corresponds to a displacement to wall height ratio (Δ_{max}/H) of about 0.037, which is well within the range of typical values for soil.

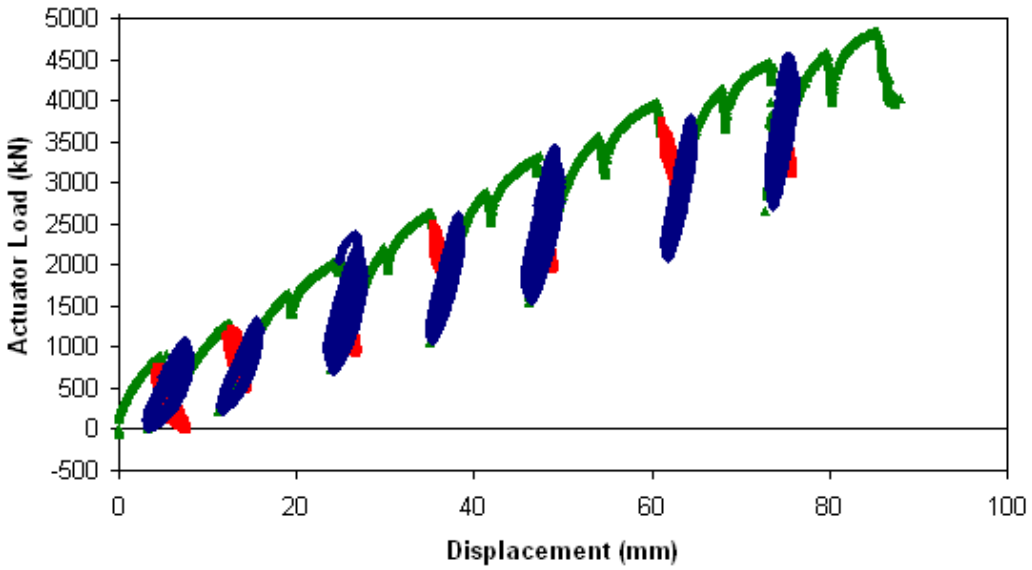

Figure 6-1 Actuator load versus pile cap displacement with densely compacted fine gravel backfill (Test 8; June 11, 2007)

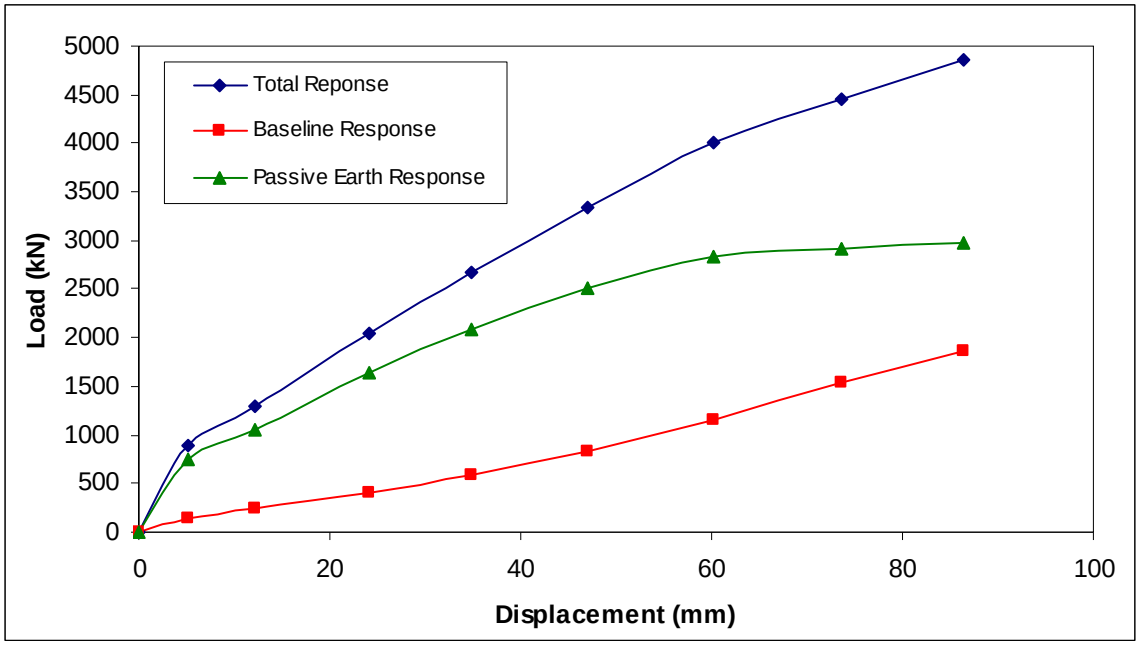

Figure 6-2 Total, baseline, and passive earth responses for pile cap with densely compacted fine gravel backfill

6.3 Calculated Passive Earth Force

Commonly used methods for calculating passive earth pressure include Rankine theory, Coulomb theory, and log-spiral theory. Log-spiral theory is typically considered the most accurate of these methods (see, for example, Cole and Rollins (2006) and Duncan and Mokwa (2001)). Three methods of estimating the development of passive pressure with wall displacement are evaluated in this section. Two of these methods, PYCAP and ABUTMENT (LSH method) involve applications of log-spiral theory and a hyperbolic load-displacement relationship. The third approach evaluated in this section is an empirical load-displacement relationship based on full-scale testing of an abutment with typical backfill conditions (see discussion of CALTRANS method in Section 4.3.3).

6.3.1 Calculated Response Using PYCAP

Passive earth resistance was calculated using the modified PYCAP spreadsheet introduced in Section 4.3.1. Table 6-2 summarizes key inputs and outputs for several cases while Figure 6-3 compares the measured passive earth response to the computed passive resistance curves from each case. The parameters in Case I are based on laboratory-determined ultimate values for shear strength, interface friction angle (which was similar for both peak and ultimate strength states, with a laboratory-derived δ/ϕ ratio of about 0.61) and initial modulus. The initial modulus (32100 kPa) used in PYCAP analysis for densely compacted fine gravel was derived from a constrained consolidation test, as well as for all of the cases, corresponds with the "preloaded or compacted" range for dense sands and gravels recommended by Duncan and Mokwa (2001). For Case I, the calculated load-displacement curve vastly overestimates the measured response. The

Table 6-2 Parameter summary for case comparison in PYCAP for densely compacted fine gravel backfill

Parameter	Case I	Case II	Case III	Case IV
ϕ (°)	50.0	50.0	50.0	44.0
c (kPa)	13.2	0	13.2	4.0
δ (°)	31	31	8	27
γ_m (kN/m^3)	21.7	21.7	21.7	21.7
E (kPa)	32100	32100	32100	32100
ν	0.3	0.3	0.3	0.3
k (kN/mm)	190	190	190	190
Δ_{max} (mm)	62	62	62	62
Δ_{max}/H	0.037	0.037	0.037	0.037
R_f	0.30	0.48	0.76	0.75
R_{3D}	2.00	2.00	1.72	1.95
K_p	35.7	35.6	11.2	17.0

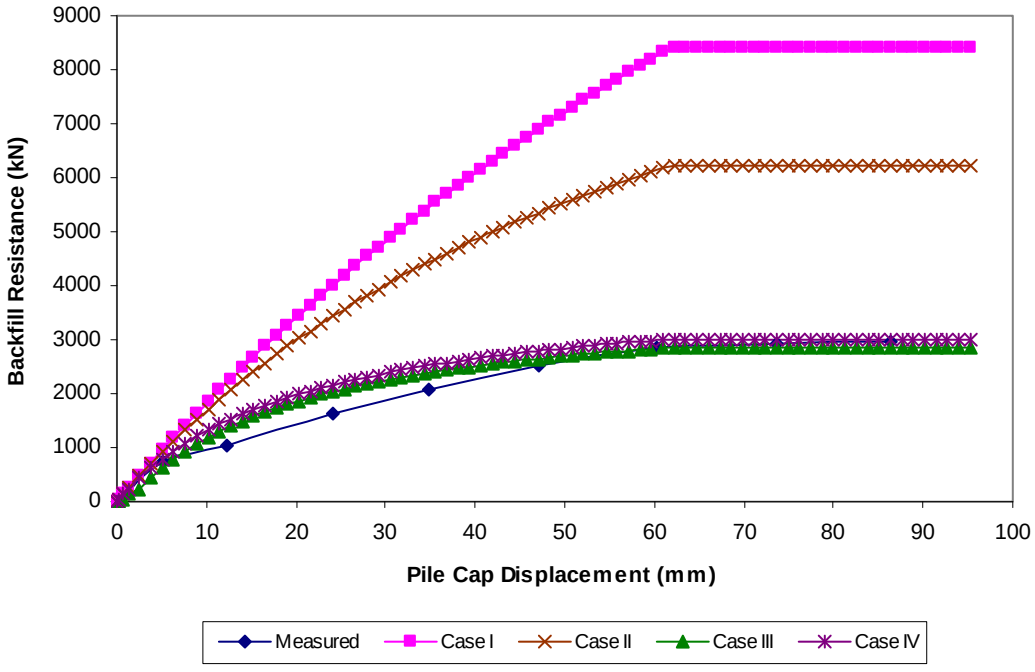

Figure 6-3 PYCAP case comparison for densely compacted fine gravel backfill

parameters in Case II are similar to Case I, but cohesion has been neglected. The resulting load-displacement curve is closer to, but still over 100% more than, the measured resistance. In Case III, the interface friction angle has been iteratively reduced to obtain a good match between the calculated and measured load-displacement curves. The friction angle in Case IV is based on an in-situ direct shear test staged using a single sample over three normal pressures. The cohesion intercept from the in-situ test, 19.7 kPa, has been reduced to a nominal value of 4 kPa, and the δ/ϕ ratio is the same laboratory-based value used in Cases I and II. The resulting curve for Case IV provides the best match with the measured resistance curve.

6.3.2 Calculated Response Using ABUTMENT (LSH)

The LSH method was also used to compute the passive earth resistance. Table 6-3 summarizes key input and output parameters for several cases while Figure 6-4 displays the measured and calculated passive resistance curves for each of the analyzed cases. As in the PYCAP analysis, Case I is based strictly on laboratory-determined ultimate values for shear strength and interface friction angle (which was similar for both peak and ultimate strength states, with a δ/ϕ ratio of about 0.61). The ε_{50} value was determined from simple lab tests and is within the range of values recommended in Shamsabadi et al. (2007). Similar to PYCAP, the calculated load-displacement curve from Case I parameters greatly overestimates the measured curve. The changes made in Cases II and III are the same changes made to the corresponding cases in the PYCAP analysis. If cohesion is included, the interface friction angle must be greatly reduced to obtain a good match. Case IV uses the results of an in-situ direct shear test staged using

Table 6-3 Summary of LSH parameters for densely compacted fine gravel backfill

Parameter	Case I	Case II	Case III	Case IV
ϕ (°)	50.0	50.0	50.0	44.0
c (kPa)	13.2	0	13.2	4.0
δ (°)	31	31	8	27
γ_m (kN/m^3)	21.7	21.7	21.7	21.7
ε_{50}	0.004	0.004	0.004	0.004
ν	0.3	0.3	0.3	0.3
R_f	0.98	0.98	0.98	0.98
R_{3D}	2.00	2.00	1.72	1.95
K_{ph}	36.3	25.0	17.7	16.0

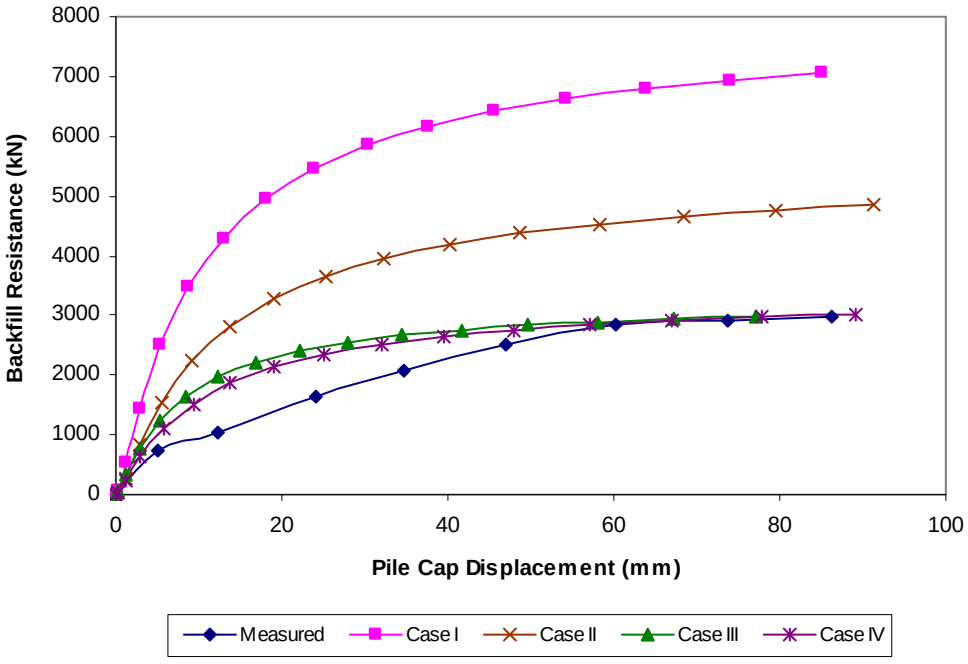

Figure 6-4 Comparison of measured and LSH-based calculated passive resistance for densely compacted fine gravel backfill

one sample over three normal pressures for the friction angle. In this case, the apparent cohesion from that test has been reduced to a nominal value of 4.0 kPa. This is the value used by Shamsabadi et al. (2007) in their analyses of the Cole and Rollins (2006) tests with a similar backfill material. The resulting curve for Case IV provides a good match with the measured curve. While Case III provides the best match with the measured curve (since the interface friction angle was iteratively determined to obtain such a match), the parameters represented by Case IV provide the most reasonable description of the measured load-displacement curve. In all cases, the calculated resistance in the middle portion of the load-displacement curves is significantly higher than the measured resistance.

6.3.3 Calculated Response Using CALTRANS

Passive earth resistance based on the CALTRANS method is shown in Figure 6-5. In the case of densely compacted fine gravel, the method under-predicts peak passive resistance by approximately 50%.

6.4 Response to Cyclic Actuator Loading

After slowly pushing the pile cap to each target displacement, alternating combinations of cyclic actuator loads and dynamic shaker loads were applied to the test foundation. The response of the pile cap to the small displacement amplitude loading cycles from the actuator is presented and discussed in this section. Figure 6-6 shows the loop displacement amplitude, stiffness, loop area, and damping ratio for the pile cap with densely compacted fine gravel backfill as a function of pile cap displacement. Values are

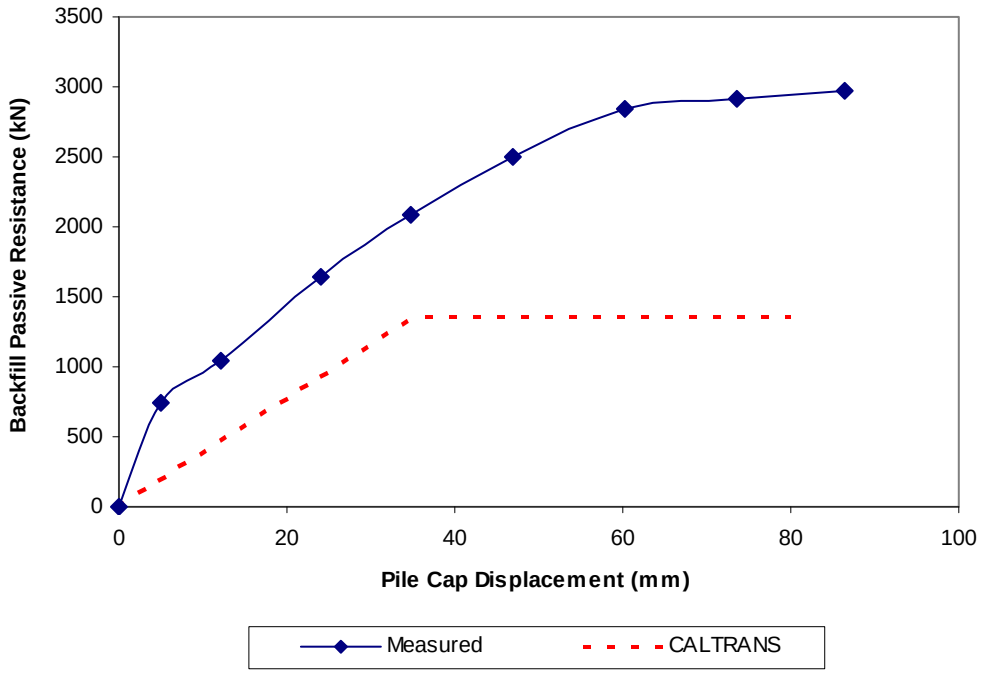

Figure 6-5 Comparison of measured and CALTRANS-based passive resistance for densely compacted fine gravel backfill

based on the median of the 15 low frequency cycles performed at each displacement level. Loop displacement amplitude decreases fairly linearly from just under 2.5 mm to about 1.25 mm as the pile cap displacement into the backfill increases. The stiffness increases from 200 to 500 kN/mm with increasing cap displacement; this appears to be due to greater mobilization of the backfill soil's passive strength and pile stiffness. The rate of stiffness increase for densely compacted fine gravel appears to continue rising in the last few displacement intervals when the ultimate passive resistance of the soil is assumed to be reached, which may indicate that passive resistance is still mobilizing. The loop area remains fairly constant around 1200 kN-mm. The damping ratio exhibits some of the saw-tooth behavior seen in other tests due to the alternating order of the static

and dynamic cyclic loading phases, remaining around 20% throughout testing until the last two static pushes, when it drops to about 15%.

6.5 Response to Dynamic Shaker Loading

After slowly pushing the pile cap to each target displacement, alternating combinations of small displacement cyclic actuator loads and dynamic shaker loads were applied to the test foundation. The response of the pile cap to the small displacement dynamic shaker loading is presented and discussed in this section. The first row of graphs in Figure 6-7 shows loop displacement amplitude as well as loop displacement amplitude normalized by the cyclic amplitude of net applied force from the shaker and actuators as functions of the forcing frequency. The second and third rows of graphs show the calculated reloading stiffness and damping, respectively, of the pile cap system. These parameters are presented in terms of forcing frequency in the left column. If non-linear behavior is present, these properties will also depend on the displacement amplitude; hence, in the right column, these parameters are shown in terms of the displacement amplitude. The data appear to suggest that both frequency and displacement amplitude must be considered when interpreting test results. The individual line series shown in the graphs represent different static pile cap displacement levels in which dynamic shaker cycles were applied before the low frequency actuator cycles.

The peaks in the normalized displacement amplitude graph correspond to the damped natural frequency, which increases from about 7.5 to 8 Hz with increasing cap displacement. Dynamic stiffness ranges from slightly under 400 to almost 1000 kN/mm as a function of frequency, peaking about 2 Hz before the damped natural frequency, then

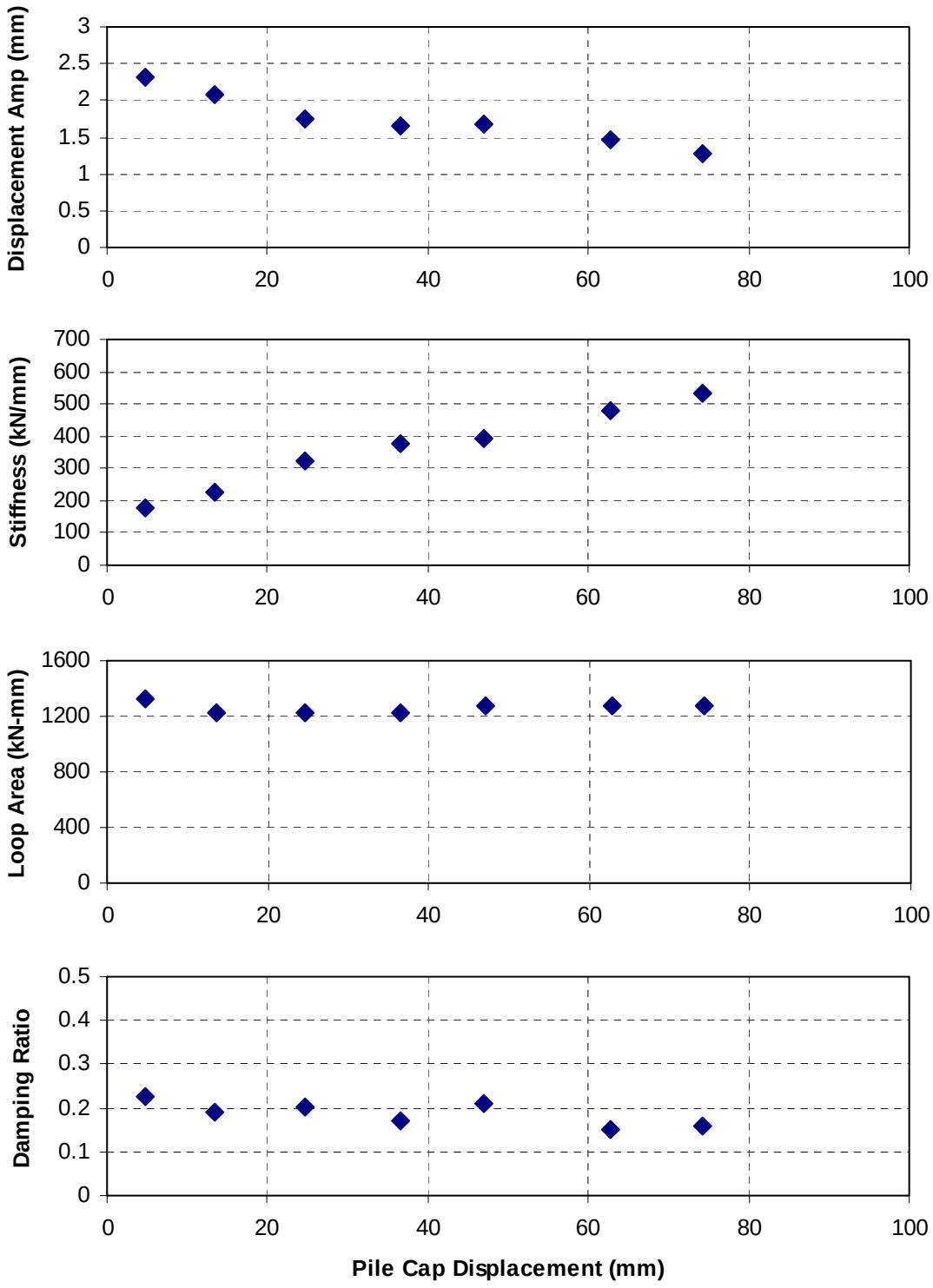

Figure 6-6 Summary of response to cyclic actuator loadings for pile cap with densely compacted fine gravel backfill

decreasing, and then increasing again about 1 Hz after the damped natural frequency. The stiffness generally increases with increasing pile cap displacement until a shaker frequency and loop displacement amplitudes of about 8.5 Hz and 0.5 mm, respectively, where the trend reverses.

Calculated damping values vary greatly with respect to forcing frequency and displacement amplitude. The minimum damping appears to be less than 5% at about 5.5 Hz and 10 Hz (at least for the 13 mm displacement interval), and about 0.25 and 1 mm of displacement amplitude, respectively. At frequencies between 5.5 and 10 Hz and displacement amplitudes between 0.25 and 1 mm, the damping ratio increases up to about 45% (corresponding with the calculated decreasing stiffness) until dropping again at about 8.5 Hz. Unfortunately, the normalized displacement amplitudes were such that the half-power bandwidth approach could not be used. As stated previously in Section 5.4, the observed variations in stiffness and damping with frequency are likely due to variations in phase between passive earth forces (whether acting on the piles or on the pile cap itself) and the inertial force from the foundation as suggested by Tokimatsu et al. (2004) in their work with large shaking table models of pile cap foundation systems. Some variation is also likely due to the simple lumped, constant, mass model used.

6.6 Comparison of Cyclic Actuator Loading and Dynamic Shaker Responses

Figure 6-7 includes displacement amplitude, stiffness, and damping ratios from the actuator-driven cycles (~ ¾ Hz) at the displacement levels given for the shaker-derived values (points in dashed ovals). The actuator-based values shown are averaged from actuator cycles run at previous and subsequent pile cap displacement levels. These

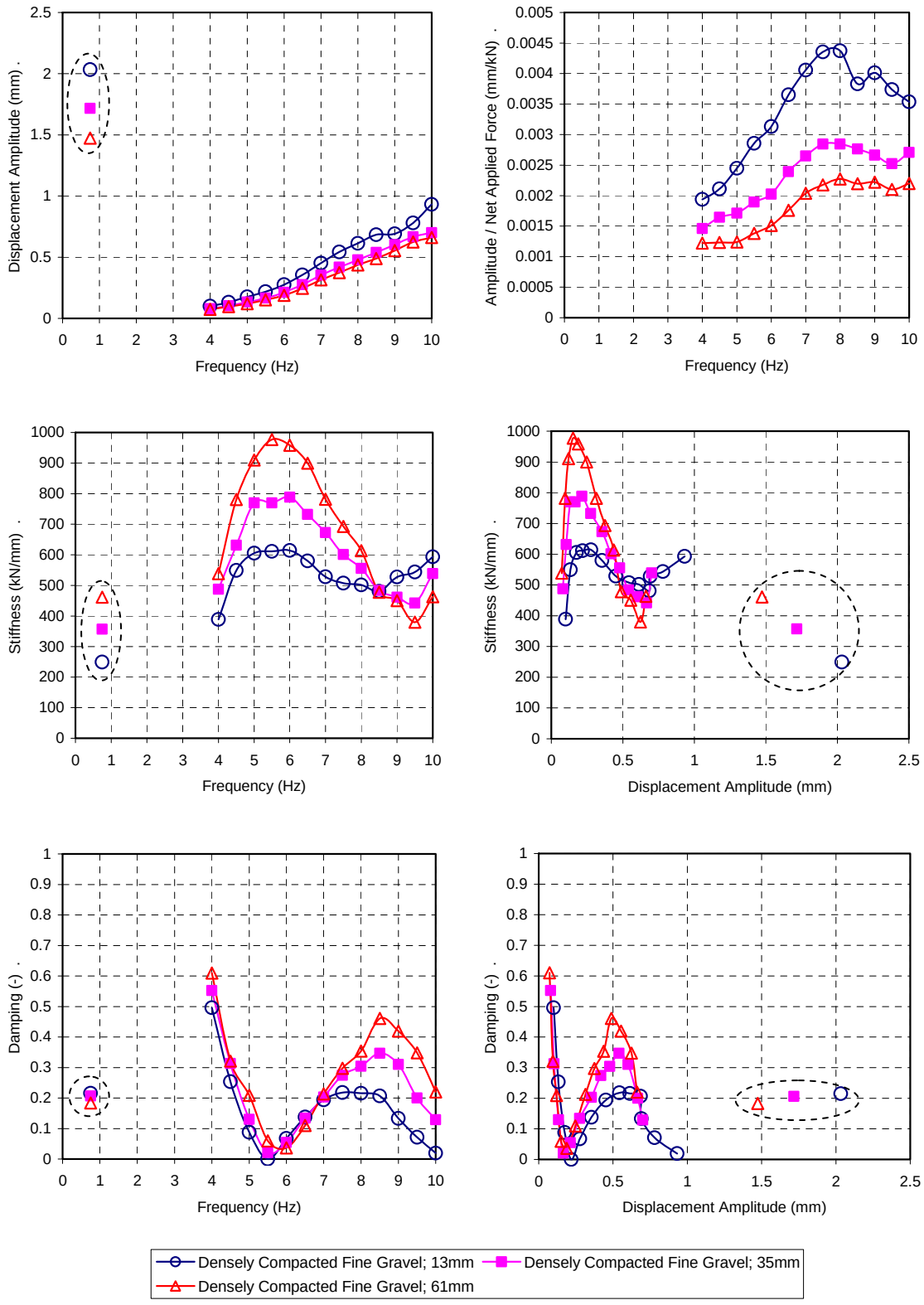

Figure 6-7 Summary of response to dynamic shaker loadings for pile cap with densely compacted fine gravel backfill

averages represent stiffness and damping values that would have been calculated if the actuator cycles had been performed before the shaker cycles. It is difficult to compare the static and dynamic methods in terms of frequency because of the difference in the associated displacement amplitudes (the shaker cannot generate large forces, and hence displacements, at low frequencies).

The largest displacement amplitudes reached by the dynamic shaker loadings were typically 0.75 mm or less. The average displacement amplitude reached by the cyclic actuator loadings was between 1.5 and 2 mm. This disparity is large enough to make comparison between the two methods problematic, except at the highest dynamic loading frequencies. On average, the stiffness under the shaker-based dynamic loading appears to be about 30% higher than the stiffness under the actuator-driven cyclic loading conditions. The equivalent damping ratio under cyclic loading conditions (about 20%) is well within the damping range observed under dynamic loading conditions.

6.7 Passive Earth Pressure Distributions

A vertical array of six earth pressure cells evenly distributed in the central portion of the pile cap face was used to make direct measurements of passive earth pressure from the backfill soil. These measurements were made in addition to the load-displacement response data from the actuators. Figure 6-8 shows the pressure measured by the pressure cells with depth at the end of each static push interval.

The pressure cells show the expected general trends of increasing pressure with depth and increasing magnitude with increasing cap displacement. A departure from the typical representation of increasing pressure with depth is apparent for the pressures

measured at the 0.42 m and 1.26 m pressure cells. These cells record an increase in pressure with increasing cap displacement but show a decrease in pressure relative to the cell immediately above them. In the last three static pushes, the pressure cell at 0.98 m appears to start to manifest similar behavior as the pressure cells at 0.42 m and 1.26 m; however, since the behavior develops at the end of the test, rather than occurring throughout, it is unlikely that the same mechanism is at play. A precise explanation for this behavior is not readily available, but it may be due to variability of density with lift thickness during compaction. The bottom-most pressure cell appears to offer progressively smaller increases in pressure as the cap displacement increases, resulting in an apparently negligible increase in pressure during the final static push. This appears to be consistent with the concept of the backfilling approaching its ultimate capacity.

Figure 6-9 shows the backfill force calculated by multiplying each measured pressure by the corresponding contributory areas of the pile cap face. In general, the resulting force-displacement curve has a similar trend to the actuator-based curve, but it is systematically lower. Applying a multiplier of 1.67 (the inverse of 0.6 determined in Section 4.5) to the cell-based curve improves the match with the actuator-based curve, although the mobilization of ultimate passive resistance is not apparent.

6.8 Cracking and Vertical Movement of Backfill

Figure 6-10 is a two part plot showing the effect of static and dynamic testing on the surface of the densely compacted fine gravel backfill area. The first part of the figure is a map of the surface cracks that developed during each static push of the pile cap. The surface cracks in the backfill indicate that failure surfaces are present within the soil.

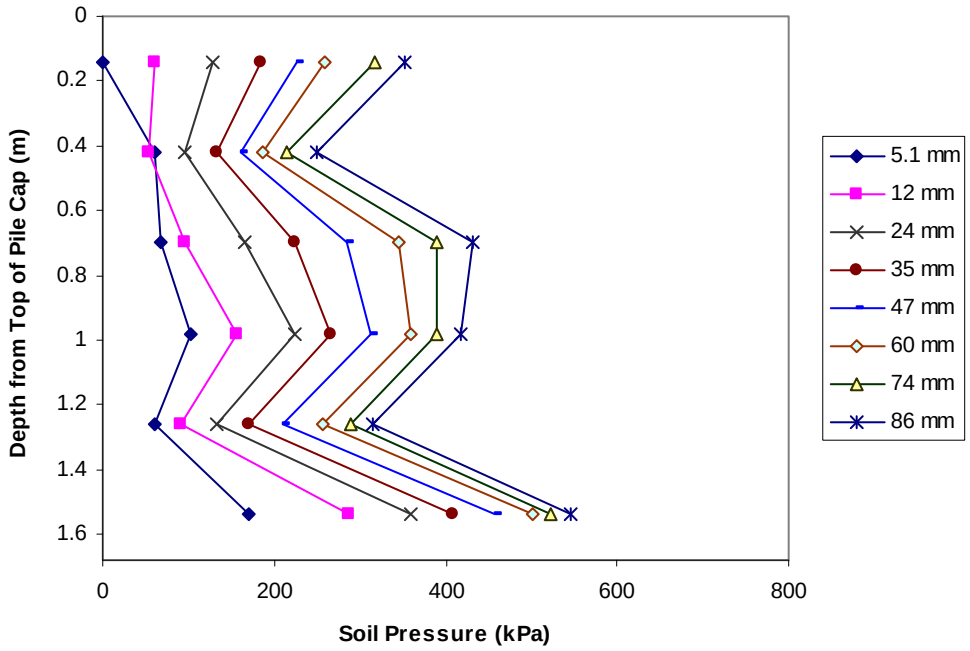

Figure 6-8 Earth pressure distribution as a function of pile cap displacement with densely compacted fine gravel backfill

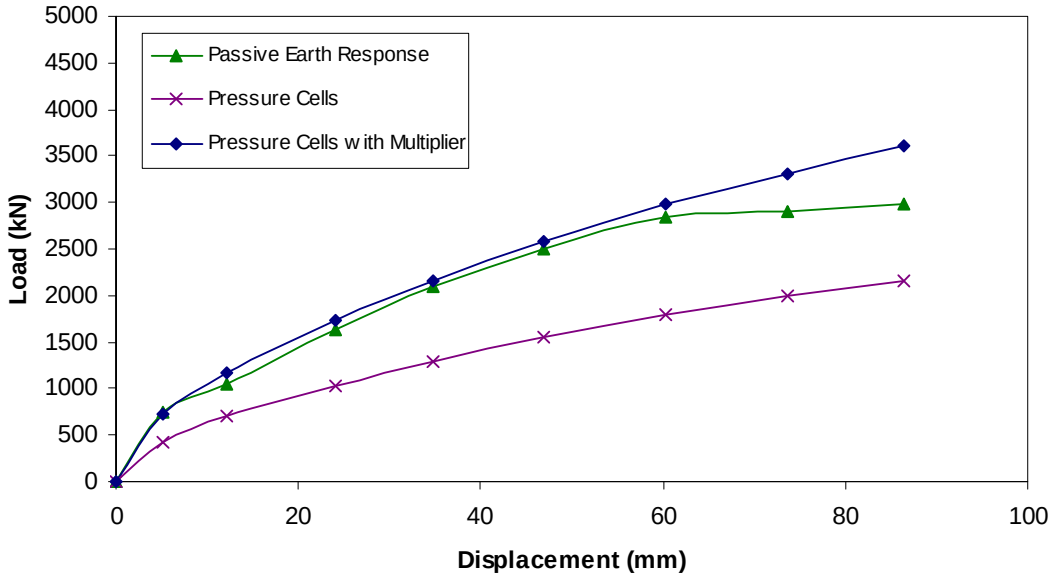

Figure 6-9 Comparison of earth forces based on actuators and pressure cells for densely compacted fine gravel backfill

The fine gravel material has some apparent cohesion (manifest by the stability of the backfill face when excavated), which helps in the identification of backfill cracking. Several of the cracks are concentrated around the edges of the cap face. These cracks are due to the internal shear stresses radiating out from the cap face and are consistent with a three dimensional shape of the failure zone. A horizontal group of cracks located 3 to 4 m from the center of the pile cap face may indicate the where early failure surfaces developed and began to daylight. The cracks extending without a particular pattern from the face of the cap out to about 3 m may be associated with near surface heave effects and/or horizontal shoving of the surface rather than larger-scale shear failure.

The second part of the figure is a contour map of the change in elevation along the surface of the backfill area during testing. The typical elevation change, as represented by the median elevation change in a given row (parallel to the face of the cap) of grid nodes, is about 30 mm at 1.83 m from the pile cap face. The contour map shows that at 3.05 m the maximum elevation change at one individual survey node is over 60 mm. Calculations in PYCAP indicate that a log-spiral failure surface should daylight at approximately 6.1 m from the face of the cap. As can be seen in the figure, most of the elevation change occurred within the first 6 m of backfill; hence, it is reasonable to expect that the failure surface daylights in the vicinity of the PYCAP analysis prediction.

The correlation between the backfill heave and the log-spiral failure surface is illustrated in Figure 6-11, where the failure surface calculated in the spreadsheet program PYCAP daylights close to where the heave profile becomes negligible. The log-spiral failure surface shown in the figure was computed using the best-fit parameters discussed in Section 6.3.1: a soil friction angle of 44° with a nominal cohesion of 4 kPa and an

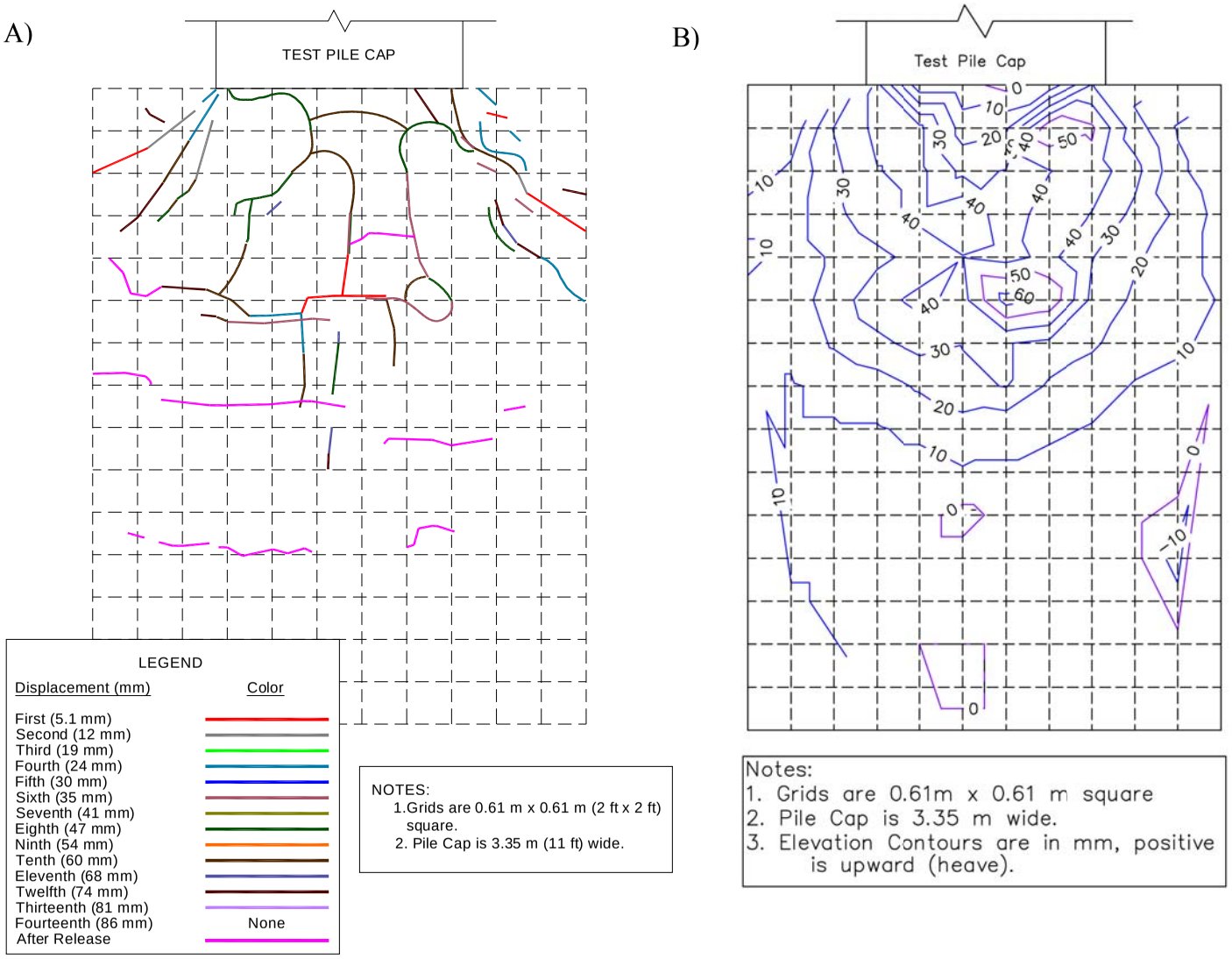

Figure 6-10 Crack pattern (A) and heave contour (B) maps for densely compacted fine gravel backfill

interface friction angle of 27°, corresponding to a δ/ϕ ratio of 0.6 as determined from laboratory direct shear testing (i.e., Case IV). The heave profile in the figure is magnified ten times to make the elevation change more appreciable.

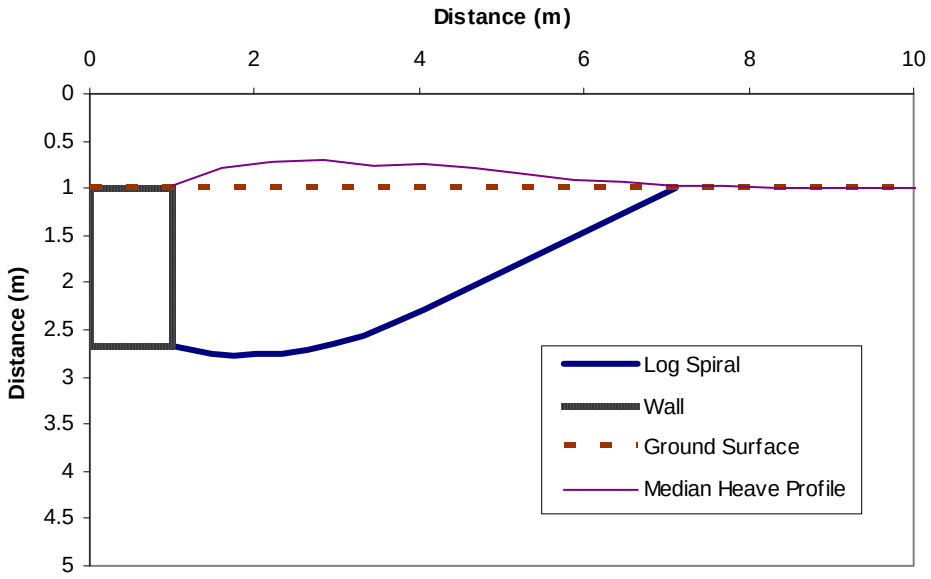

Figure 6-11 Heave profile with best-fit log-spiral failure surface from PYCAP for densely compacted fine gravel backfill

6.9 Horizontal Movement of Backfill

String potentiometers were used to measure movement in the backfill. Figure 6-12 shows the movement of each of the monitoring points in the densely compacted fine gravel backfill compared to the movement of the pile cap face. The backfill displacement ranges from 87 mm (100% of cap displacement) at the cap face to 9 mm (11% of cap displacement) at 5.5 m from the cap face. This translational movement represents the

amount of the pile cap displacement not absorbed through compressive strain up to the monitoring point.

Figure 6-13 shows the compressive strain corresponding to each static push of the pile cap. The compressive strain ranges from 0.028 to 0.003 within the backfill zone. The strain distribution is high at the cap face, as expected, but the highest strain occurs at about 3 m from the cap face. This high strain level located in the middle of the backfill area may be associated with the development of progressive slip planes as soil friction is mobilized, but the exact mechanism is unclear. A simple explanation for the erratic strain behavior in the figure is not readily available; however, some of the variation from interval to interval may indicate the potential sensitivity of the string potentiometer measurements to differential pushing of the pile cap (not all the monitoring stakes were on the same end of the cap face) and tipping of the monitoring stakes themselves. Movement of the stakes could explain the presence of some negative strain amounts in the calculations. However, it does appear that stresses are transmitted some significant distance throughout this well compacted backfill.

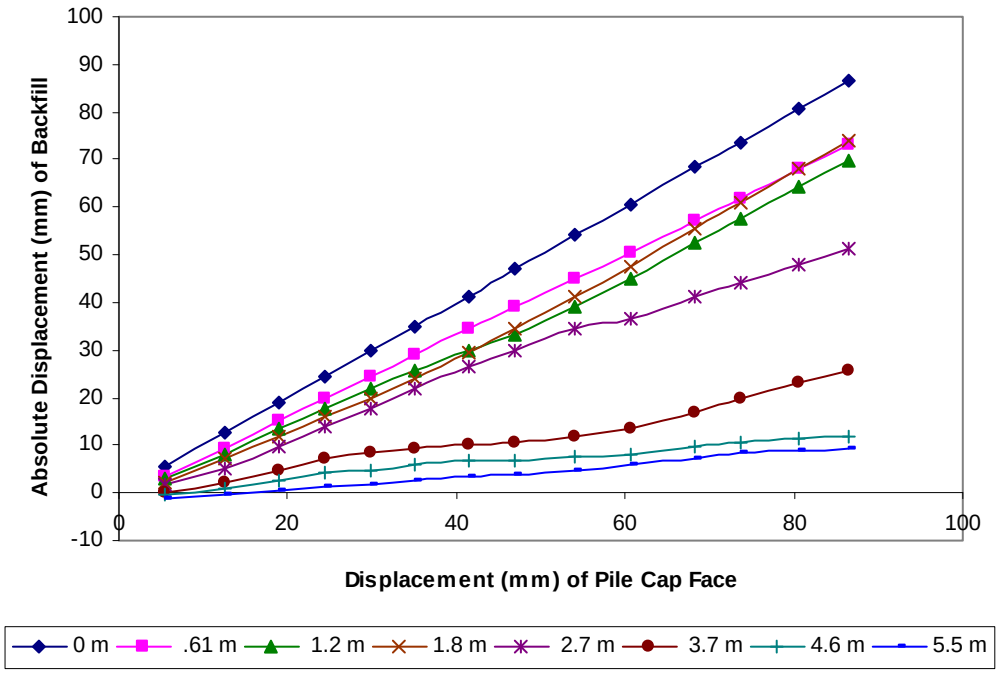

Figure 6-12 Displacement of monitoring points in densely compacted fine gravel backfill

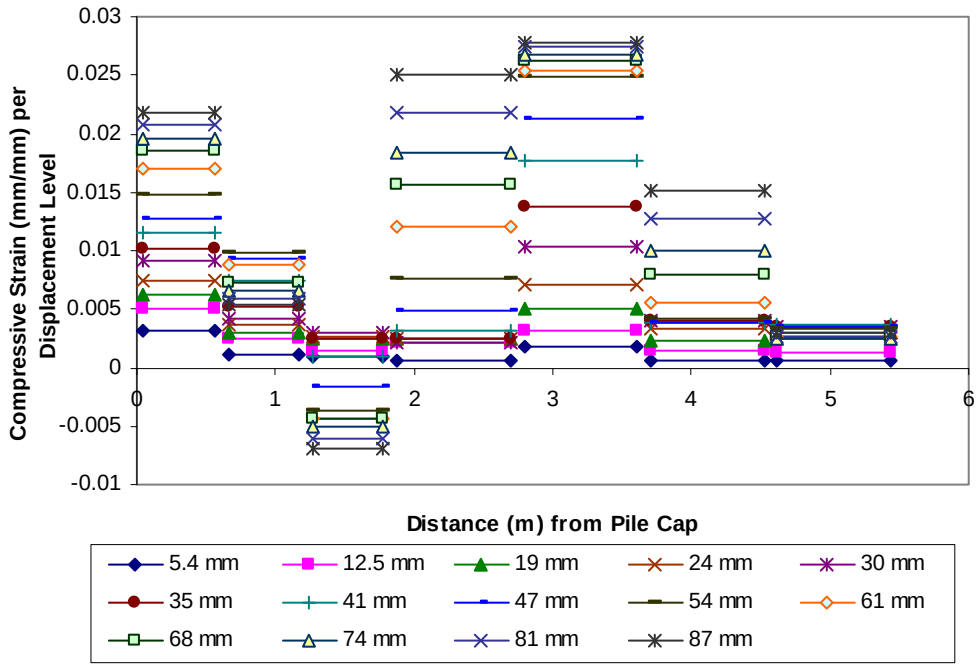

Figure 6-13 Strain per displacement level for densely compacted fine gravel backfill

7 Pile Cap with Loosely Compacted Fine Gravel

7.1 General

The pile cap with loosely compacted fine gravel backfill was tested on June 6, 2007. Table 7-1 summarizes the test in terms of loads and displacements measured at the end of each "static push" with the actuators. The table also indicates the order in which actuator-driven cyclic loads and shaker-based dynamic loads were applied. At some displacement increments, cyclic and dynamic loadings were not applied in order to help assure that the test foundation displaced sufficiently into the backfill for the load path to return to the static-backbone loading curve. No significant deviations from the general test procedure occurred during this test.

Table 7-1 Summary of test with loosely compacted fine gravel backfill

Displacement Interval	Displacement (mm)	Actuator Load (kN)	Actuator Cycles	Shaker Cycles
1	6.3	531	First	Second
2	17	546	Second	First
3	24	636	First	Second
4	30	713	None	None
5	35	997	Second	First
6	42	1127	None	None
7	49	1461	First	Second
8	56	1595	None	None
9	62	1926	Second	First
10	69	2066	None	None
11	75	2388	First	Second

7.2 Load-Displacement Response

Figure 7-1 shows the entire actuator load verses pile cap displacement relationship for the test with loosely compacted fine gravel backfill. Static pushes, actuator cycles, and shaker cycles are represented by green, blue, and red data points, respectively. Section 4.2 provides some discussion relative to the interpretation of this data. As shown in Figure 7-1, and made clearer in Figure 7-2, the loosely compacted fine gravel test exhibits a sizeable loss of resistance after the cyclic and dynamic loadings which accompanied the first two displacement intervals.

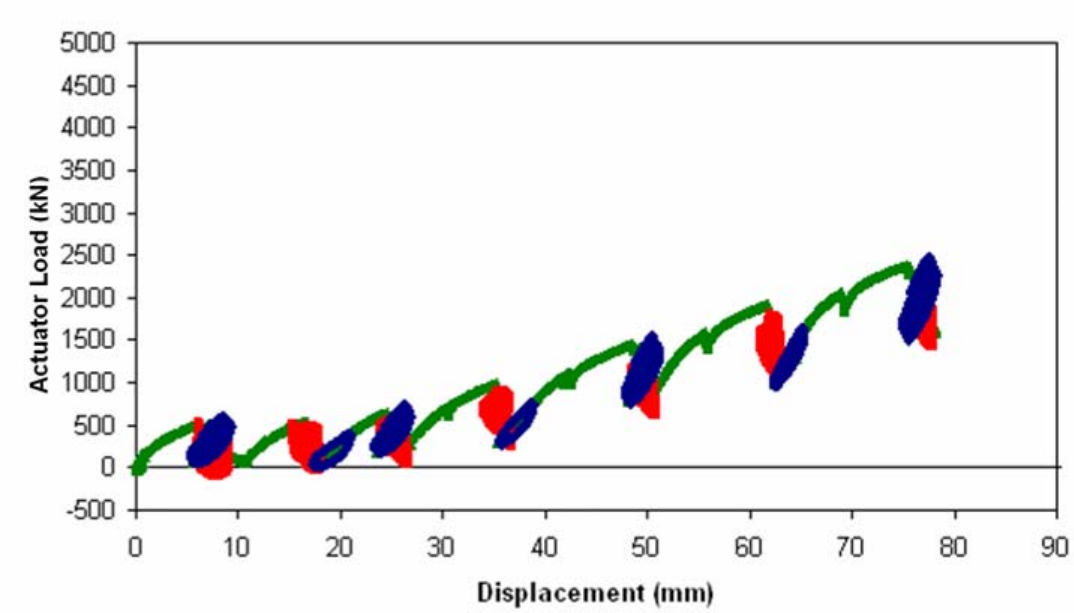

Figure 7-1 Actuator load versus pile cap displacement with loosely compacted fine gravel backfill (Test 7; June 6, 2007)

Figure 7-2 shows three load-displacement response curves for the pile cap: one for the response with backfill in place (the "total" response, which is the equivalent monotonic response, or "backbone" curve, derived from the data shown in Figure 7-1); one for the response with no backfill present (the "baseline" response); and one showing

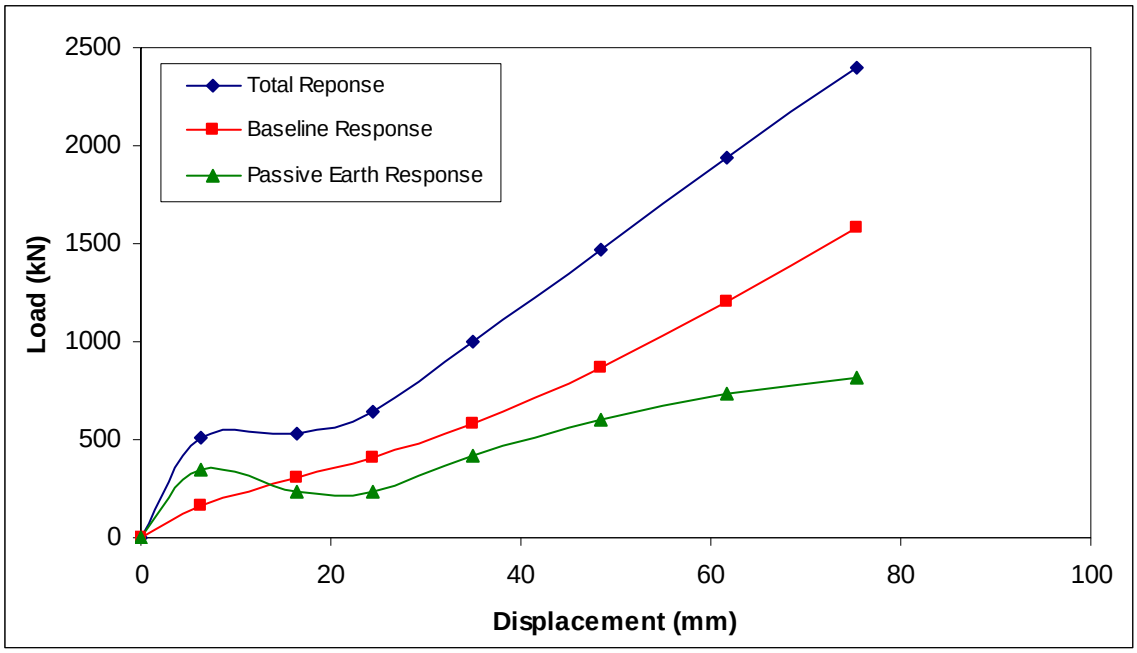

Figure 7-2 Total, baseline and passive earth responses for the pile cap with loosely compacted fine gravel backfill

the passive earth response of the backfill (obtained by subtracting the baseline response from the total response). After the initial push, the loosely compacted fine gravel backfill provides slightly less additional resistance than the resistance initially provided by the piles and cap acting by themselves, as shown in the figure. The test does not appear to mobilize a peak resistance by the conclusion of testing. This may be consistent with the observation by Clough and Duncan (1991) that a loose or medium dense material will require two to four times more displacement to fully mobilize passive resistance than a dense material. The maximum passive earth resistance from this test, which was about 820 kN, was recorded at the end of the final static push. The backfill resistance may have continued to increase if the pile cap had been pushed to greater displacement levels. The figure shows that a significant amount of resistance has developed by 6 mm of displacement, after which the backfill appears to lose passive earth resistance and then

recover it as the pile cap displacement increases. This unexpected behavior may be due to the effects of cyclic and dynamic loadings, or possibly to a small error in the baseline response. These effects are magnified by the relatively small passive resistance of the backfill at the displacement interval in question.

7.3 Calculated Passive Earth Force

Commonly used methods for calculating passive earth pressure include Rankine theory, Coulomb theory, and log-spiral theory. Log-spiral theory is typically considered the most accurate of these methods (see, for example, Cole and Rollins (2006) and Duncan and Mokwa (2001)). Three methods of estimating the development of passive pressure with wall displacement are evaluated in this section. Two of these methods, PYCAP and ABUTMENT (LSH method) involve applications of log-spiral theory and a hyperbolic load-displacement relationship. The third approach evaluated in this section is an empirical load-displacement relationship based on full-scale testing of an abutment with typical backfill conditions (see discussion of CALTRANS method in Section 4.3.3).

7.3.1 Calculated Response Using PYCAP

Passive earth resistance was calculated using the modified PYCAP spreadsheet introduced in Section 4.3.1. Table 7-2 summarizes key inputs and outputs for several cases analyzed while Figure 7-3 compares the measured passive earth response to the computed passive resistance curves from each case. Case I uses laboratory-determined ultimate values for shear strength parameters, and results in a predicted passive resistance nearly six times greater than the measured resistance. The initial modulus value used in Case I is consistent with the "preloaded or compacted" range for a loose sand or gravel

given by Duncan and Mokwa (2001), and is also consistent with the "normally loaded" range for a medium to dense soil. In Case II, the cohesion intercept was ignored and the interface friction angle was reduced to better match the measured passive resistance. With the interface friction angle at a nominal value of 2°, Case II results in a predicted resistance that matches the measured resistance to within 5%. With so little interface friction, the solution is essentially a Rankine passive earth pressure solution using the laboratory determined soil friction angle. Case III employs in-situ direct shear test results for the shear strength parameters and a δ/ϕ ratio of 0.6 (which is equivalent to the ratio found in interface friction angle testing with densely compacted fine gravel). Case III results in a resistance estimate over 200% greater than the measured response. In Case IV, the cohesion intercept is neglected and the interface friction angle has been iteratively reduced to provide a match to the measured resistance. Like Case II, Case IV estimates the passive resistance to within 5% of the measured passive resistance curve. Using the Rankine method (omitting the nominal 4 degrees of interface friction) with the field test-derived soil friction angle of 43° yields an ultimate passive force of about 710 kN, which is within 15% of the measured ultimate resistance. However, a similarly close match is also obtained in Case V by reducing the peak soil friction found in the staged in-situ direct shear test, 43°, to 65% of its original value (i.e., taking the inverse tangent of 65% of the tangent of 43°) which results in a friction angle of 31 degrees. This approach is similar to the one-third reduction approach suggested by Terzaghi and Peck (1967) when evaluating bearing capacity in loose granular soils and the anticipated failure mode is local or punching shear.

Table 7-2 Summary of PYCAP parameters for loosely compacted fine gravel backfill

Parameter	Case I	Case II	Case III	Case IV	Case V
ϕ (°)	44.9	44.9	43	43	31
c (kPa)	27.1	0.0	4.8	0.0	0.0
δ (°)	27	2	26	4	31
γ_m (kN/m^3)	19.3	19.3	19.3	19.3	19.3
E (kPa)	23500	23500	23500	23500	23500
ν	0.3	0.3	0.3	0.3	0.3
k (kN/mm)	140	140	140	140	130
Δ_{max} (mm)	124	124	124	124	124
Δ_{max} /H	0.074	0.074	0.074	0.074	0.074
R_f	0.64	0.95	0.90	0.95	0.95
R_{3D}	2.00	1.49	1.88	1.48	1.54
K_p	18.8	6.3	15.1	6.2	6.4

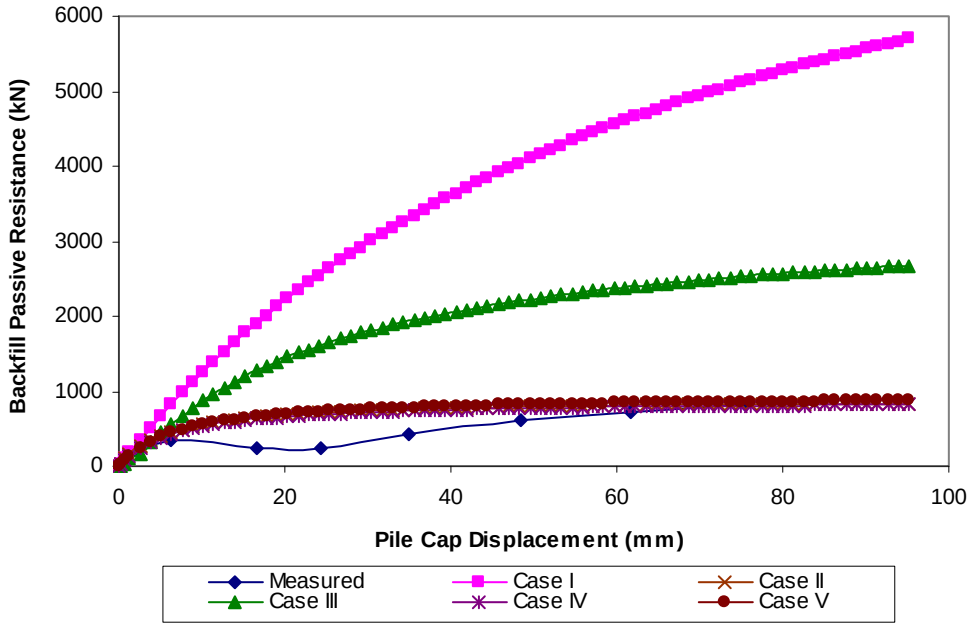

Figure 7-3 Comparison of measured and PYCAP-based calculated passive resistance for loosely compacted fine gravel backfill

7.3.2 Calculated Response Using ABUTMENT (LSH)

Along with PYCAP, the LSH method was also used to calculate passive resistance. Table 7-3 summarizes key input and output parameters for several cases while Figure 7-4 compares the measured passive resistance curve to the calculated resistance curves for each case. In Case I, laboratory direct shear test results are used to determine ultimate strength parameters, producing a poor match with the measured earth pressure curve. In Case II, cohesion is neglected and the interface friction angle has been iteratively reduced to better match the measured resistance; this reduced interface friction angle is the same as that used in Case II of the PYCAP-based analyses. Case III employs in situ direct shear results for soil friction angle and cohesion and a δ/ϕ ratio of 0.6, as in the PYCAP analysis. Using these parameters, the Case III theoretical curve over-estimates the maximum passive resistance by about 190%, similar to the result obtained using PYCAP. The interface friction angle in Case IV was iteratively reduced to provide a match between the predicted resistance and the measured response. Both Case II and Case IV provide matches within 5% of the measured resistance curve at the maximum displacement interval. It appears, in the case of the loosely compacted fine gravel that the computed prediction of passive resistance significantly overestimates the actual value unless a lower friction angle is used or the interface friction is drastically reduced, or even eliminated. Case IV appears to provide the best estimate of passive resistance for loosely compacted fine gravel backfill.

Table 7-3 Summary of LSH parameters for loosely compacted fine gravel backfill

Parameter	Case I	Case II	Case III	Case IV
ϕ (°)	44.9	44.9	43	43
c (kPa)	27.1	0	4.8	0
δ (°)	27	2	26	4
γ_m (kN/m^3)	19.3	19.3	19.3	19.3
ε_{50}	0.005	0.005	0.005	0.005
ν	0.3	0.3	0.3	0.3
R_f	0.98	0.98	0.98	0.98
R_{3D}	2.00	1.49	1.88	1.48
K_{ph}	33.6	6.5	15.1	6.5

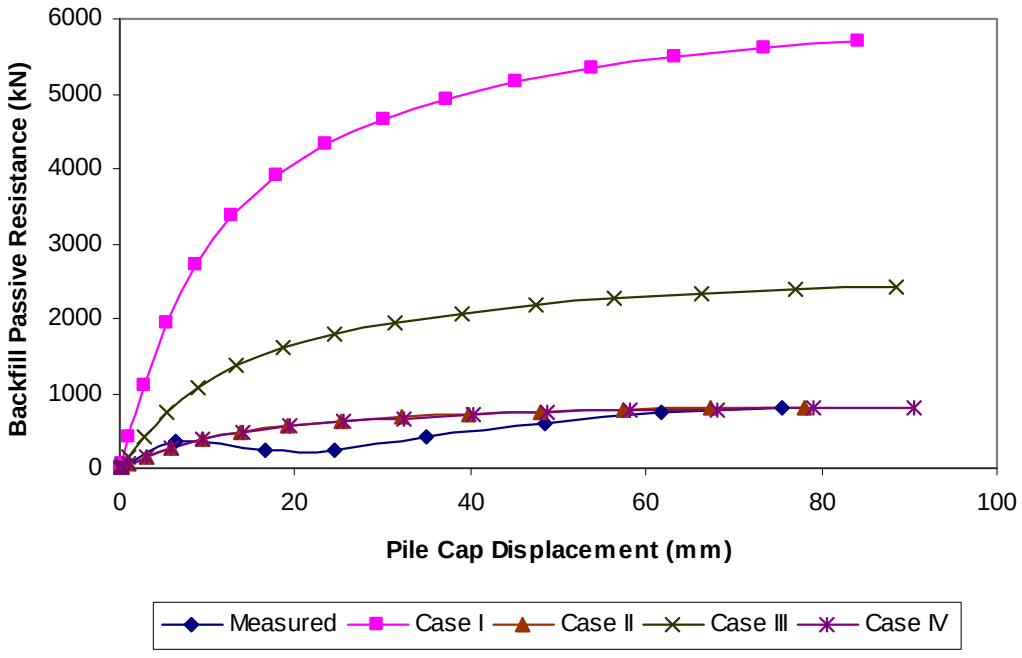

Figure 7-4 Comparison of measured and LSH-based calculated resistance for loosely compacted fine gravel backfill

7.3.3 Calculated Response Using CALTRANS

Passive earth resistance based on the CALTRANS method is shown Figure 7-4. In this case, the method over-predicts peak passive resistance by approximately 67%.

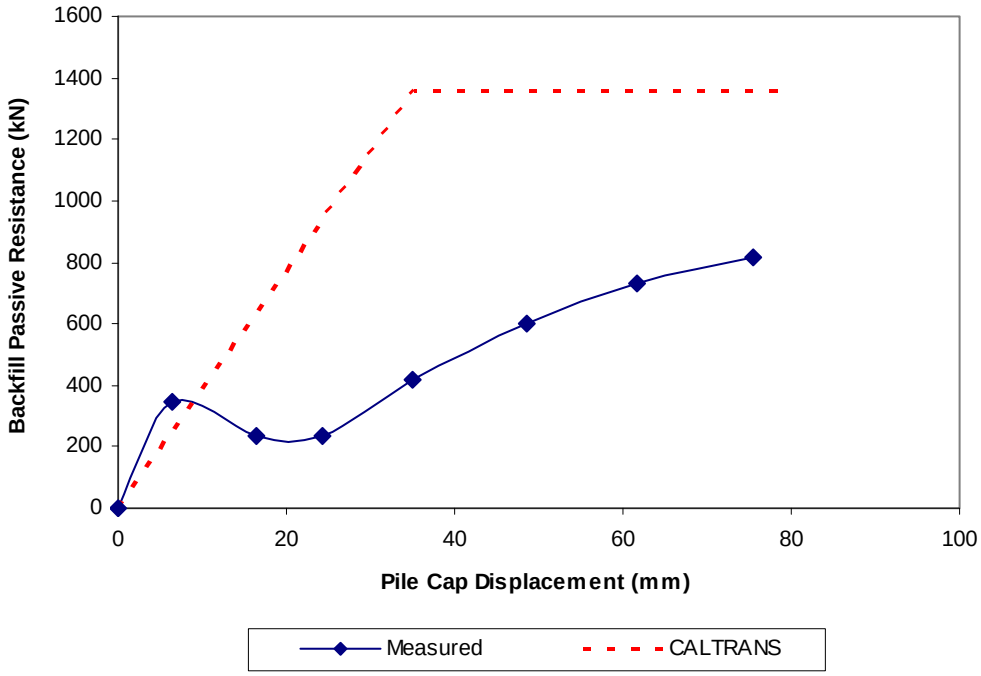

Figure 7-5 Comparison of measured and CALTRANS-based passive resistance for loosely compacted fine gravel backfill

7.4 Response to Cyclic Actuator Loading

After slowly pushing the pile cap to each target displacement, alternating combinations of small displacement cyclic actuator loads and dynamic shaker loads were applied to the test foundation. The response of the pile cap to the small displacement amplitude loading cycles from the actuator is presented and discussed in this section.

Figure 7-6 shows the loop displacement amplitude, stiffness, loop area, and damping ratio for the pile cap with loosely compacted fine gravel backfill as a function of pile cap displacement. Values are based on the median of the 15 low frequency cycles performed at each displacement level Loop displacement amplitude decreases slightly from about 1.75 mm to just under 1.5 mm, with a median displacement amplitude of about 1.6 mm, as the pile cap displacement increases. The stiffness increases from 100 to almost 300 kN/mm with increasing cap displacement; this appears to be due to greater mobilization of the backfill soil's passive strength and pile stiffness. The saw-toothed trend visible in other tests due to alternating cyclic and dynamic loading is exhibited in the stiffness and displacement amplitude data. The damping ratio also exhibits some oscillatory behavior with increasing cap displacement, decreasing in a fairly linearly from a peak of 31% to 19% with a median value of approximately 24%. The stiffness and damping values are more similar to those calculated from the baseline test than those calculated with the densely compacted backfill present.

7.5 Response to Dynamic Shaker Loading

After slowly pushing the pile cap to each displacement interval, alternating combinations of small displacement cyclic actuator loads and dynamic shaker loads were applied to the test foundation. The response of the pile cap to small displacement dynamic shaker loading is presented and discussed in this section. The first row of graphs in Figure 7-7 shows loop displacement amplitude as well as loop displacement amplitude normalized by the cyclic amplitude of net applied force from the shaker and actuators as functions of the forcing frequency. The second and third rows of graphs

show the calculated reloading stiffness and damping, respectively, of the pile cap system. In the left column, these parameters are shown in terms of forcing frequency. If non-linear behavior is present, these properties will also depend on the displacement amplitude; hence, in the right column, these parameters are shown on terms of the displacement amplitude. The data appear to suggest that both frequency and displacement amplitude must be considered when interpreting test results. The individual line series shown in all of the graphs represent different static pile cap displacement levels in which dynamic shaker cycles were applied before the low frequency actuator cycles.

The peaks in the normalized displacement amplitude graph correspond to the damped natural frequency, which increases from 6.5 to 7 Hz with increasing cap displacement. The dynamic reloading stiffness ranges between about 200 to about 350 kN/mm in the range of frequencies tested. In terms of displacement amplitude, the stiffness stays close to 200 kN/mm until a loop displacement of about 1.25 mm, when the stiffness increases dramatically. Calculated damping values vary greatly with respect to forcing frequency and displacement amplitude. The minimum damping appears to be less than 5% at 5.5 Hz and 0.4 mm of displacement amplitude. At higher frequencies, the damping ratio increases up to about 35% (as the stiffness decreases) until dropping again at 7.5 to 8 Hz. Using the half-power bandwidth method to interpret the normalized displacement amplitudes yields damping ratios of 25, 23, and 24% for the three pile cap displacement levels shown. The stiffness and damping ratio generally increase with increasing pile cap displacement; however, at relatively large loop displacement amplitudes (1 mm and greater), this trend appears to reverse. As stated previously in

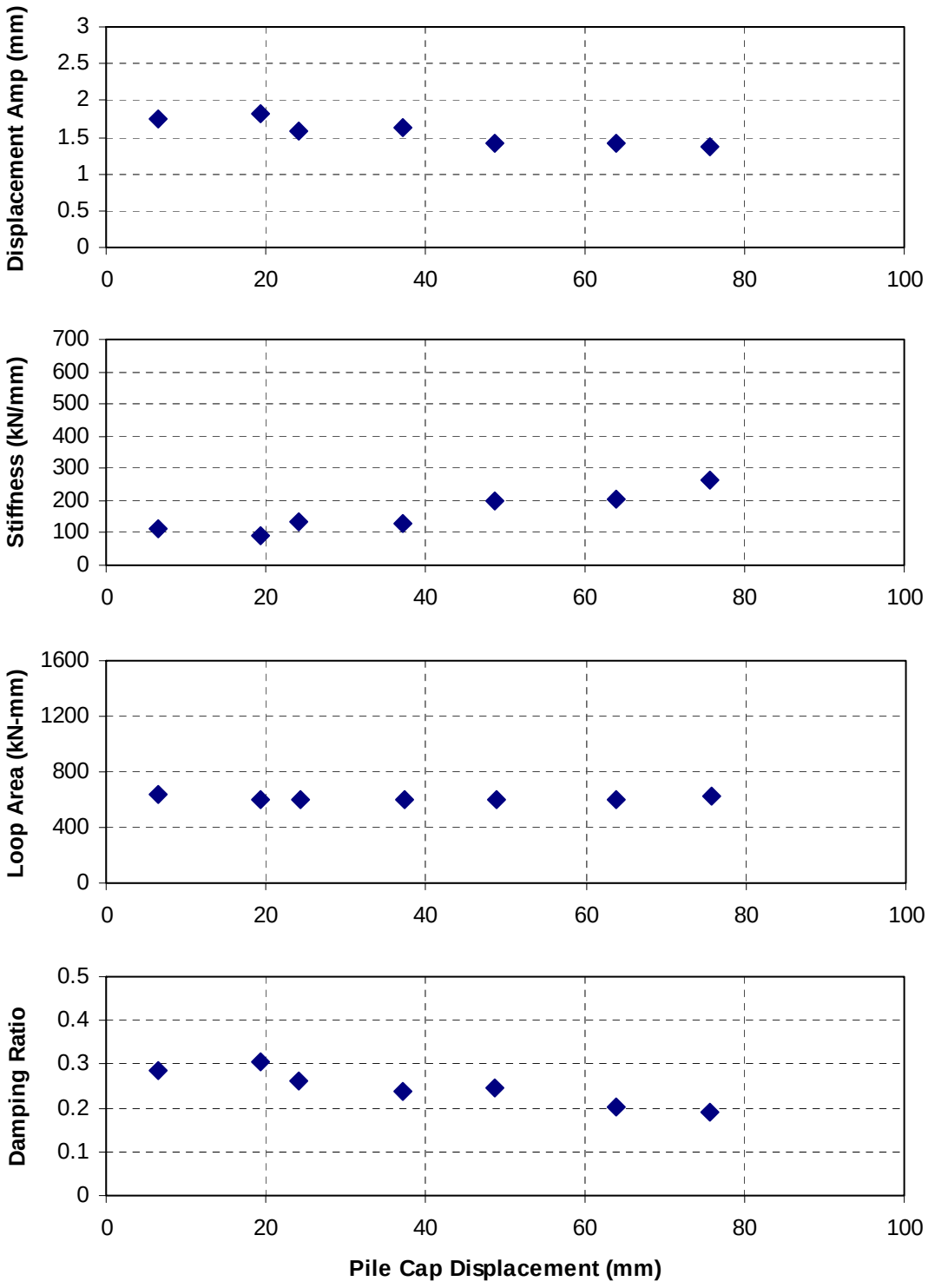

Figure 7-6 Summary of response to cyclic actuator loadings for pile cap with loosely compacted fine gravel backfill

Section 5.4, the observed variations in stiffness and damping with frequency are likely due to variations in phase between passive earth forces (whether acting on the piles or on the pile cap itself) and the inertial force from the foundation as suggested by Tokimatsu et al. (2004) in their work with large shaking table models of pile cap foundation systems. Some variation is also likely due to the simple lumped, constant, mass model used.

7.6 Comparison of Cyclic Actuator and Dynamic Shaker Responses

Included in Figure 7-7 are displacement amplitude, stiffness, and damping ratio calculated from the actuator-driven cycles (~ ¾ Hz) at the represented pile cap displacement levels (points in dashed ovals). The actuator-based values shown are averaged from actuator cycles run at previous and subsequent pile cap displacement levels. These averages represent stiffness and damping values that would have been calculated if the actuator cycles and been performed before the shaker cycles. It is difficult to compare the static and dynamic methods in terms of frequency because of the difference in the associated displacement amplitudes (the shaker cannot generate large forces, and hence displacements, at low frequencies).

The dynamic shaker loadings at 10 Hz resulted in maximum displacement amplitudes of about 1.4 mm for the first two pile cap displacement levels shown, and 1.1 mm for the last pile cap displacement level shown. These values are somewhat similar to those obtained during actuator cycling. For the second and third cap displacement levels shown, the actuator-based stiffnesses are within the shaker-based stiffness range, albeit at the lower end, near 200 kN/mm. The actuator-based damping ratio (ranging from about 20 to 30%) compares favorably with the 23 to 25% damping

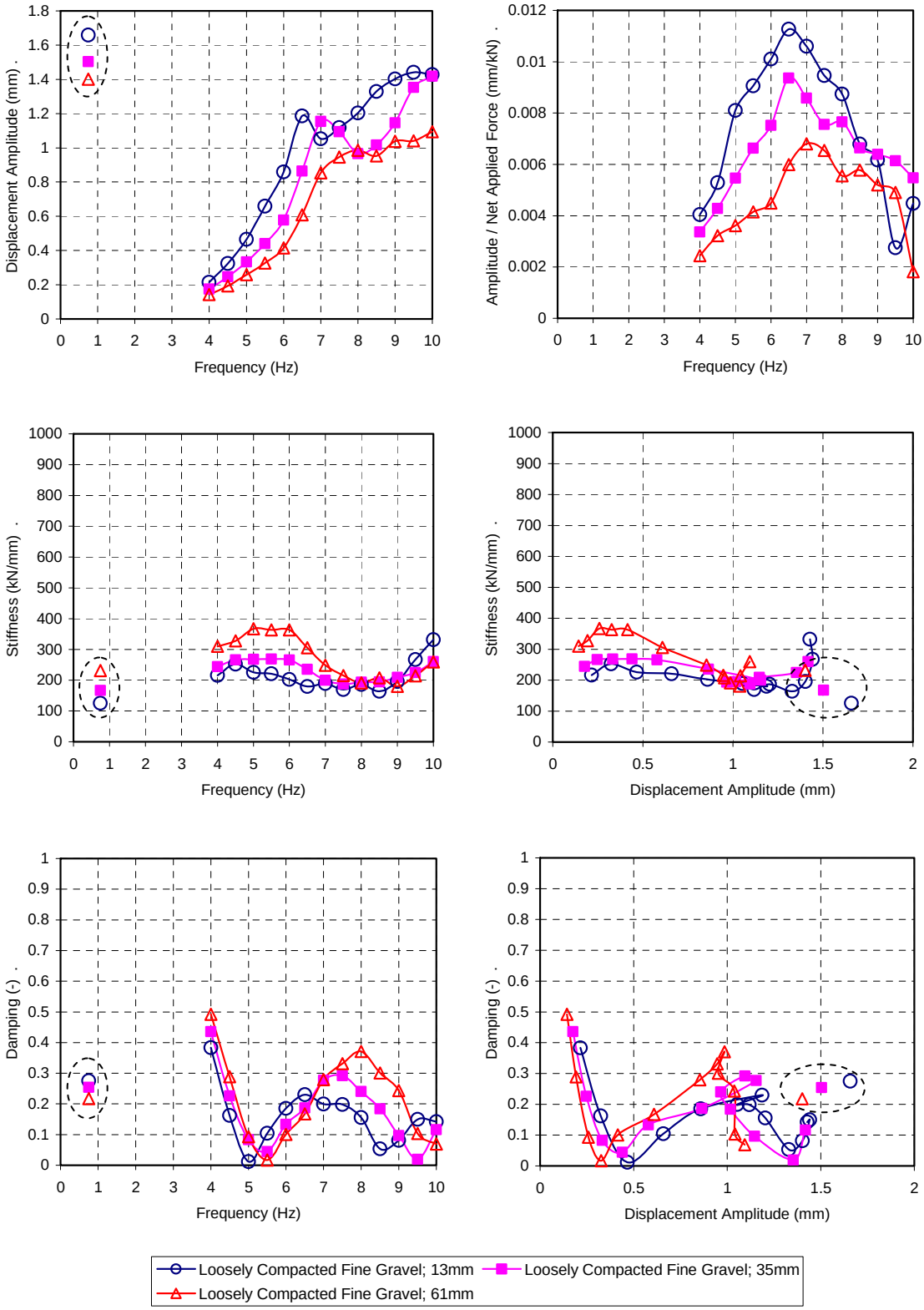

Figure 7-7 Summary of response to dynamic shaker loadings for pile cap with loosely compacted fine gravel backfill

ratio computed with the half-power band width approach and is within the range calculated using the shaker-based load-displacement loops. The similarities between the stiffness and damping values for the two different frequency ranges appear to suggest that dynamic loadings do not significantly increase the apparent resistance of the pile cap relative to slowly applied cyclic loadings.

7.7 Passive Earth Pressure Contributions

A vertical array of six earth pressure cells evenly distributed in the central portion of the pile cap face was used to make direct measurements of passive earth pressure from the backfill soil. Figure 7-8 shows the pressure measured by the pressure cells with depth at the end of each static push interval.

The profiles suggest that the reactive pressure from the backfill is concentrated near a depth of 1 m. The measured pressure distribution does not appear to match the typical representation of increasing pressure with depth. However, this may, in part, be a result of the soil mass not having developed a well defined, ultimate failure state. The pressure cell closest to the ground surface shows little increase in pressure from the first push to the last, which appears to indicate that ultimate resistance near the top develops well before the resistance mobilizes at deeper depths. The trend in the lowest pressure cell is consistent with that observed in other tests, decreasing with increasing displacement after initially recording some pressure development (as discussed in Section 4.5). The pressure cell above it unexpectedly displays a similar trend, decreasing from some pressure to nearly zero pressure after the second displacement level. A precise explanation for this behavior is not readily available. Little change in the pressure

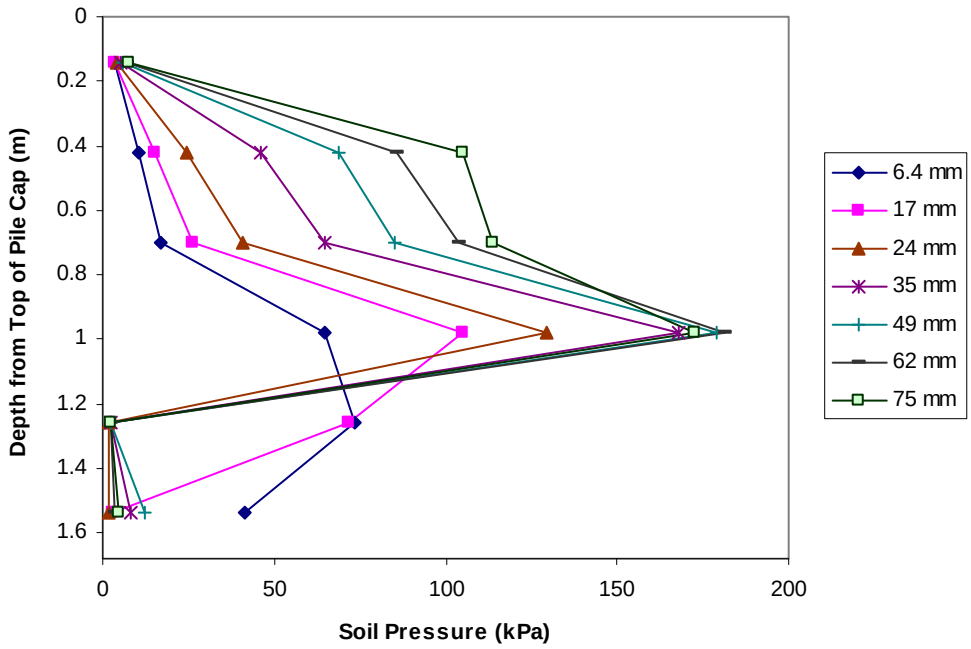

Figure 7-8 Earth pressure distribution as a function of pile cap displacement with loosely compacted fine gravel

profiles during the last few displacement intervals, which appears to suggest that the soil adjacent to the cap is approaching its ultimate resistance.

Figure 7-9 shows the backfill force computed by multiplying each measured pressure by the corresponding contributory areas of the pile cap face. In general, the resulting force-displacement curve has a similar trend to the actuator-based curve, but it is systematically lower. The unexpected drop in the actuator-based load-displacement curves near 16 mm after the second loading interval is not reflected in the pressure cell-derived resistance. Applying a multiplier of 1.67 (the inverse of 0.6 determined in Section 4.5) to the cell-based curve improves the match with the actuator-based curve. The ultimate passive resistance appears to mobilize in the pressure cell curves, whereas for the actuator curves such mobilization is not as well defined.

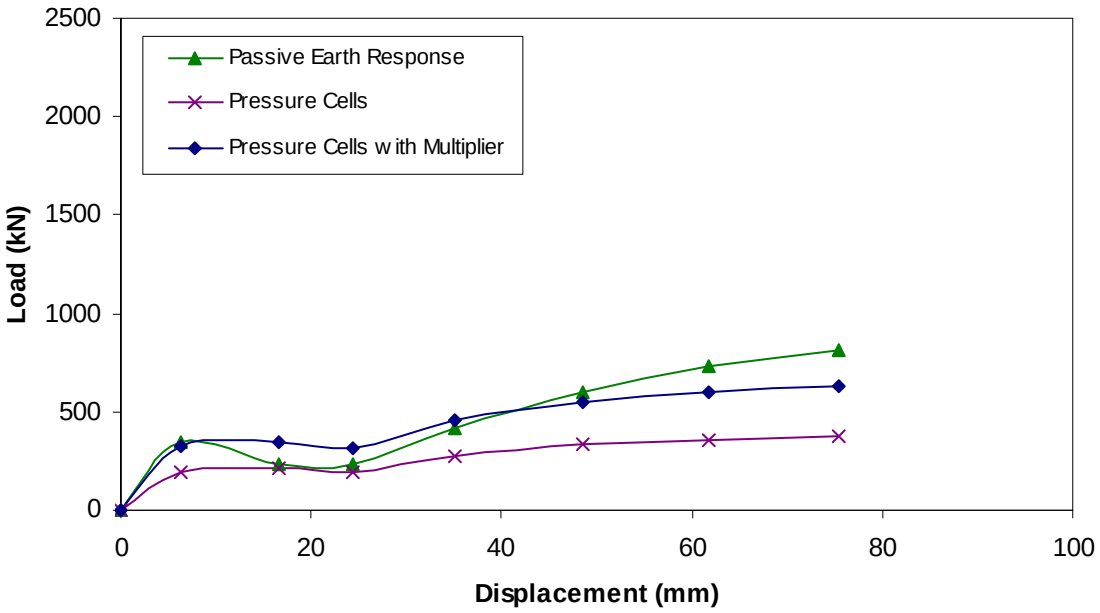

Figure 7-9 Comparison of earth forces based on actuators and pressure cells for loosely compacted fine gravel backfill

7.8 Cracking and Vertical Movement of Backfill

Figure 7-10 is a two part plot showing the effect of static and dynamic testing on the surface of the loosely compacted fine gravel backfill area. The first part of the figure is a map of the surface cracks that developed during each static push of the pile cap. The surface cracks in the backfill indicate that failure surfaces are present within the soil.

Low cohesion in the loosely compacted fine gravel backfill, along with the dynamic vibration due to the eccentric mass shaker, caused the soil grains to shift during testing, potentially obscuring cracks. The figure shows a large number of cracks that formed during the first pile cap displacement interval, with loadings from subsequent displacement intervals producing fewer cracks. Cracks from later pushes into the loosely

compacted fine gravel backfill occurred largely within 2 m of the cap. The orientation and distribution of the cracks seem to suggest a punching failure mechanism in the loosely compacted fine gravel backfill material instead of a mobilization of passive resistance.

The second part of the figure is a contour map of the change in elevation along the surface of the backfill area during testing. The typical elevation change, as represented by the median elevation change in a given row (parallel to the face of the cap) of grid nodes, is about 3 mm of both heave and settlement. As much as 20 mm of settlement occurred directly adjacent to the pile cap face, though some of this decrease in elevation may be due to loss of material near the boundaries of the backfill zone. Most of the heave occurred away from the pile cap face, with the settlement occurring within 4 m of the pile cap face.

The correlation between the failure surface and the settlement characteristics of the backfill is illustrated in Figure 7-11, where the median vertical displacement profile is given alongside a log-spiral failure surface. The log-spiral failure surface shown below was computed in PYCAP using the best-fit parameters discussed in section 7.3.1: a soil friction angle of 43° with no cohesion and a nominal interface friction angle of 4° (i.e., Case IV). The low interface friction angle used to calculate the log-spiral solution produces a failure surface that resembles a Rankine failure wedge rather than a log-spiral failure surface. This appears to be consistent with the backfill settlement at the pile cap face and the relative lack of heave in the backfill area.

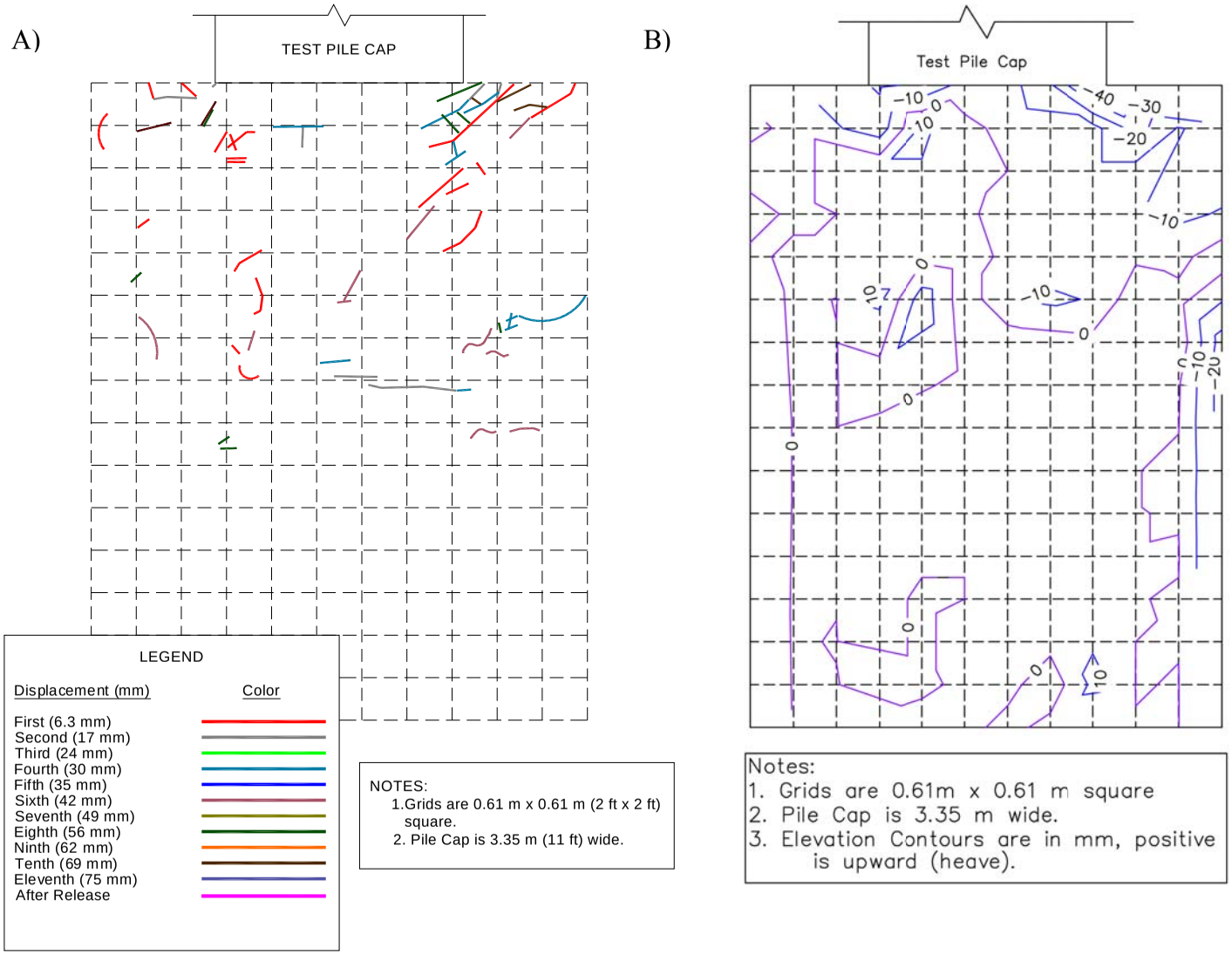

Figure 7-10 Crack pattern (A) and heave contour (B) maps for loosely compacted fine gravel backfill

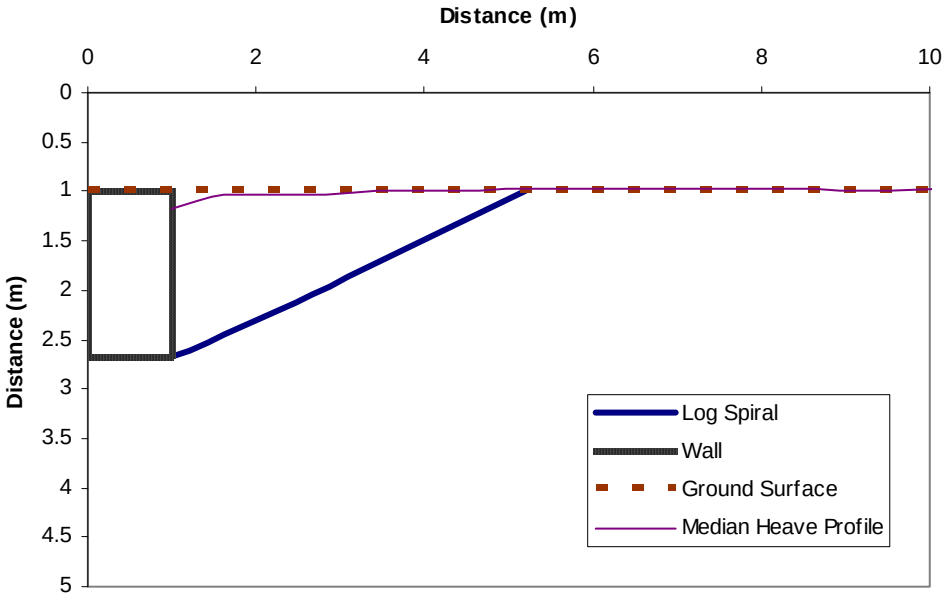

Figure 7-11 Heave profile with best-fit log-spiral failure surface from PYCAP for loosely compacted fine gravel backfill

7.9 Horizontal Movement of Backfill

String potentiometers were used to measure movement in the backfill. Figure 7-12 shows the movement of each of the monitoring points in the loosely compacted fine gravel backfill compared to the movement of the pile cap face. Movement at 1.2 m away from the pile cap face appears to be greater than at 0.6 m from the face of the pile cap. This is likely partially due to backfill settlement immediately in front of the pile cap, which may have caused the first monitoring point to shift toward the pile cap while no such negative movement occurred at the second monitoring point. The string potentiometers recorded a considerable amount of negative displacement in the loosely compacted fine gravel test, particularly at 3.7 m and 5.5 m from the pile cap face. A

negative displacement in Figure 7-12 indicates that the monitoring point moves toward the pile cap while the pile cap moves into the backfill. Background noise (data spikes caused by small electrical shorts) and other difficulties are common in the raw data and are impossible to eliminate altogether. Even considering the error that these elements may have introduced into the data, it is possible that small negative movements may have occurred in the backfill. According to the contour map of the backfill after testing, the backfill experienced a fair amount of settlement. The monitoring points were located within range of the settlement and may have shifted along with the backfill as it settled, thus generating negative movements.

After the first three pushes of the pile cap, the backfill displacement is generally positive. The relatively small amount of change at the point farthest from the pile cap suggests that most of the displacement of the cap has been absorbed in the backfill area up to that point. This observation may indicate that the initial negative displacement recorded at this monitoring point may be due to an unknown error source.

Figure 7-13 shows the compressive strain corresponding to each static push of the pile cap. The compressive strain ranges from about 0.09 to 0.005 within the backfill zone. The 0.6 m interval closest to the cap experiences by far the most compressive strain, in this case about three times the strain in any other interval. In the loosely compacted fine gravel backfill, the compressive strain appears to decrease rapidly and incrementally as the distance between the monitoring point and the pile cap face increases. Minor variation from interval to interval may indicate the potential sensitivity of the string potentiometer measurements to differential pushing of the pile cap (not all the monitoring stakes were on the same end of the cap face) and tipping of the monitoring

stakes themselves. Movement of the stakes could explain the presence of some negative strain amounts in the calculations. Generally speaking, the strain appears to decrease logarithmically with distance away from the cap.

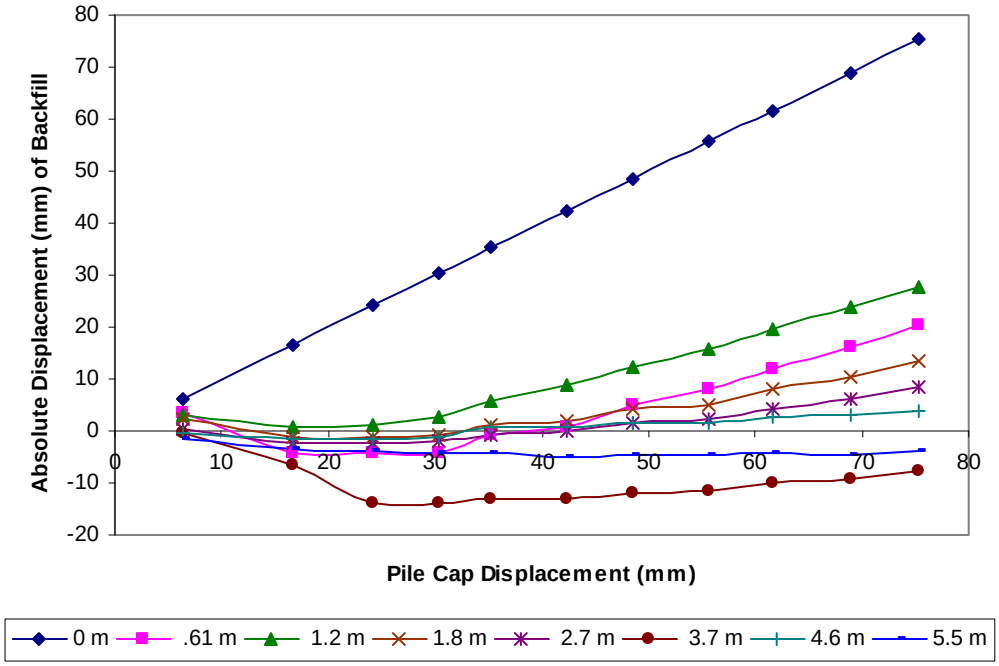

Figure 7-12 Displacement of monitoring points in loosely compacted fine gravel backfill

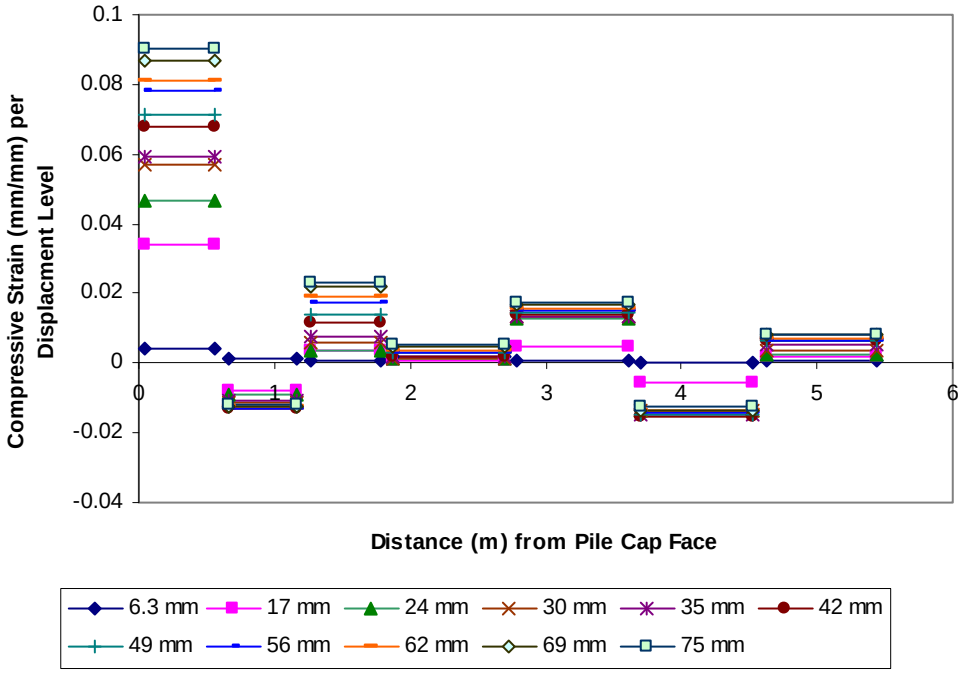

Figure 7-13 Strain per displacement level for loosely compacted fine gravel backfill

8 Pile Cap with Densely Compacted Coarse Gravel Backfill

8.1 General

The pile cap with densely compacted coarse gravel backfill was tested on June 26, 2007. Table 8-1 summarizes the test in terms of loads and displacements measured at the end of each "static push" with the actuators. The table also indicates the order in which actuator-driven cyclic loads and shaker-based dynamic loads were applied. At certain displacement increments, cyclic and dynamic loadings were not applied in order to help assure that the test foundation displaced sufficiently into the backfill for the load path to return to the static-backbone loading curve. Some deviation from the general test procedure occurred during this test; that is, the maximum shaker frequency from the fourth displacement interval onward was limited to 9 Hz and no shaker loadings were applied during the last displacement interval due to progressive breakdown of the shaker. The resistance of the pile cap with the densely compacted coarse gravel backfill approached the maximum load capacity of loading system and the reaction foundation.

8.2 Load-Displacement Response

Figure 8-1 shows the entire actuator load verses pile cap displacement relationship for the test, with static pushes, actuator cycles and shaker cycles being

Table 8-1 Summary of test with densely compacted coarse gravel backfill

Displacement Interval	Displacement (mm)	Actuator Load (kN)	Actuator Cycles	Shaker Cycles
1	5.0	881	First	Second
2	11	1308	Second	First
3	17	1812	First	Second
4	23	2261	Second	First
5	30	2672	None	None
6	36	3133	First	Second
7	42	3410	None	None
8	49	3859	Second	First
9	56	4115	None	None
10	62	4480	First	Second
11	69	4671	None	None
12	75	4923	First	None

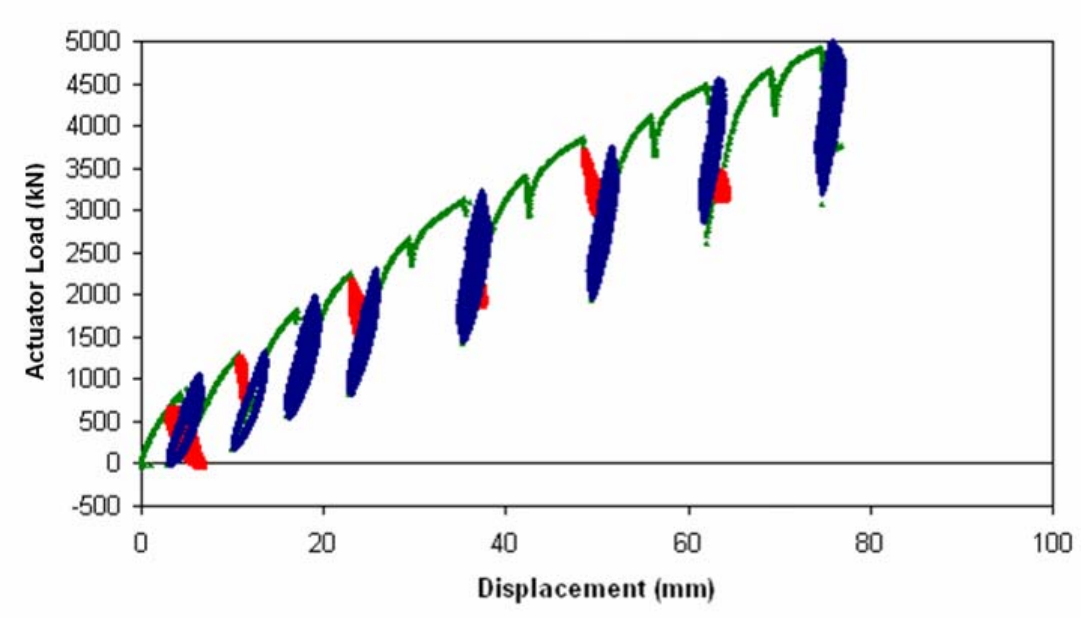

Figure 8-1 Actuator load versus pile cap displacement with densely compacted coarse gravel backfill (Test 12; June 26, 2007)

represented by green, blue, and red data points, respectively. Section 4.2 provides some discussion relative to the interpretation of this data.

Figure 8-2 shows three load-displacement response curves for the pile cap: one for the response with backfill in place (the "total" response, which is the equivalent monotonic response or backbone curve derived from the data shown in Figure 8-1); one for the response with no backfill present (the "baseline" response); and one showing the passive earth response of the backfill (obtained by subtracting the baseline response from the total response).

The curves show that total response and baseline response appear to increase at different rates until approximately 74 mm of displacement, the final displacement level for the test. The baseline and total responses appear increase at a similar rate, causing the passive earth response to level off. Unfortunately, limits on the load capacity of the equipment prevented the research team from displacing the pile cap to higher levels, which would have enabled us to confirm full mobilization of passive resistance. Based on the data, the ultimate passive resistance of the backfill appears to be about 3380 kN at about 74 mm of displacement, corresponding to a wall displacement to height ratio (Δ_{max}/H) of about 0.044.

8.3 Calculated Passive Earth Response

Commonly used methods for calculating passive earth pressure include Rankine theory, Coulomb theory, and log-spiral theory. Log-spiral theory is typically considered the most accurate of these methods (see, for example, Cole and Rollins (2006) and Duncan and Mokwa (2001)). Three methods of estimating the development of passive

pressure with wall displacement are evaluated in this section. Two of these methods, PYCAP and ABUTMENT (LSH method) involve applications of log-spiral theory and a hyperbolic load-displacement relationship. The third approach evaluated in this section is an empirical load-displacement relationship based on full-scale testing of an abutment with typical backfill conditions (see discussion of CALTRANS method in Section 4.3.3).

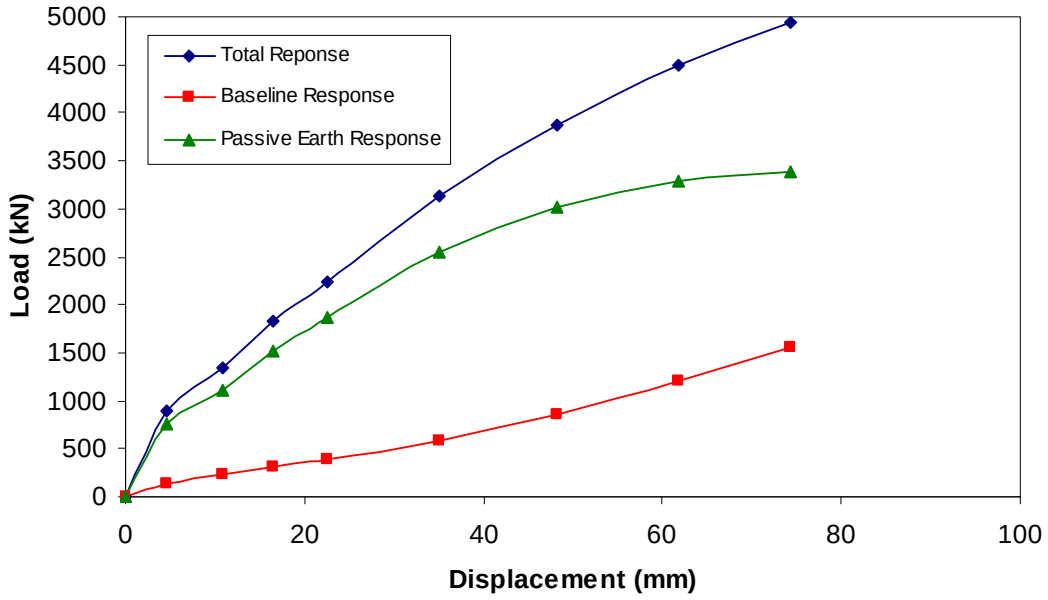

Figure 8-2 Total, baseline, and passive earth responses for pile cap with densely compacted coarse gravel backfill

8.3.1 Calculated Response Using PYCAP

Passive earth resistance was calculated using the modified PYCAP spreadsheet introduced in Section 4.3.1. Table 8-2 summarizes key inputs and outputs for several cases while Figure 8-3 shows the measured passive resistance curve alongside the calculated passive resistance curves for each case. Case I uses a soil friction angle

obtained from a correlation proposed by Duncan (2004) (as mentioned in Section 3.4.2) and a δ/φ ratio of 0.6. The initial modulus, 39700 kPa, corresponds to the recommended range for dense preloaded or compacted sand and gravel presented by Duncan and Mokwa (2001). The calculated load-displacement response using Case I overestimates the measured resistance by about 200%. In Case II, the interface friction angle was iteratively reduced to obtain a good match between the calculated and measured curves. In-situ direct shear test results were used for the soil friction angle and cohesion intercept in Case III and the interface friction angle is based on a δ/ϕ ratio of 0.6 found by interface direct shear testing in the laboratory for the densely compacted fine gravel. The larger particles prevented a similar test with the coarse gravel. Case III underestimates the ultimate passive resistance by about 4%. Case IV also employs in-situ direct shear parameters, but the δ/ϕ ratio is changed to 0.75, a commonly assumed value. Case IV overestimates the ultimate passive resistance by about 16%. In Case V the interface friction angle is iteratively changed within the range used in Cases III and IV in order to match the recorded data. Case V was tailored to provide the best match between the computed and measured passive responses and will therefore be referred to as the "best fit" case. However, Case III provides an excellent match with minimal manipulation of the field-derived parameters. The Case III parameters could reasonably be used to predict the capacity of this particular soil type for design purposes. Cole and Rollins (2006) and Rollins and Sparks (2002) also used P-154 coarse gravel materials in their tests. Their in-situ direct shear tests found friction angles of 40 and 42° with cohesion intercepts of 7.2 kPa and 0 kPa, respectively. The gravel used in Cole and Rollins (2006) and Rollins and Sparks (2002) had unit weights of 23.1 and 23.6 kN/m^3 and required wall

Table 8-2 Parameter summary for case comparison in PYCAP for densely compacted coarse gravel backfill

Parameter	Case I	Case II	Case III	Case IV	Case V
ϕ (°)	54	54	41	41	41
c (kPa)	0	0	13.69	13.69	13.69
δ (°)	32.4	11.0	24.6	30.8	26.0
γ_m (kN/m^3)	21.8	21.8	21.8	21.8	21.8
E (kPa)	39700	39700	39700	39700	39700
ν	0.3	0.3	0.3	0.3	0.3
k (kN/mm)	240	240	240	240	240
Δ_{max} (mm)	0.044	0.044	0.044	0.044	0.044
Δ_{max}/H	74	74	74	74	74
R_f	0.21	0.80	0.82	0.78	0.81
R_{3D}	2.00	1.98	1.77	1.89	1.80
K_p	55.0	17.5	12.4	15.4	13.1

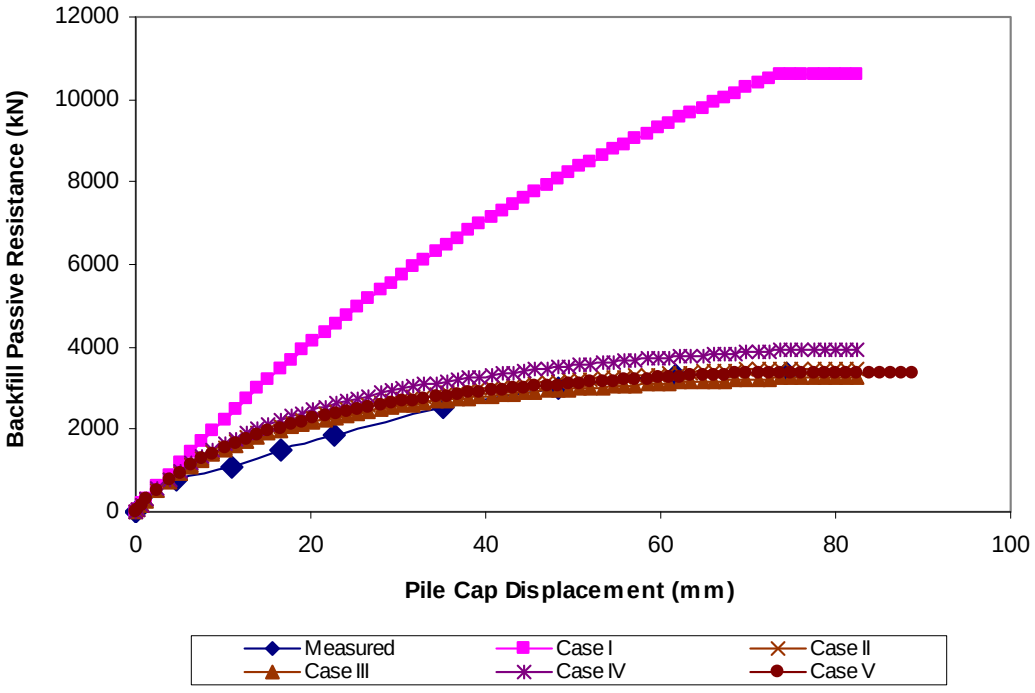

Figure 8-3 PYCAP case comparison for densely compacted coarse gravel

movements that were 3.5 and 6% of the height, respectively, to mobilize the full passive earth response. These parameters were analyzed using PYCAP for comparison with the results obtained using the Case III parameters (the in-situ direct shear results with a δ/ϕ ratio of 0.6). The Cole and Rollins, Rollins and Sparks, and Case III parameters matched the measured resistance to within roughly 10%, all underestimating the measured results. This favorable comparison with published parameters, along with a favorable match to the measured data, lends validity to the use of the field direct shear values. The friction angle based on the Duncan (2004) correlation was too large to produce a reasonable match with the measured results.

8.3.2 Calculated Response Using ABUTMENT (LSH)

Passive earth resistance was also calculated using the LSH method. Table 8-3 summarizes key inputs and outputs for several cases while Figure 8-4 shows the measured and calculated passive resistance curves for each case. The soil friction angle used in Case I was estimated using the Duncan (2004) correlation mentioned in the previous section. Absent load-deformation laboratory tests due to the large particle sizes of the coarse gravel backfill, the strain at which 50% of the failure strength occurs (ε_{50}) was estimated by examining the load-displacement curve (Figure 8-2) and finding the displacement level at which the soil mass reaches 50% of its peak resistance, and then examining the measured differential displacement and calculated compressed strain along the surface of the backfill (Figure 8-12 and Figure 8-13) and averaging the strain from the two strain intervals closest to the cap face and confirming the result by comparing it with typical values. The interface friction angle was determined by using a δ/ϕ ratio of 0.6,

Table 8-3 Parameter summary for case comparison in ABUTMENT for densely compacted coarse gravel

Parameter	Case I	Case II	Case III	Case IV
ϕ (°)	54	54	41	41
c (kPa)	0	0	13.7	13.7
δ (°)	32.4	11	24.6	30.75
γ_m (kN/m^3)	21.8	21.8	21.8	21.8
ε_{50}	0.0037	0.0037	0.0037	0.0037
ν	0.3	0.3	0.3	0.3
R_f	0.98	0.98	0.98	0.98
R_{3D}	2	1.98	1.77	1.89
K_{ph}	39.0	18.2	17.1	18.8

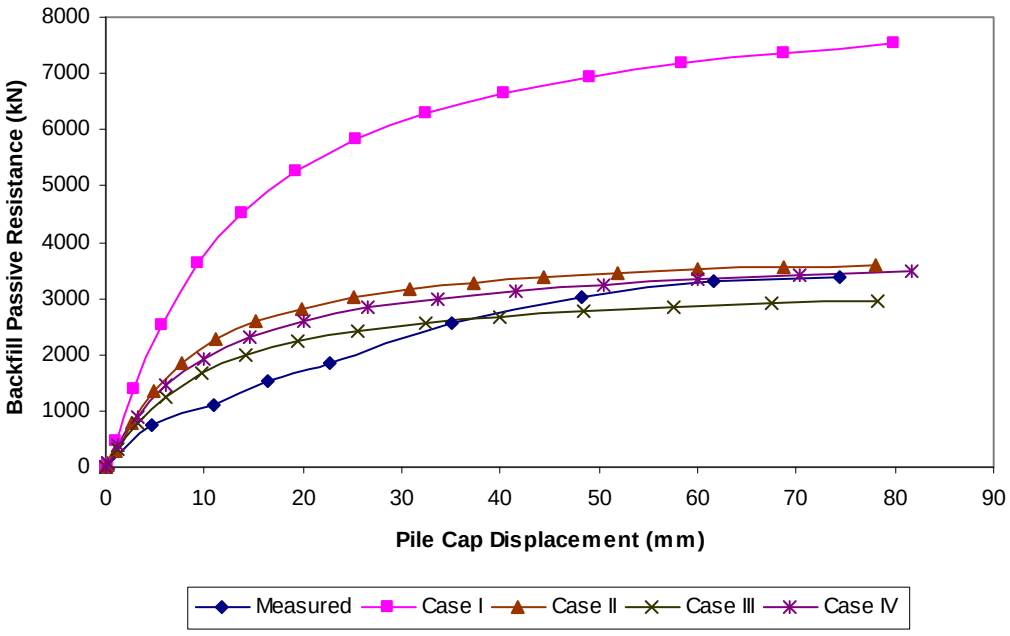

Figure 8-4 ABUTMENT case comparison for densely compacted coarse gravel backfill

consistent with laboratory determined soil and interface friction values from the densely compacted fine gravel backfill. With the exception of the ε_{50} value, these are the same parameters used in Case I for the PYCAP analysis. Likewise, Cases II through IV use the same parameters as in the PYCAP analysis. Using the LSH method, the resistance predicted using Case I parameters overpredicts the measured response by over 130%. Case II overestimates the measured peak by about 6.5%. Case III underestimates the measured curve by about 12.5%. The Case IV parameters (with a δ/ϕ ratio of 0.75) estimate the resistance to within 5% of the measured resistance. The Case IV parameters provide the best match to the measured data with little manipulation to the field derived strength parameters.

8.3.3 Calculated Response Using CALTRANS

Passive earth resistance based on the CALTRANS method is shown in Figure 8-5. In this case, the method under-predicts peak passive resistance by almost 60%.

8.4 Response to Cyclic Actuator Loading

After slowly pushing the pile cap to each target displacement, alternating combinations of cyclic actuator loads and dynamic shaker loads were applied to the test foundation. The response of the pile cap to the small displacement amplitude loading cycles from the actuator is presented and discussed in this section. Figure 8-6 shows the loop displacement amplitude, stiffness, loop area, and damping ratio for the pile cap with densely compacted coarse gravel backfill as a function of pile cap displacement. Values are based on the median of 15 low frequency cycles performed at each displacement

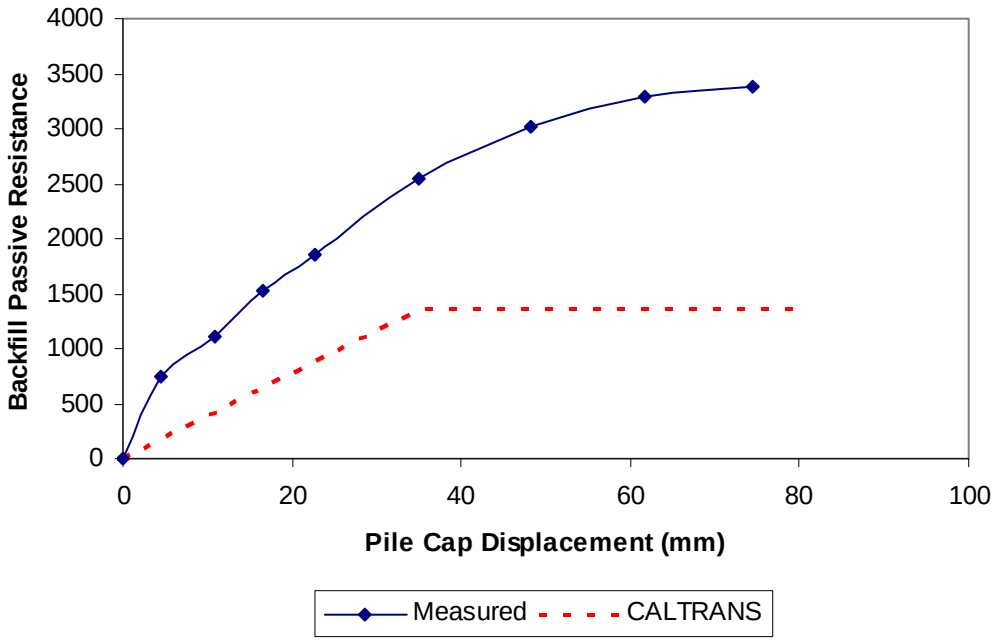

Figure 8-5 Comparison of measured and CALTRANS-based passive resistance for densely compacted coarse gravel backfill

level. Loop displacement decreases almost linearly from 1.8 to 1.1 mm as the pile cap displacement into the backfill increases, with a median displacement of 1.5 mm. The stiffness increases from 240 to 630 kN/mm as the cap displacement increases; this appears to be due to greater mobilization of the backfill soil's passive strength and pile stiffness. The rate of stiffness increase appears to level off in the last couple of displacement intervals as the passive resistance of the backfill approaches its ultimate value. The loop area remains fairly constant at each displacement interval. The same alternating trend seen in other tests due to changing the order of cyclic and dynamic loading phases is apparent in the stiffness and damping data. With a dramatic increase in stiffness and a relatively constant loop area, the relatively constant damping ratio, with a median value of 18%, is somewhat surprising.

8.5 Response to Dynamic Shaker Loading

After slowly pushing the pile cap to each target displacement, alternating combinations of small displacement cyclic actuator loads and dynamic shaker loads were applied to the test foundation. The response of the pile cap to the small displacement dynamic shaker loading is presented and discussed in this section. The first row of graphs in Figure 8-7 shows loop displacement amplitude as well as loop displacement amplitude normalized by the cyclic amplitude of net applied force from the shaker and actuators as functions of the forcing frequency. The second and third rows of graphs show the calculated reloading stiffness and damping, respectively, of the pile cap system. These parameters are shown in terms of forcing frequency in the left column. If non-linear behavior is present, these properties will also depend on the loop displacement amplitude; hence, in the right column, these parameters are shown in terms of the displacement amplitude. The data appear to suggest that both frequency and displacement amplitude must be considered when interpreting test results. The individual line series shown in the graphs represent different static pile cap displacement levels in which dynamic shaker cycles were applied before the low frequency actuator cycles.

The peaks in the normalized displacement amplitude graph correspond to the damped natural frequency, which appears to remain at approximately 7.5 Hz for all static displacement levels shown. Reloading stiffness ranges from approximately 400 to 1000 kN/mm, peaking 1.5 to 2 Hz, depending on pile cap displacement into the backfill, before the damped natural frequency and descending thereafter to about 500 kN/mm. The stiffness data shows similar peaking trends when plotted as a function of displacement, with peak stiffness occurring at displacement amplitudes of about 0.2 mm.

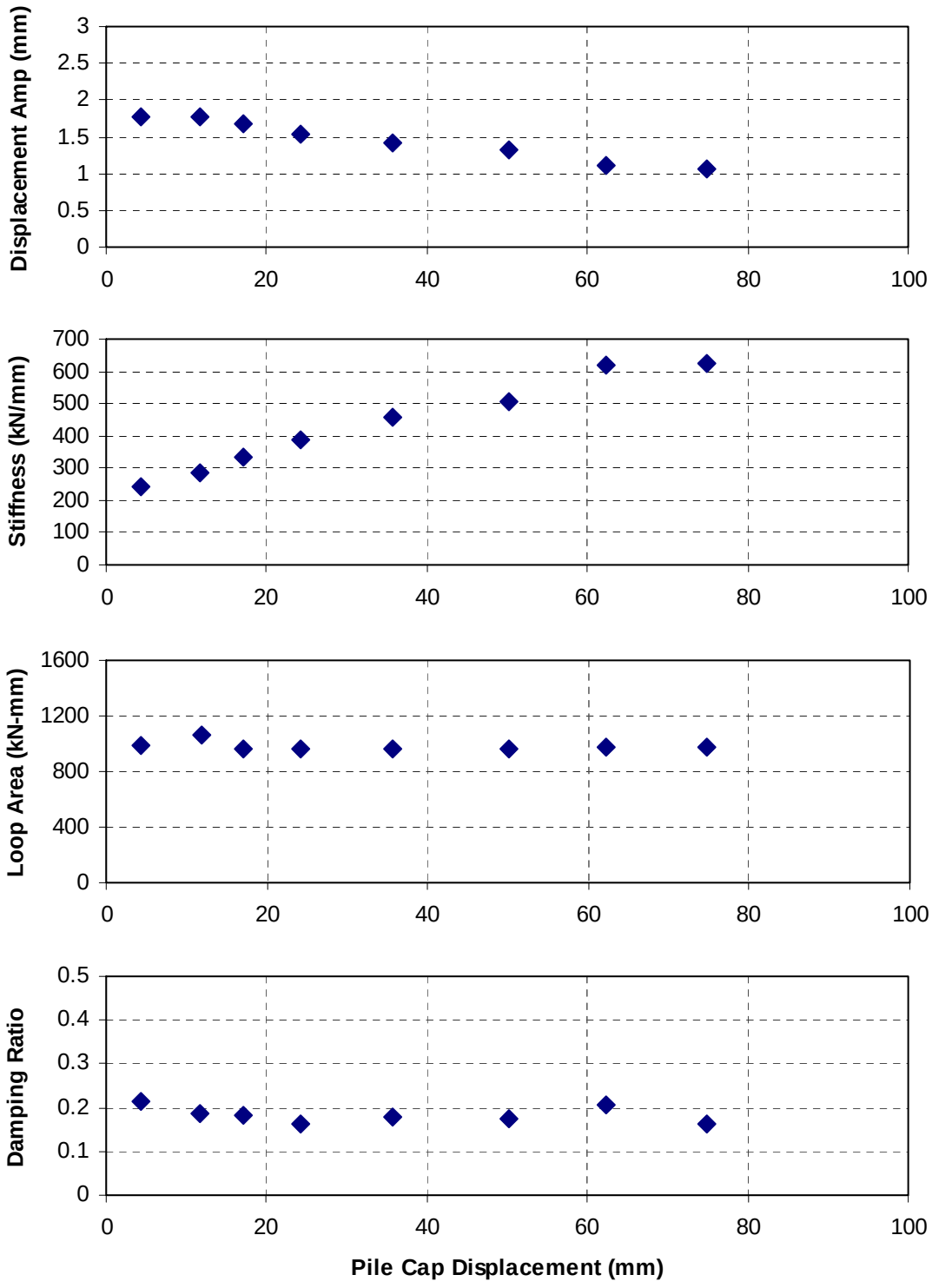

Figure 8-6 Summary of response to cyclic actuator loadings for pile cap with densely compacted coarse gravel backfill

The stiffness data generally increases in stiffness with increasing pile cap displacement. Calculated damping values vary greatly with respect to forcing frequency and displacement amplitude. The minimum damping appears to be less than 5% at about 6 Hz and 0.2 mm of displacement amplitude (i.e., the zone of peak stiffness). At higher frequencies and displacements, the damping ratio increases up to about 30 to 40% (corresponding with decreasing stiffness), depending on pile cap displacement, until dropping again at about 8.5 Hz (where the rate of stiffness decrease appears to level off). Unfortunately, due to the shape of the normalized displacement amplitude curves, the half-power bandwidth approach could not be used. As stated previously in Section 5.4, the observed variations in stiffness and damping with frequency are likely due to variations in phase between passive earth forces (whether acting on the piles or on the pile cap itself) and the inertial force from the foundation as suggested by Tokimatsu et al. (2004) in their work with large shaking table models of pile cap foundation systems. Some variation is also likely due to the simple lumped, constant, mass model used.

8.6 Comparison of Cyclic Actuator and Dynamic Shaker Responses

Figure 8-7 includes displacement amplitude, stiffness, and damping ratios from the actuator-driven cycles (~ ¾ Hz) at the displacement levels given for the shaker derived values (points in dashed ovals). The actuator-based values shown are averaged from actuator cycles run at previous and subsequent pile cap displacement levels. These averages represent stiffness and damping values that would have been calculated if the actuator cycles had been performed before the shaker cycles. In terms of frequency, it can be difficult to compare the static and dynamic methods because of the difference in

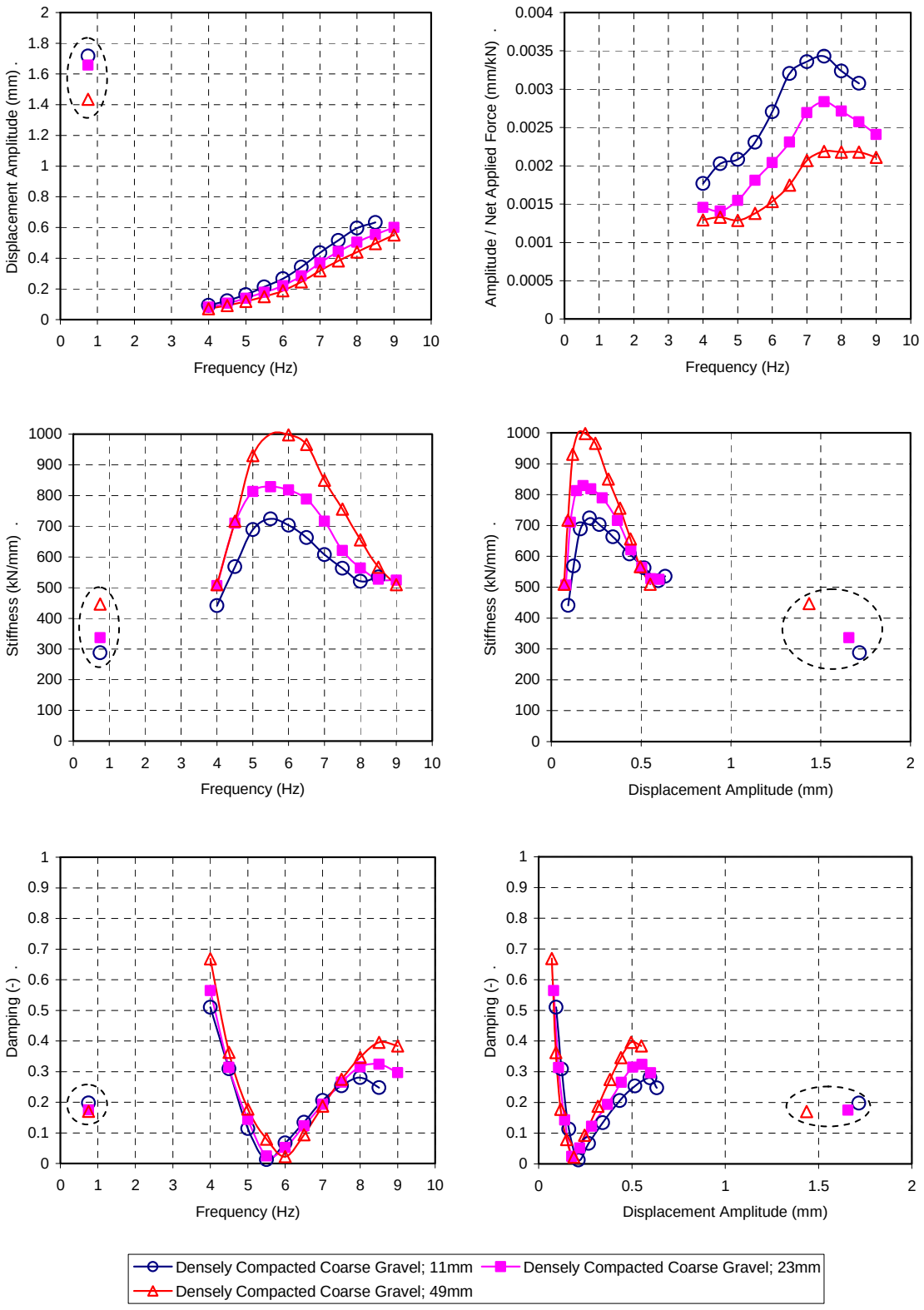

Figure 8-7 Summary of response to dynamic shaker loadings for pile cap with densely compacted coarse gravel backfill

the associated displacement amplitudes (the shaker cannot generate large forces, and hence displacements, at low frequencies).

The large resistance provided by the densely compacted coarse gravel caused the displacement amplitudes from the dynamic shaker loading to be too small for results to be consistent enough between the two types of loading for comparison (a range of 1.4 to 1.7 mm from the actuators versus less than 0.6 mm from the shaker). Extrapolation of the general trends from the dynamic shaker loading data to the displacement amplitude levels from the cyclic actuator loading is impractical due to the curvilinear nature of the trends.

8.7 Passive Earth Pressure Distributions

A vertical array of six earth pressure cells evenly distributed in the central portion of the pile cap was used to measure the passive earth pressure from the backfill soil directly. These measurements were made in addition to the load-displacement response data from the actuators. Figure 8-8 shows the pressure measured by the pressure cells with depth at the end of each static push interval.

The pressure cells show the expected general trends of increasing pressure with depth and increasing magnitude with increasing pile cap displacement. However, the pressure cells at 0.42 m and 1.26 m appear to go against the expected trends by decreasing relative to the pressure cell above them; as a result, the measured pressure distribution does not match the typical representation of pressure increasing with depth. This same behavior was observed in the case of the densely compacted fine gravel backfill, suggesting that the variations are due to either the measuring devices themselves

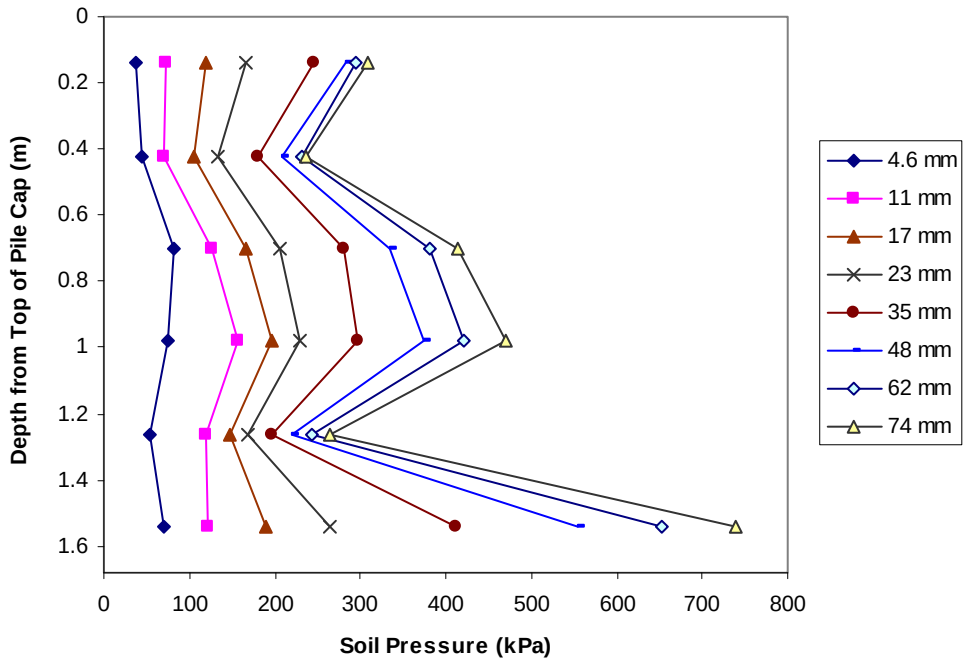

Figure 8-8 Earth pressure distribution as a function of pile cap displacement with densely compacted coarse gravel

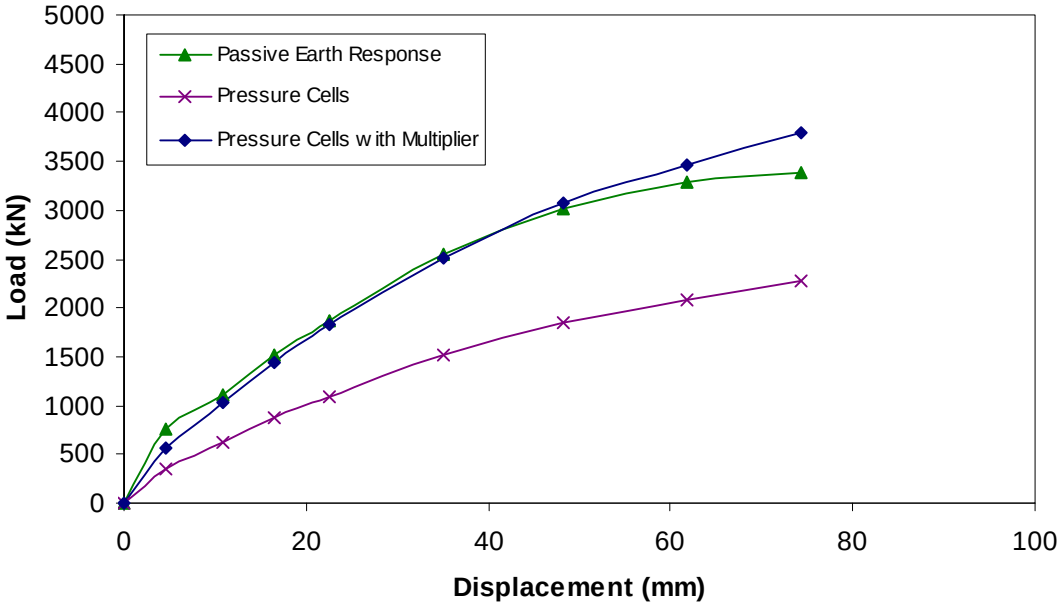

Figure 8-9 Comparison of earth forces based on actuators and pressure cells for densely compacted coarse gravel backfill

or to differential compaction across lift thickness. The irregularities in the pressure cell profile discussed in Section 4.5 are not present in this case. The rate of pressure increase appears to slow in the last several pile cap displacement intervals, indicating that the passive resistance of the backfill may be approaching its fully mobilized resistance.

Figure 8-9 shows the backfill force calculated by multiplying each measured pressure by the corresponding contributory areas of the pile cap face. In general, the resulting force-displacement curve has a similar trend to the actuator-based curve, but it is systematically lower. Applying a multiplier of 1.67 (the inverse of 0.6 determined in Section 4.5) to the cell-based curve provides an improved match with the actuator-based curve, although the pressure cell-based curve suggests that the ultimate passive resistance may not be mobilized until a further displacement level. This observation, however, hinges on the validity of an assumed, constant multiplier).

8.8 Cracking and Vertical Movement of Backfill

Figure 8-10 is a two part plot showing the effect of static and dynamic testing on the surface of the densely compacted coarse gravel backfill area. The first part of the figure is a map of the surface cracks that formed during each static push of the pile cap. Surface cracks in the backfill indicate the presence of failure surfaces within the soil.

Due to the cohesionless, coarse-grained nature of the material, coupled with dynamic vibration from the eccentric mass shaker, the soil grains tended to shift during testing, potentially obscuring cracks. A thin layer of fine-grained material was spread over the densely compacted coarse gravel to avoid crack obfuscation during the course of the test. The majority of the cracks are concentrated around the edges of the pile cap

face. These cracks are caused by internal shear stresses radiating out from the cap face and are consistent with a three dimensional shape of the failure zone. Another group of cracks occur in the center of the backfill zone, including several cracks oriented in the direction of pile cap movement, which may be due to localized failure surfaces caused by shifting particles as the backfill displaces. The pink horizontal cracks distributed through the central region of the backfill zone occurred as the soil relaxed after the pile cap was unloaded and are not forcibly related to shear failure planes due to loading.

The second part of the figure is a contour map of the change in elevation along the surface of the backfill area during testing. The typical elevation change, as represented by the median elevation change in a given row (parallel to the face of the cap) of grid nodes, is about 35 mm at 1.2 m from the pile cap face. The heave ranges to about 45 mm within about a meter and a half from the pile cap face. Calculations in PYCAP indicate that a log-spiral failure surface should daylight at approximately 6 m from the face of the cap. While the contour map shows heave occurring throughout the entire backfill, the bulk of the heave occurs within the first 4 or 5 m of the backfill zone, with the heave at greater distances generally less than 10 mm higher than the original backfill surface elevation. As the rate of elevation change beyond 6 m is minimal, it is reasonable to expect that the failure surface daylights in the vicinity of the PYCAP prediction.

The correlation between the heave profile and log-spiral failure surface is illustrated by the cross-sectional view in Figure 8-11, in which the failure surface calculated in the spreadsheet program PYCAP using the best-fit parameters discussed in Section 8.3.1: in-situ test-based soil friction and cohesion values of 44° and 13.7 kPa, respectively, with an interface friction angle of 26° iterated to match the measured

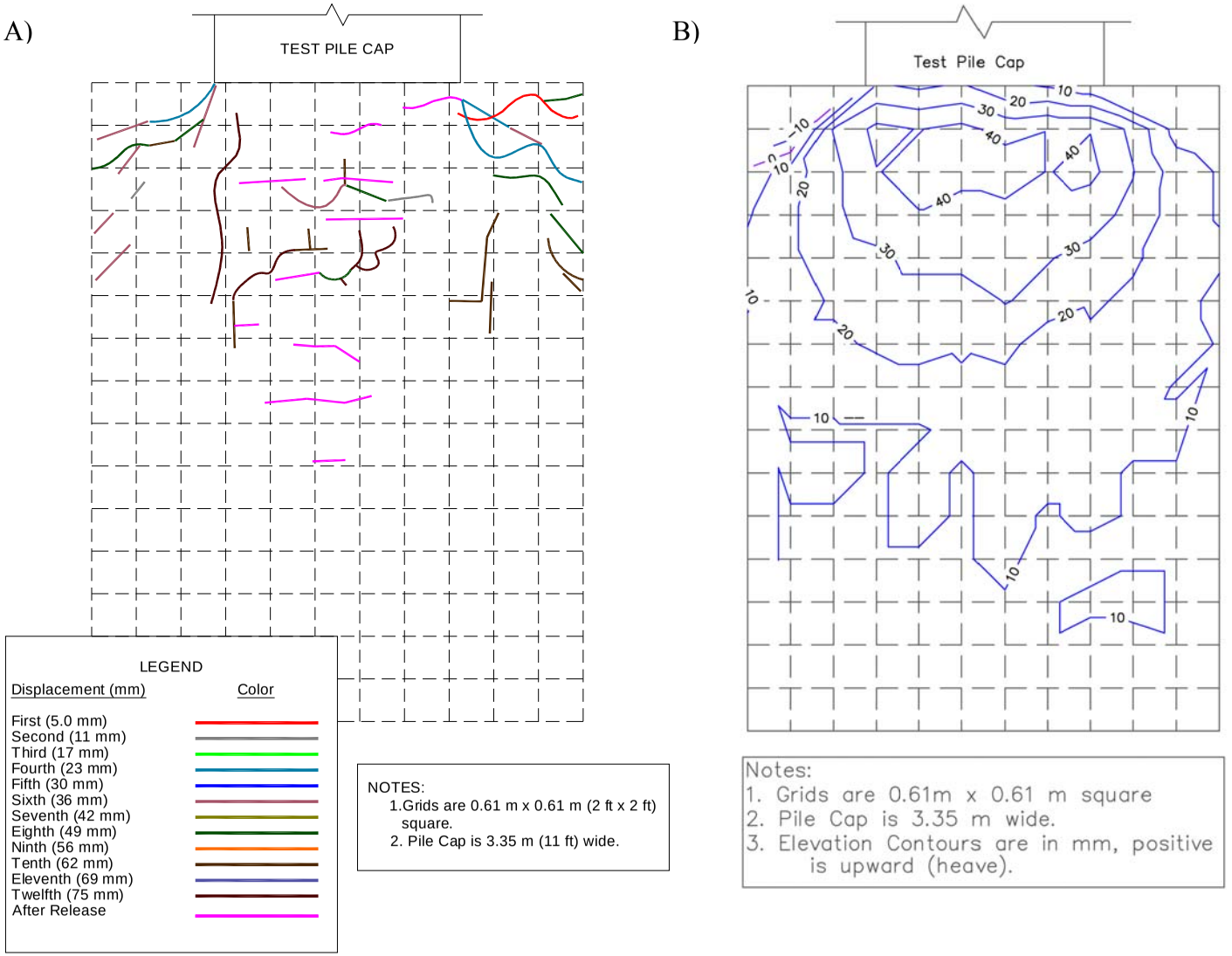

Figure 8-10 Crack pattern (A) and heave contour (B) maps for densely compacted coarse gravel backfill

response (i.e., Case V). The log-spiral surface daylights close to where the elevation change becomes negligible. In the densely compacted coarse gravel backfill, the sudden change in elevation in the area immediately in front of the pile cap suggests a fairly strong interaction between the backfill and the wall surface; hence, the best-fit parameters were chosen to reflect that interaction. The heave profile shown in the figure is magnified ten times to make the elevation change more appreciable.

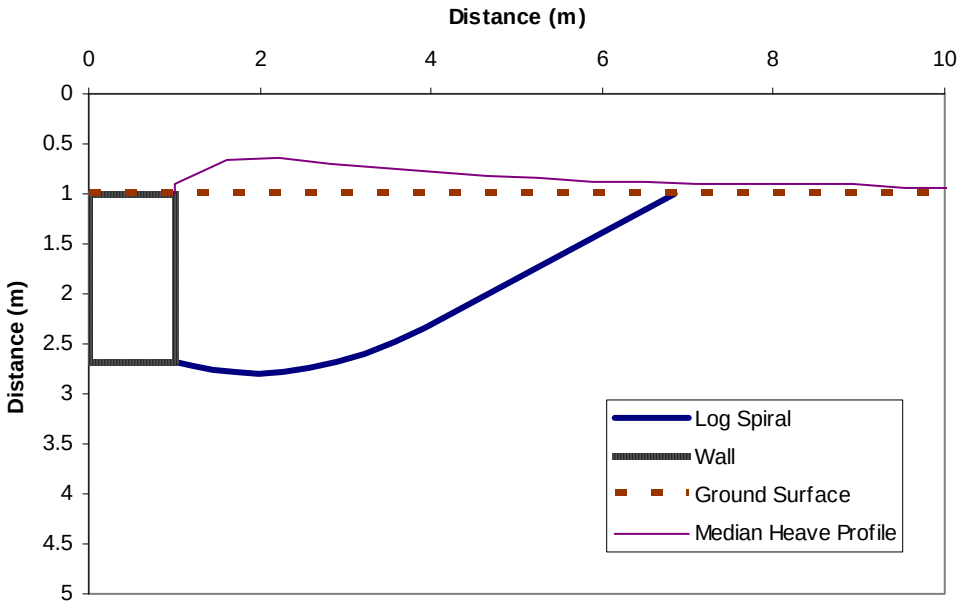

Figure 8-11 Heave profile for densely compacted coarse gravel compared with log-spiral failure surface from PYCAP

8.9 Horizontal Movement of Backfill

String potentiometers were used to measure movement in the backfill. Figure 8-12 shows the movement of each of the monitoring points in the densely compacted

coarse gravel backfill compared to the movement of the pile cap face. The backfill displacement ranges from 75 mm (100% of cap displacement) at the cap face to 15 mm (20% of cap displacement) at 5.5 m from the cap face. The translational movement at the monitoring point 5.5 m from the cap face represents the amount of the pile cap displacement not absorbed through compressive strain up to that point.

Figure 8-13 shows the compressive strain corresponding to each static push of the pile cap. The 0.6-m interval closest to the cap experiences the most compressive strain for a given displacement level, in this case almost twice the strain in any other interval. With the exception of the second 0.6-m interval, which appears to strain much less than the intervals both before and after it, the compressive strain in the remainder of the intervals is fairly evenly distributed. It is possible that some of the strain beyond 1.2 m from the face of the cap is associated with the development of progressive slip planes as soil friction is mobilized. The potential sensitivity of the string potentiometer measurements to differential pushing of the pile cap (not all the monitoring stakes were on the same end of the cap face) may be indicated by minor variations from interval to interval. Tipping of the monitoring stakes themselves may also affect the variations shown in the figure. In this particular case, some of the strain shown in the first interval may occur in the second interval, which would make the distribution more uniform with distance, but still highest near the face of the pile cap.

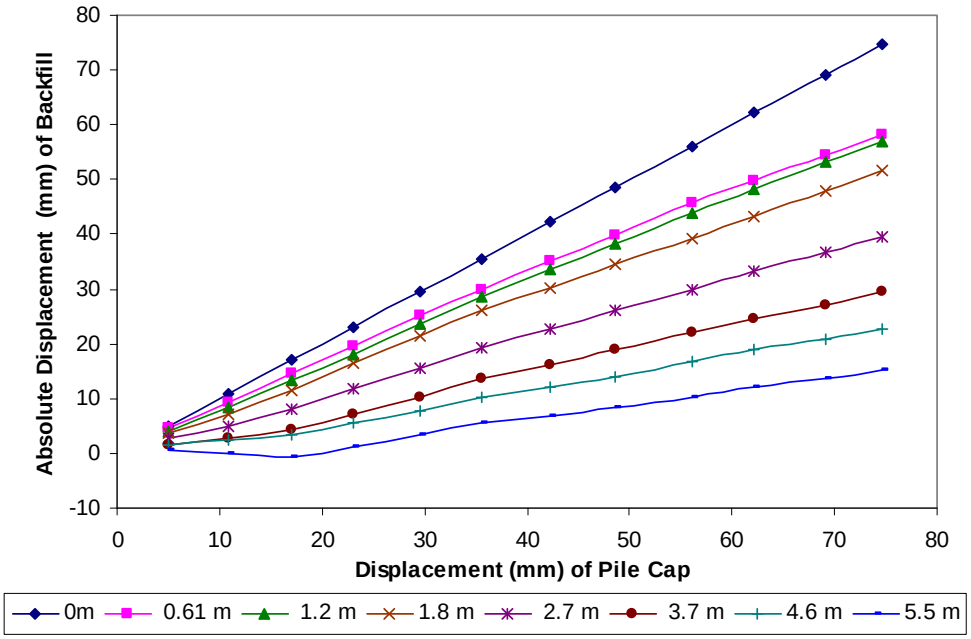

Figure 8-12 Displacement of monitoring points in densely compacted coarse gravel backfill

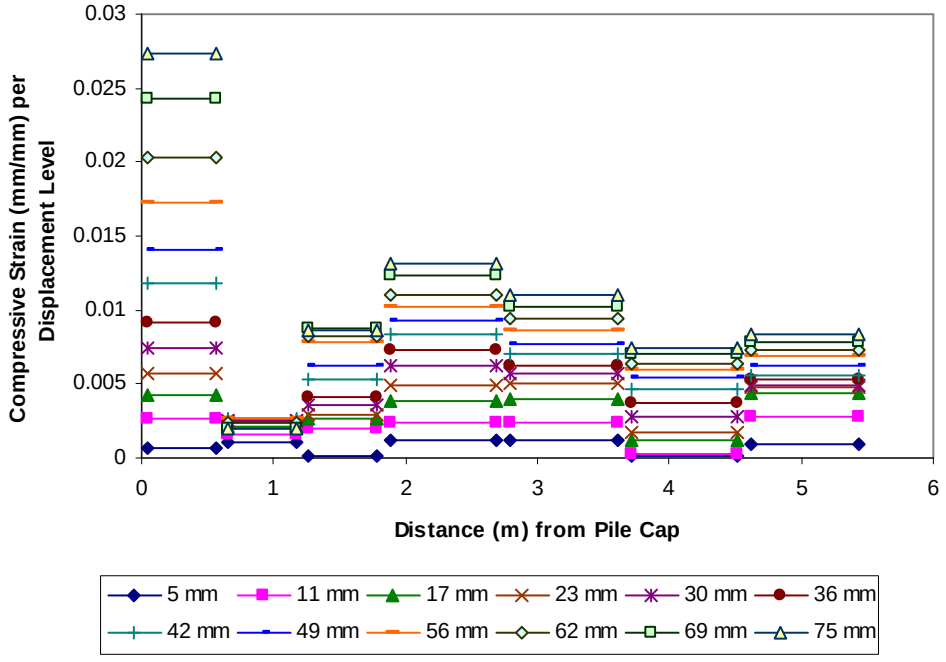

Figure 8-13 Strain per displacement level for densely compacted coarse gravel backfill

9 Pile Cap with Loosely Compacted Coarse Gravel Backfill

9.1 General

The pile cap with loosely compacted coarse gravel backfill was tested on June 21, 2007. Table 9-1 summarizes the test in terms of loads and displacements measured at the end of each "static push" with the actuators. The table also indicates the order in which actuator-based cyclic loads and shaker-based dynamic loads were applied. At some displacement increments, cyclic and dynamic loadings were not applied in order to help assure that the test foundation displaced sufficiently into the backfill for the load path to return to the static-backbone loading curve. No significant deviations from the general test procedure occurred during this test.

9.2 Load-Displacement Response

Figure 9-1 shows the entire actuator load verses pile cap displacement relationship for the test with loosely compacted coarse gravel. Static pushes, actuator cycles and shaker cycles are represented by green, blue, and red data points, respectively. Section 4.2 provides some discussion relative to the interpretation of this data. Unlike the loosely compacted fine gravel, the loosely compacted coarse gravel did not exhibit a substantial loss of resistance after the first couple sets of cyclic and dynamic loadings.

Table 9-1 Summary of test with loosely compacted coarse gravel backfill

Displacement Interval	Displacement (mm)	Actuator Load (kN)	Actuator Cycles	Shaker Cycles
1	6.9	490	First	Second
2	15	639	None	None
3	22	990	Second	First
4	29	925	None	None
5	35	1311	First	Second
6	42	1313	None	None
7	47	1705	Second	First
8	53	1741	None	None
9	58	2157	First	Second
10	64	2226	None	None
11	70	2652	Second	First
12	77	2719	None	None
13	82	3082	First	Second

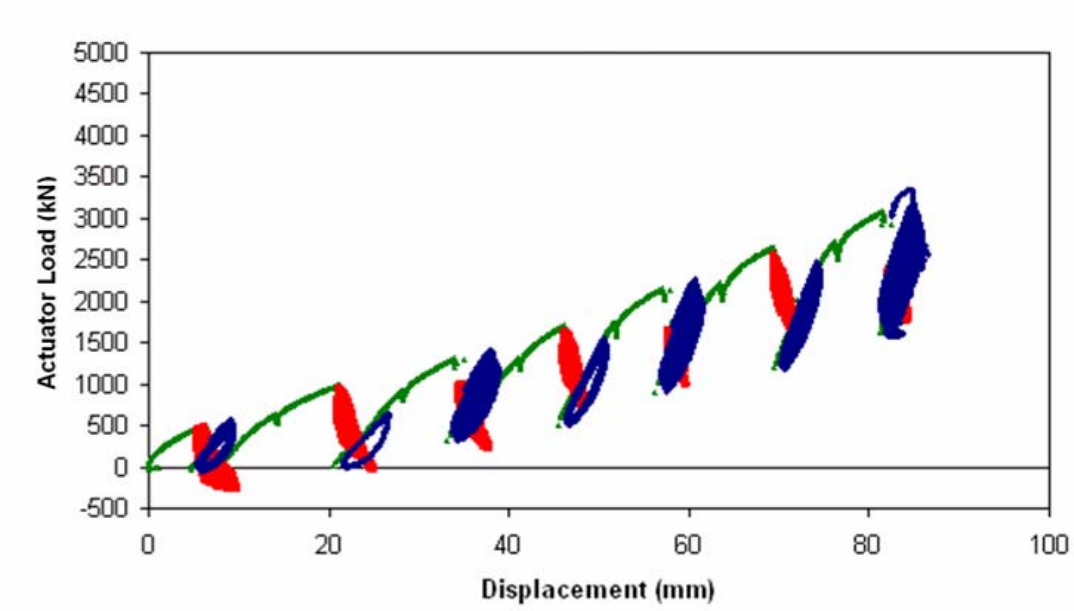

Figure 9-1 Actuator load versus pile cap displacement with loosely compacted coarse gravel backfill (Test 10; June 21, 2007)

Figure 9-2 shows three load-displacement response curves for the pile cap: one for the response with backfill in place (the "total" response, which is the equivalent monotonic response or backbone curve derived from the data shown in Figure 9-1); one for the response with no backfill present (the "baseline" response); and one showing the passive earth response of the backfill (obtained by subtracting the baseline response from the total response).

The curves show that total response and baseline response increase at different rates until the end of testing for the loosely compacted coarse gravel backfill material. At about 60 mm, the total response and baseline response curves appear to increase at a similar rate, but the backfill response merely seems to experience a gentle slope change,

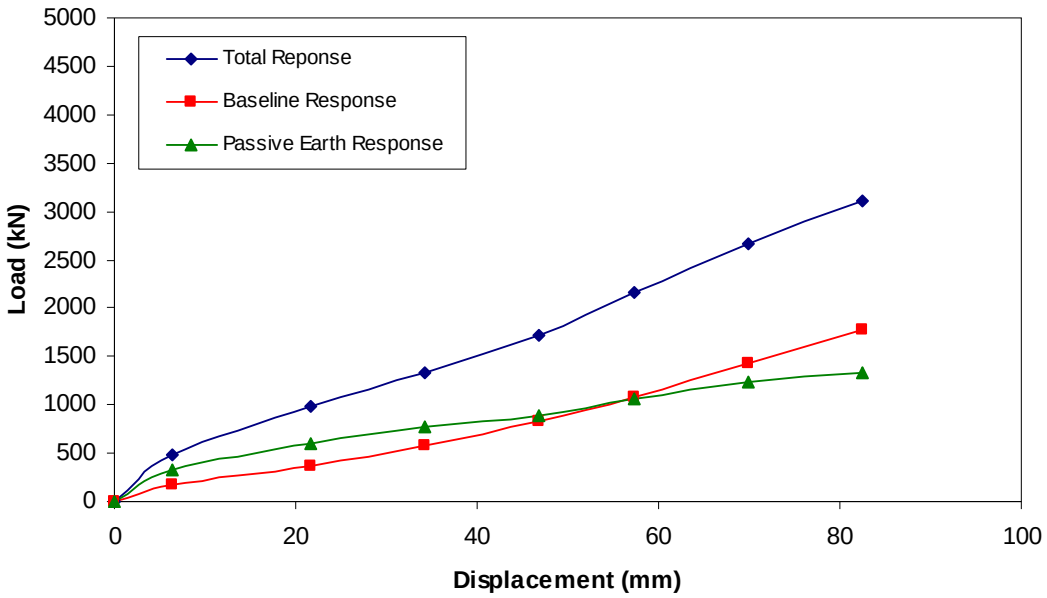

Figure 9-2 Total, baseline, and passive earth responses for pile cap with loosely compacted coarse gravel backfill

which makes it difficult to determine when the backfill resistance is fully mobilized. The resistance likely would have increased past the 1340 kN maximum value had the backfill been allowed to continue displacing into the soil. The ultimate passive resistance of the backfill is assumed to develop at a pile cap displacement of 148 mm – twice that developed during the densely compacted coarse gravel backfill test, as suggested by Clough and Duncan (1991) for a loose or medium dense material relative to a dense material. This displacement will be used in subsequent analyses, which will be presented later in this thesis, and corresponds to a displacement to wall height ratio of about 0.088, or say 9%.

9.3 Calculated Passive Earth Forces

Commonly used methods for calculating passive earth pressure include Rankine theory, Coulomb theory, and log-spiral theory. Log-spiral theory is typically considered the most accurate of these methods (see, for example, Cole and Rollins (2006) and Duncan and Mokwa (2001)). Three methods of estimating the development of passive pressure with wall displacement are evaluated in this section. Two of these methods, PYCAP and ABUTMENT (LSH method) involve applications of log-spiral theory and a hyperbolic load-displacement relationship. The third approach evaluated in this section is an empirical load-displacement relationship based on full-scale testing of an abutment with typical backfill conditions (see discussion of CALTRANS method in Section 4.3.3).

9.3.1 Calculated Response Using PYCAP

Passive earth resistance was calculated using the modified PYCAP spreadsheet introduced in Section 4.3.1. Table 9-2 summarized key inputs and outputs for several

cases while Figure 9-3 compares the measured passive earth response to the computed passive resistance curves from each case. Case I uses the friction angle correlation developed by Duncan (2004) as discussed in Section 3.4.2 and results in a computed ultimate passive resistance that is 233% greater than the measured resistance. The initial soil modulus value used in these analyses, 19150 kPa, is consistent with the loose to medium values in the "normally loaded" range given by Duncan and Mokwa (2001) and is at the very low end of the range of loose "preloaded or compacted" sand and gravel. In Case II, the interface friction angle was iteratively reduced to a very low value to provide a better match with the ultimate passive resistance, and results in an estimate of resistance that is within 5% of the measured backfill response. In-situ direct shear test results determined the soil friction angle in Case III and the interface friction angle was estimated using a δ/ϕ ratio of 0.6, based on laboratory results from the densely compacted fine gravel backfill material. The Case III curve does not match the measured ultimate passive resistance as nicely as that provided by Case II parameters, however, the Case III parameters provide an estimate that is within 16% of the measured resistance and provides a good representation of the soil behavior. Case IV is similar to Case III, except an assumed δ/ϕ ratio of 0.75 is used. Case IV overestimates the measured response by about 40%. The Case II parameters obviously provide the best match to the measured passive earth response and are referred to as the "best fit" parameters for this soil. Case III provides a reasonable match with little parameter manipulation, which makes it a good choice for design situations. Hence, the Case III parameters are considered the "most representative" parameters. In Case V, the shear strength parameters found during the in-situ direct shear test for the loosely compacted coarse gravel are reduced to 85% of their

Table 9-2 Parameter summary for case comparison in PYCAP for loosely compacted coarse gravel backfill

Parameter	Case I	Case II	Case III	Case IV	Case V
ϕ (°)	50	50	40	40	35.5
c (kPa)	0	0	0	0	0
δ (°)	30	4.2	24	30	35.5
γ_m (kN/m^3)	20.23	20.23	20.23	20.23	20.23
E (kPa)	19150	19150	19150	19150	19150
ν	0.3	0.3	0.3	0.3	0.3
k (kN/mm)	120	120	120	120	120
Δ_{max} (mm)	0.088	0.088	0.088	0.088	0.088
Δ_{max}/H	148	148	148	148	148
R_f	0.67	0.92	0.90	0.88	0.91
R_{3D}	2.00	1.64	1.72	1.82	1.72
K_p	33.9	9.3	11.1	13.7	9.2

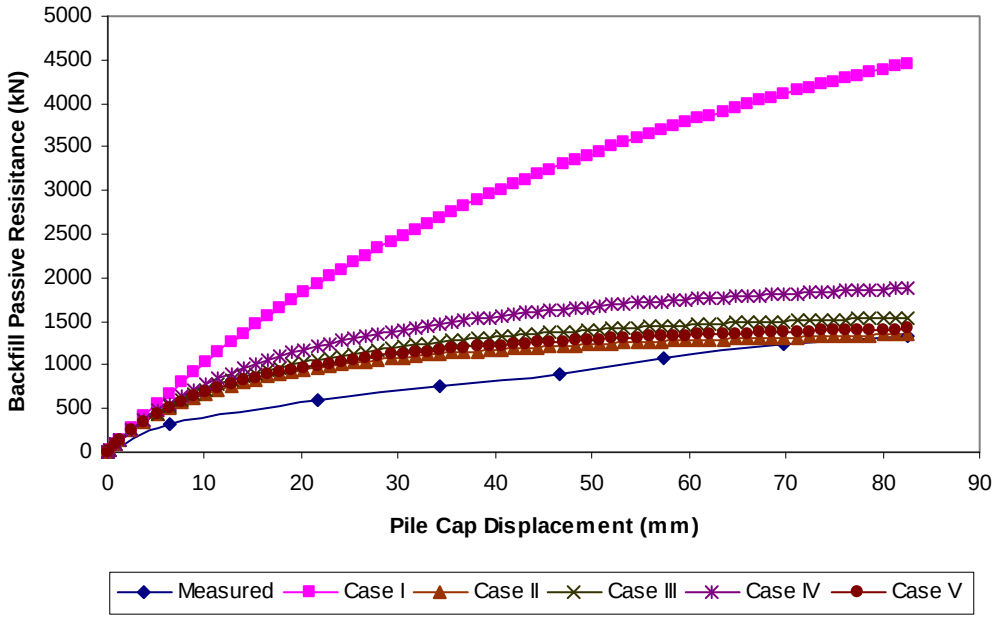

Figure 9-3 PYCAP case comparison for loosely compacted coarse gravel backfill

original value (the tangent of the original densely compacted coarse gravel friction angle was multiplied by 0.85 and the inverse tangent of that value became the new soil friction angle for the loosely compacted coarse gravel). As the Figure 9-3 shows, the match obtained using the reduced parameters is quite reasonable. As stated previously in Section 7.3.1, this approach resembles that suggested by Terzaghi and Peck (1967) for dealing with local shear effects for the bearing capacity of loose to medium sands; however, the fraction of shear strength used is 85% rather than 67% as suggested by Terzaghi and Peck. Additional discussion regarding this matter is presented in Section 10.2.

9.3.2 Calculated Response Using ABUTMENT (LSH)

Passive earth resistance was also calculated using the LSH method. Table 9-3 summarizes key inputs and outputs for several cases while Figure 9-4 shows the measured and calculated passive resistance curves for each case. Case I is based on the Duncan (2004) correlation equation mentioned in the previous section and overestimates the measured resistance by nearly 200%. In Case II, the interface friction angle is reduced to provide a better match with the measured response. Case III uses in-situ direct shear test results for the friction angle and a δ/ϕ ratio of 0.6, resulting in a calculated load-displacement curve that compares favorably with the measured passive resistance. Case II and Case III both result in excellent estimates of the measured resistance. Case IV is similar to Case III, except the δ/ϕ ratio is assigned a typical value of 0.75. Case IV overestimates the measured curve by about 15%, but matches the initial portion of the curve about as well as Cases II and III. As the parameters from Case II and Case III

Table 9-3 Parameter summary for case comparison in ABUTMENT for loosely compacted coarse gravel backfill

Parameter	Case I	Case II	Case III	Case IV
ϕ (°)	50	50	40	40
c (kPa)	0	0	0	0
δ (°)	30	4.2	24	30
γ_m (kN/m^3)	20.2	20.2	20.2	20.2
ε_{50}	0.0074	0.0074	0.0074	0.0074
ν	0.3	0.3	0.3	0.3
R_f	0.98	0.98	0.98	0.98
R_{3D}	2.00	1.64	1.72	1.82
K_{ph}	24.4	9.8	9.7	10.6

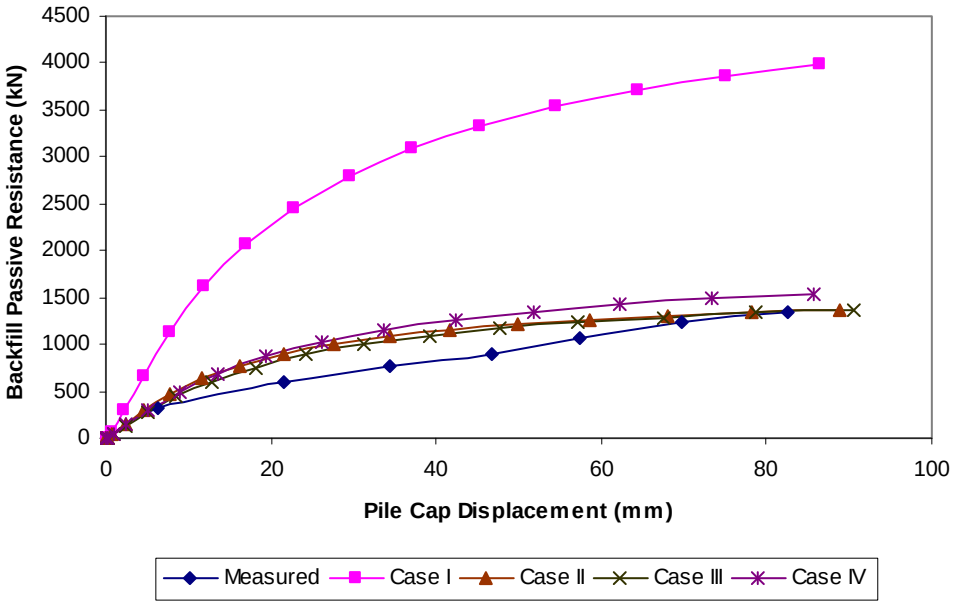

Figure 9-4 ABUTMENT case comparison for loosely compacted coarse gravel backfill

result in similar predictions, the Case III parameters, which involve less manipulation of the available data, are the most representative parameters for this material and the best parameters for design using the LSH method.

9.3.3 Calculated Response Using CALTRANS

The CALTRANS method was used to estimate passive resistance, as shown in Figure 9-5. For the loosely compacted coarse gravel, the method estimates the passive resistance to within 5% of the final measured resistance; thus, the CALTRANS method provides a good match to the measured resistance at the displacement levels reached during testing for this material. This is unexpected due to wall type and backfill background considerations of the method. The initial stiffness from the CALTRANS method is much too high to realistically represent the loading behavior of the loosely compacted coarse gravel backfill, and it appears that the method would underestimate the resistance if the pile cap were to be pushed to higher displacement levels.

9.4 Response to Cyclic Actuator Loading

After slowly pushing the pile cap to each target displacement, alternating combinations of cyclic actuator loads and dynamic shaker loads were applied to the test foundation. The response of the pile cap to the small displacement amplitude loading cycles from the actuator is presented and discussed in this section. Figure 9-6 shows loop displacement amplitude, stiffness, loop area, and damping ratio for the pile cap with

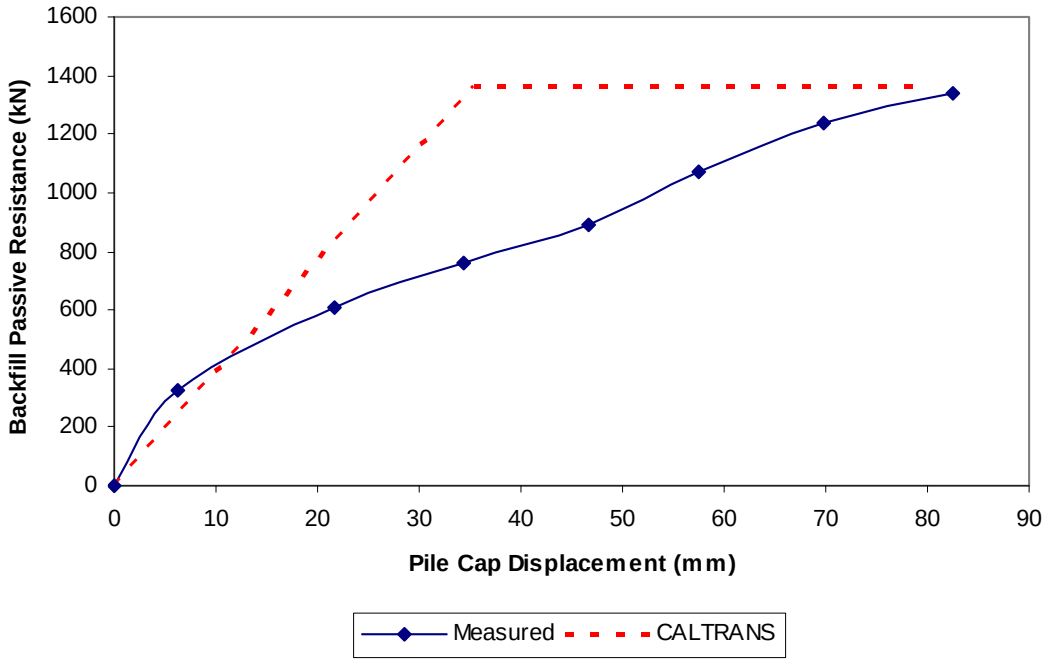

Figure 9-5 Comparison of measured and CALTRANS-based passive resistance for loosely compacted coarse gravel backfill

loosely compacted coarse gravel backfill as a function of pile cap displacement. Values are based on the median of the 15 low frequency cycles performed at each displacement level. Loop displacement amplitude ranges from about 1.9 to 2.5 mm, with a general trend of decreasing amplitude with pile cap displacement level. The stiffness increases from 100 to nearly 300 kN/mm as the cap displacement increases to about 67 mm, then decreases slightly at 82 mm, the final cap displacement level. The damping ratio decreases fairly linearly from 28% to 15% until about 67 mm of cap displacement, after which the damping ratio increases to about 20%. The median damping ratio for the cyclic actuator loading over the course of the test is 21%. The saw-tooth shaped trend seen in other tests due to the alternating order cyclic and dynamic loading is evident in each data type in Figure 9-6 to some degree. The stiffness and damping values appear to

be more similar to those calculated for the pile cap without backfill present than those calculated with the densely compacted coarse gravel backfill present.

9.5 Response to Dynamic Shaker Loading

After slowly pushing the pile cap to each target displacement, alternating combinations of small displacement cyclic actuator loads and dynamic shaker loads were applied to the test foundation. The response of the pile cap to the small displacement dynamic shaker loading is presented and discussed in this section. The first row of graphs in Figure 9-7 shows loop displacement amplitude as well as loop displacement amplitude normalized by the cyclic amplitude of net applied force from the shaker and actuators as functions of the forcing frequency. The second and third rows of graphs show the calculated reloading stiffness and damping, respectively, of the pile cap system. These parameters are shown in terms of forcing frequency in the left column. If non-linear behavior is present, these properties will also depend on the loop displacement amplitude; hence, in the right column, these parameters are shown in terms of the displacement amplitude. The data appear to suggest that both frequency and displacement amplitude must be considered when interpreting test results. The individual line series shown in the graphs represent different static pile cap displacement levels in which dynamic shaker cycles were applied before the slowly applied actuator cycles.

The peaks in the normalized displacement amplitude graph correspond to the damped natural frequency of the system, which appears to remain at approximately 7 Hz as the pile cap displaces farther into the backfill. Dynamic stiffness initially ranges from

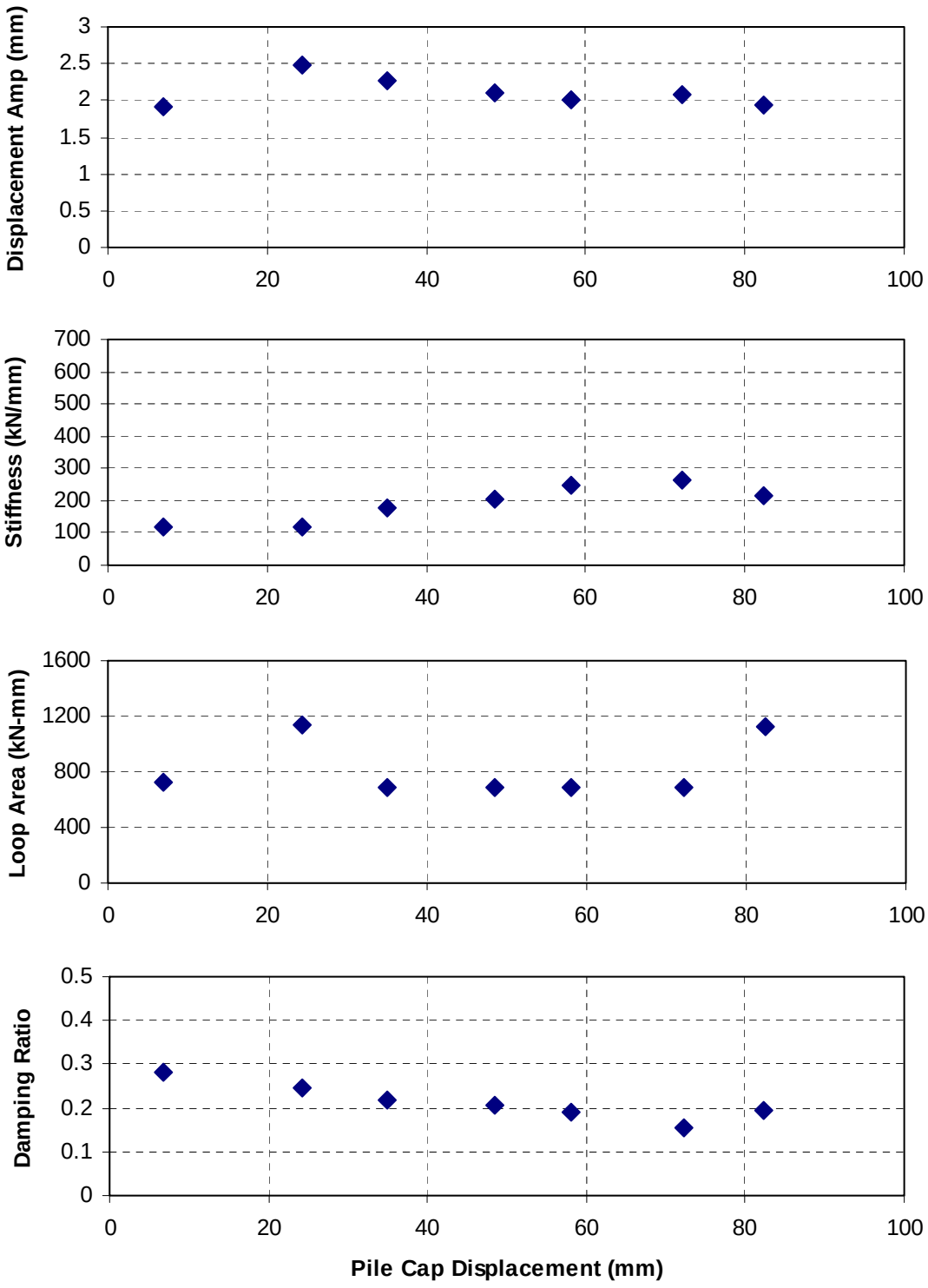

Figure 9-6 Summary of response to cyclic actuator loadings for pile cap with loosely compacted coarse gravel backfill

300 to over 500 kN/mm as a function of frequency, peaking at about 5 Hz, and then decreasing to values from just under 200 to about 100 kN/mm between 8.5 and 9.5 Hz, after which the stiffness increases to about 200 kN/mm in the last forcing frequencies of the test. Calculated damping values vary greatly with respect to forcing frequency and displacement amplitude. The minimum damping appears to be less than 5% at 5.5 Hz and at 0.3 mm of displacement amplitude. At higher frequencies and displacements, the damping ratio increases up to about 60% (roughly corresponding to the calculated decreasing stiffness) until 8.5 Hz, where the decrease in damping corresponds with the increasing stiffness. The half-power bandwidth approach was used to interpret the normalized displacement amplitude, yielding a damping ratio of 23% for the 22 and 47 mm displacement intervals. The half-power bandwidth approach could not be used for the 70 mm displacement interval due to the distribution of frequency and displacement values. As stated previously in Section 5.4, the observed variations in stiffness and damping with frequency are likely due to variations in phase between passive earth forces (whether acting on the piles or on the pile cap itself) and the inertial force from the foundation as suggested by Tokimatsu et al. (2004) in their work with large shaking table models of pile cap foundation systems. Some variation is also likely due to the simple lumped, constant, mass model used.

9.6 Comparison of Cyclic Actuator and Dynamic Shaker Responses

Figure 9-7 includes displacement amplitude, stiffness, and damping ratio calculated from the actuator-driven cycles (~ ¾ Hz) at the displacement levels given for the shaker derived values (points in dashed ovals). The actuator-based values shown are

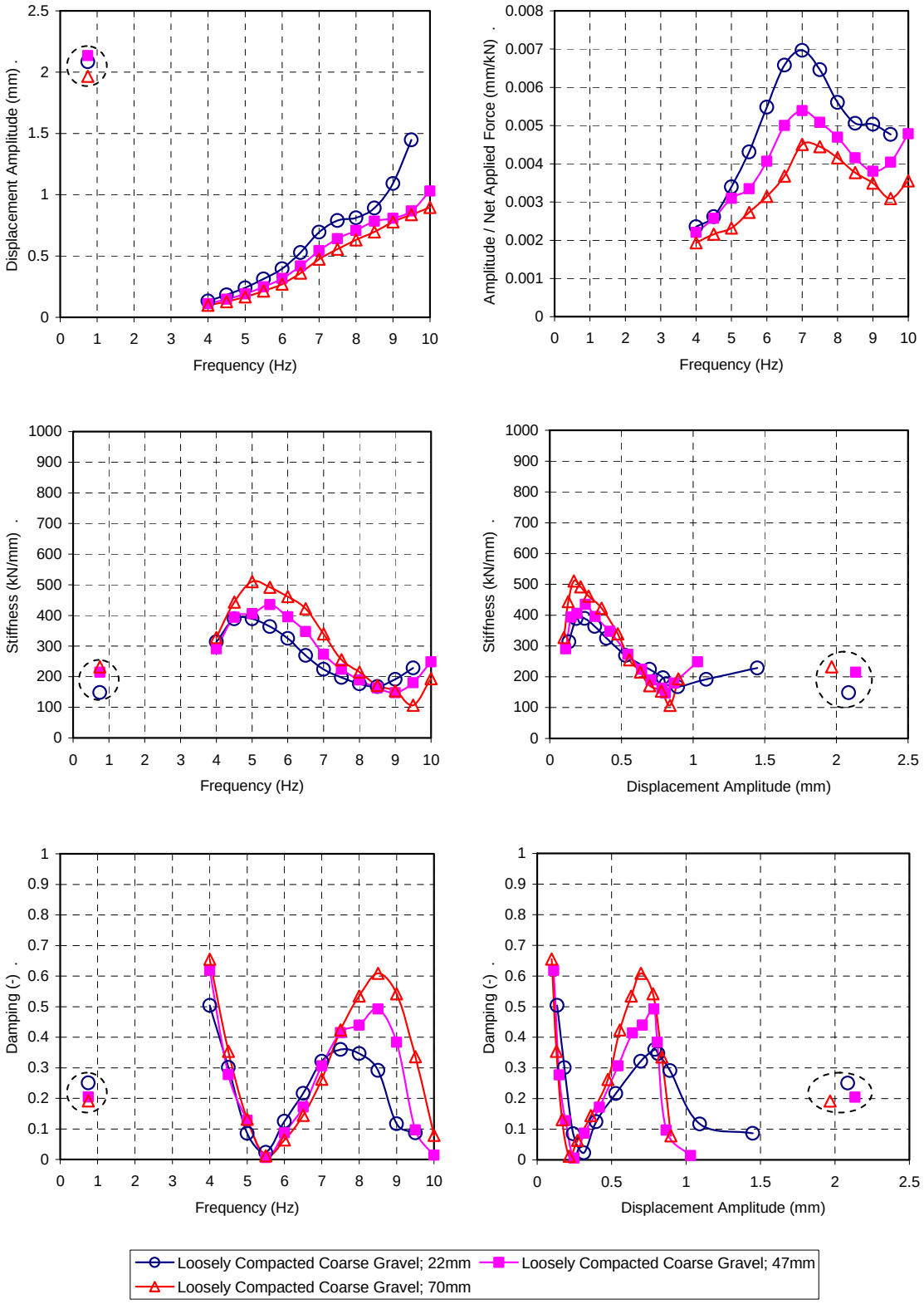

Figure 9-7 Summary of response to dynamic shaker loadings for pile cap with loosely compacted coarse gravel backfill

averaged from previous and subsequent pile cap displacement levels. These averages represent the stiffness and damping that would have been calculated if the actuator cycles had been performed before the shaker cycles. In terms of frequency, it can be difficult to compare the static and dynamic methods because of the difference in the associated loop displacement amplitudes (the shaker cannot generate large forces, and hence displacements, at low frequencies).

Maximum loop displacement levels due to dynamic shaker loading were just less than 1.5 mm for the 22 mm static push and decreased to about 1 mm for the 47 and 70 mm static pushes. Average loop displacement levels due to cyclic actuator loading were about 2 mm, which makes it difficult to compare the static and dynamic methods due to the difference in the associated loop displacement amplitudes. The shaker was unable to generate enough force in the range of forcing frequencies tested to produce comparable loop displacement amplitudes for ready comparison between cyclic and dynamic loading. The equivalent damping ratio under cyclic loading conditions (about 20%) is bracketed by the general range of damping ratios observed under dynamic loading conditions.

9.7 Passive Earth Pressure Distributions

A vertical array of six earth pressure cells evenly distributed in the central portion of the pile cap face was used to measure the passive earth pressure from the backfill soil directly. These measurements were made in addition to the load-displacement response data from the actuators. Figure 9-8 shows the pressure measured by the pressure cells with depth at the end of each static push interval.

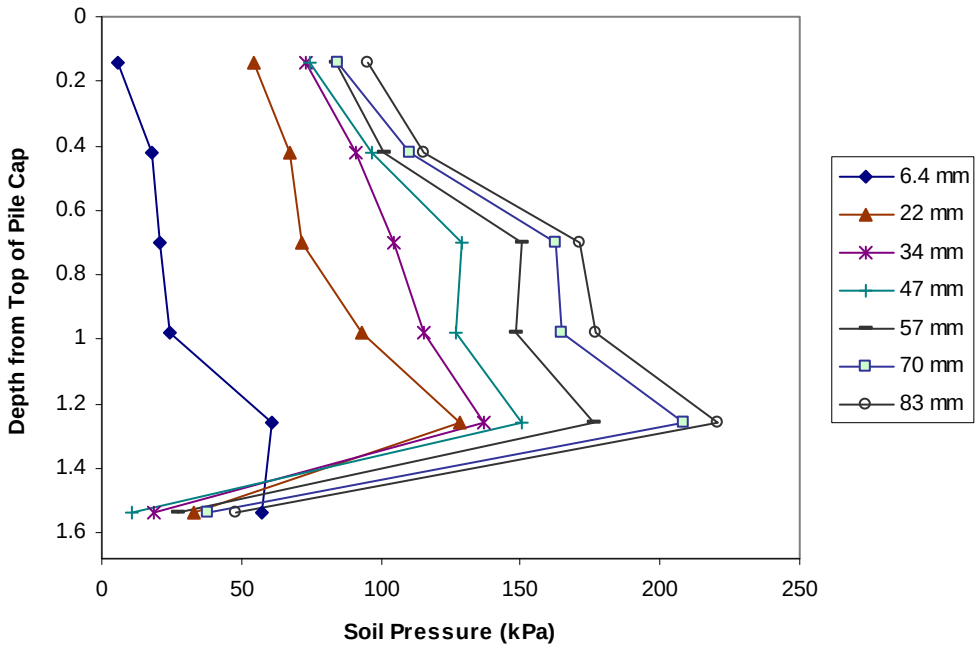

Figure 9-8 Earth pressure distribution as a function of pile cap displacement with loosely compacted coarse gravel

The pressure cells show the expected general trends of increasing pressure with depth and increasing magnitude with increasing pile cap displacement. However, for the measurements from the pressure cell farthest from the ground surface, this trend does not appear to apply. The bottom pressure cell shows a substantial amount of pressure in the first push, followed by a steady decrease to near zero pressure in subsequent pushes. The same behavior occurs in other backfill tests and is discussed in Section 4.5.

Inspection of the figure shows that after the first five displacement increments, there is a drop in measured pressure. This drop in pressure is followed by an increase in pressure followed by a drop in pressure, and so on until the end of testing. This behavior is consistent with the overall loss in resistance observed after the application of the actuator and shaker loadings. In these instances, no cyclic or dynamic loadings were

applied during interval after the pressure drop (as shown in Table 9-1) in order to help assure that sufficient displacement had occurred for the load path to return to the static-backbone loading curve before applying the cyclic and dynamic loadings again.

Figure 9-9 shows the backfill force calculated by multiplying each measured pressure by the corresponding contributory areas of the pile cap face. In general, the resulting force-displacement curve has a similar trend to the actuator-based curve, but it is systematically lower. Applying a multiplier of 1.67 (the inverse of 0.6 determined in Section 4.5) to pressures for the displacement intervals for which the load path returned to the backbone (i.e., the even-numbered intervals) provides an excellent match with the actuator-based curve. The data suggests that the loosely compacted coarse gravel backfill does not mobilize ultimate passive resistance in the displacement range evaluated during the test.

9.8 Cracking and Vertical Movement of Backfill

Figure 9-10 is a two part plot showing the effect of static and dynamic testing on the surface of the loosely compacted coarse gravel backfill area. The first part of the figure is a map of the surface cracks that developed during each static push of the pile cap. The surface cracks in the backfill indicate the presence of failure surfaces within the soil.

Due to the cohesionless, coarse-grained nature of the material, coupled with the dynamic vibration from the eccentric mass shaker, the soil grains tended to shift during testing, potentially obscuring cracks. Unlike the densely compacted coarse gravel, no fine-grained veneer was placed on the surface of the loosely compacted coarse gravel

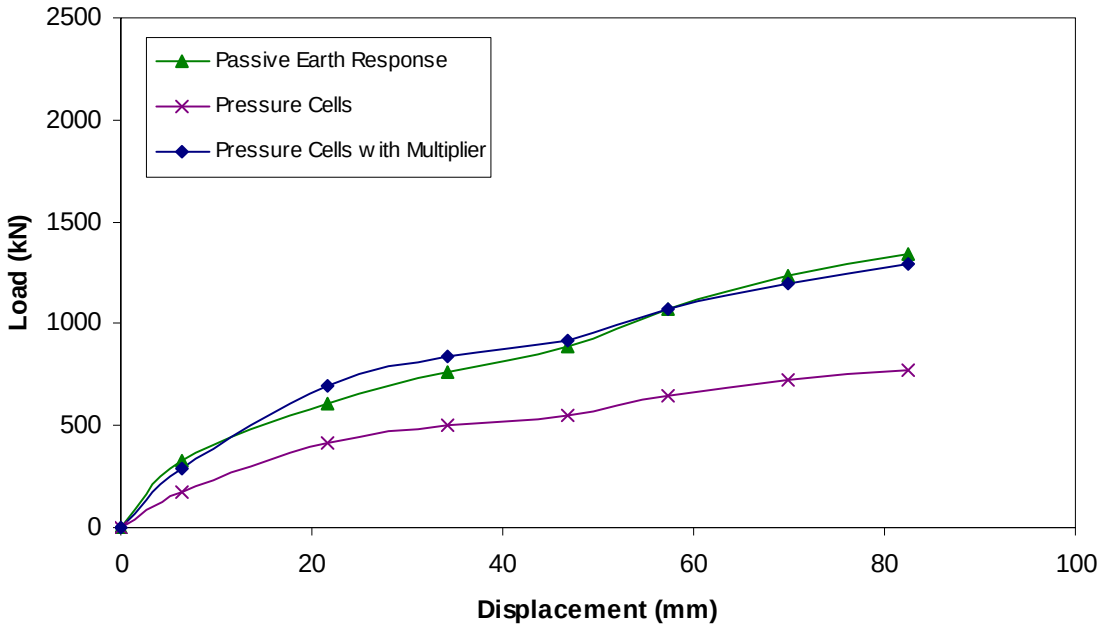

Figure 9-9 Comparison of earth forces based on actuators and pressure cells for loosely compacted coarse gravel backfill

backfill. Without a thin layer of fine material to elucidate them, it was extremely difficult to identify individual cracks along the open, granular, backfill surface. Unfortunately, too few cracks were visible enough to ascertain a stress distribution or failure pattern.

The second part of the figure is a contour map of the change in elevation along the surface of the backfill area during testing. The typical elevation change, as represented by the median elevation change in a given row (parallel to the face of the cap) of grid nodes, is about 30 mm of settlement directly adjacent to the pile cap face. The settlement ranges from 0 to over 100 mm of subsidence at individual survey nodes near the pile cap face, though some of the larger settlement values may be due to material loss near the boundaries of the backfill area, which may have affected the accuracy of the given typical settlement value near the face of the pile cap. The figure shows that most of the elevation

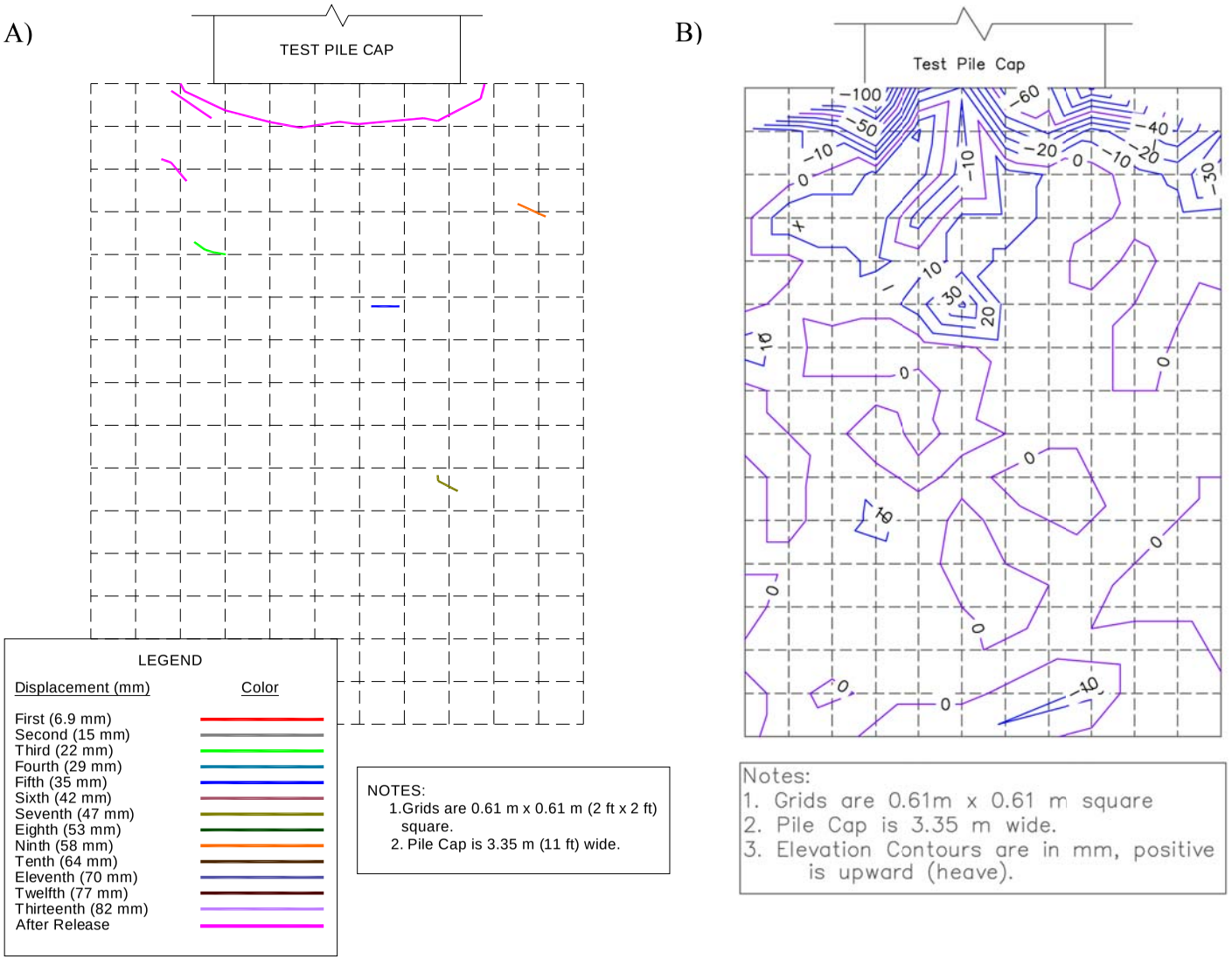

Figure 9-10 Crack pattern (A) and heave contour (B) maps for loosely compacted coarse gravel backfill

change occurred within the first meter or so of backfill. Little elevation change occurs beyond about 4 m from the face of the pile cap.

The contour map in the figure shows that the majority of the elevation change in the loosely compacted coarse gravel backfill was settlement. Figure 9-11 illustrates the correlation between the vertical movement in the backfill and the log-spiral failure surface calculated using Case III parameters for PYCAP discussed in Section 9.3.1: a friction angle of 40° based on the in-situ direct shear test results and a δ/ϕ ratio of 0.6. Also shown is the failure surface derived from Case II, which is more linear. As the figure illustrates, there is some to little curve to the log-spiral failure surface (depending on the case), suggesting that loosely compacted coarse gravel may fail according to mechanism similar to a Rankine passive failure wedge. The vertical displacement profile in the figure is magnified ten times to make the elevation change more appreciable.

9.9 Horizontal Movement of Backfill

String potentiometers were used to measure movement in the backfill. Figure 9-12 shows the movement of each of the monitoring points in the loosely compacted coarse backfill compared to the movement of the pile cap face. The backfill displacement ranges from 83 mm (100% of cap displacement) at the cap face to 5.9 mm (7% of cap displacement) at 5.5 m from the cap face. This translational movement represents the amount of the pile cap displacement not absorbed through compressive strain up to the monitoring point.

Figure 9-13 shows the compressive strain corresponding to each static push of the pile cap. The compressive strain ranges from 0.055 to 0.003 within the backfill zone. As

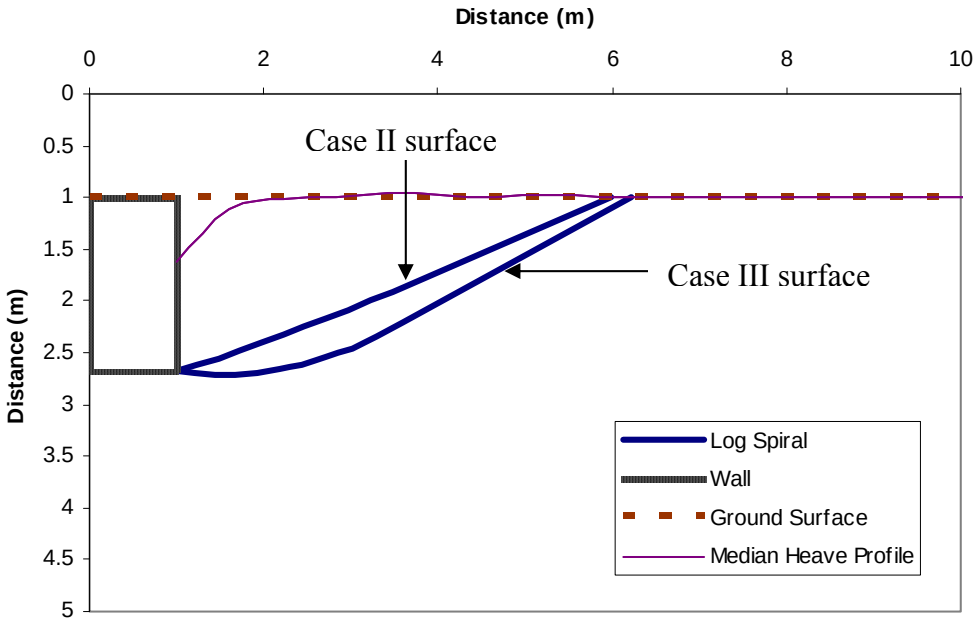

Figure 9-11 Heave profile with "best-fit" (Case II) and "most-representative" (Case III) log-spiral failure surfaces from PYCAP for loosely compacted coarse gravel

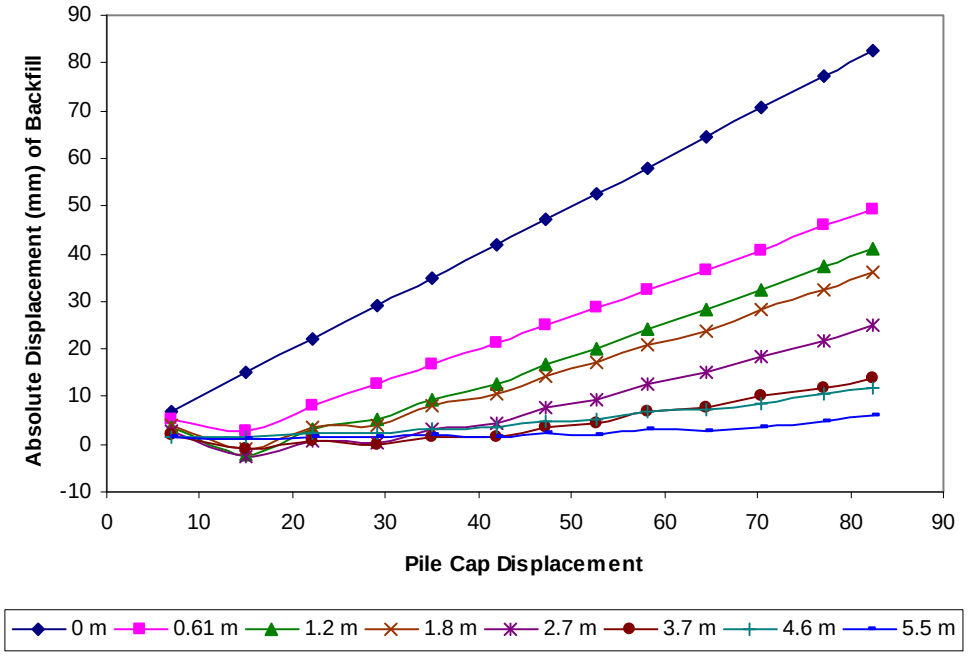

Figure 9-12 Displacement of monitoring points in loosely compacted coarse gravel backfill

expected, the strain is highest in the interval closest to the pile cap face and is relatively uniform with distance away from the cap up to the maximum distance monitored. The potential sensitivity of the string potentiometer measurements to differential pushing of the pile cap (not all the monitoring stakes were on the same end of the cap face) may be indicated by minor variations from interval to interval. Tipping of the monitoring stakes themselves during the dynamic shaking may also affect the variations visible in the figure. Movement of the stakes may also explain the presence of some negative strain values in the calculations.

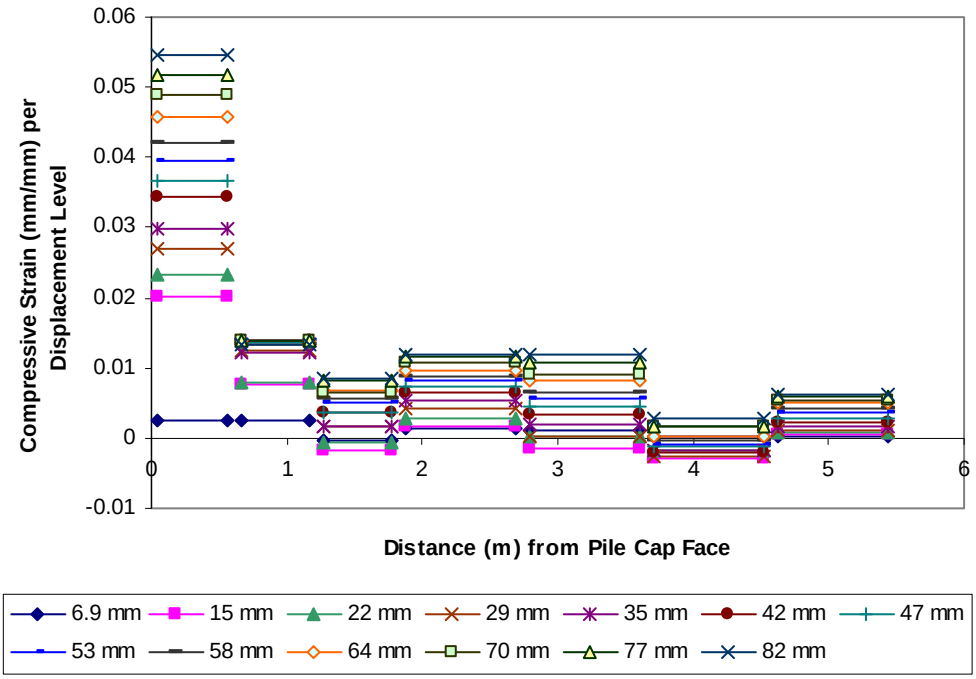

Figure 9-13 Strain per displacement level for loosely compacted coarse gravel backfill

10 Evaluation and Comparison of Different Backfill Conditions

10.1 Measured Passive Earth Resistance Based on Soil Type and Compactive Effort

One of the primary interests of this research was quantifying the passive earth resistance of different types of backfill soil compacted to different densities. As described in Section 3.4, two backfill soil types, each in two different density states, were tested. Table 10-1 summarizes the peak resistance provided by each of the backfill soil conditions along with the displacement at which the passive earth resistance is fully mobilized. Comparisons of the passive force-displacement curves for each backfill material in its loosely and densely compacted states are subsequently shown in Figure 10-1 and Figure 10-2, while the passive force-displacement curves of the two densely and loosely compacted soil types are shown in Figure 10-3 and Figure 10-4, respectively.

As shown in the table and figures, the densely compacted coarse gravel provided the most passive resistance, followed by the densely compacted fine gravel. In their loosely compacted states, up to the displacement levels tested, the fine and coarse gravel backfill materials provided only 27 and 40%, respectively, of their densely compacted load capacity. The clear difference in the peak values and shapes of the backfill resistance curves for the densely and loosely compacted backfills highlights the importance of obtaining adequate compaction. Different resistance-developing mechanisms appear to be in play when the differing patterns of horizontal strain, backfill

surface elevation change, and cracking are considered. Resistance in the densely compacted soils appears to develop as shear develops along a curvilinear failure plane. The generally good agreement between measured and calculated passive earth forces (presented for each backfill condition in previous chapters) obtained with little manipulation of the strength parameters substantiates this appraisal. The soils in the loosely compacted backfills, however, appear to compress in an area very near the pile cap face without significant strains occurring in the backfill farther away from the cap, and the resistance develops slowly, reaching values far less than the ultimate values of the densely compacted soils even after considerable deformation. This behavior is somewhat similar to a punching failure in a bearing capacity analysis where failure planes are not well defined and the resistance develops due to incremental compression of the soft or loose soil underneath (adjacent in this case).

The peak passive resistance for the loosely compacted fine and coarse gravel soils typically corresponds to the load at the end of each test; more resistance may have developed if the tests had been conducted to higher displacement levels. Constraints that

Table 10-1 Peak passive earth resistance and associated displacement for various backfill conditions

Backfill Type	Peak Resistance (kN)	Δ_{max} (mm)	Δ_{max}/H
Densely Compacted Fine Gravel	2860	62	0.037
Loosely Compacted Fine Gravel	820	≥ 64	--
Densely Compacted Coarse Gravel	3380	≈ 74	0.044
Loosely Compacted Coarse Gravel	1340	≥ 74	--

Note: the presence of the "≥" symbol indicates that the backfill did not appear to reach its ultimate strength by the maximum displacement level of the test; peak resistance in such cases are the maximum observed resistance.

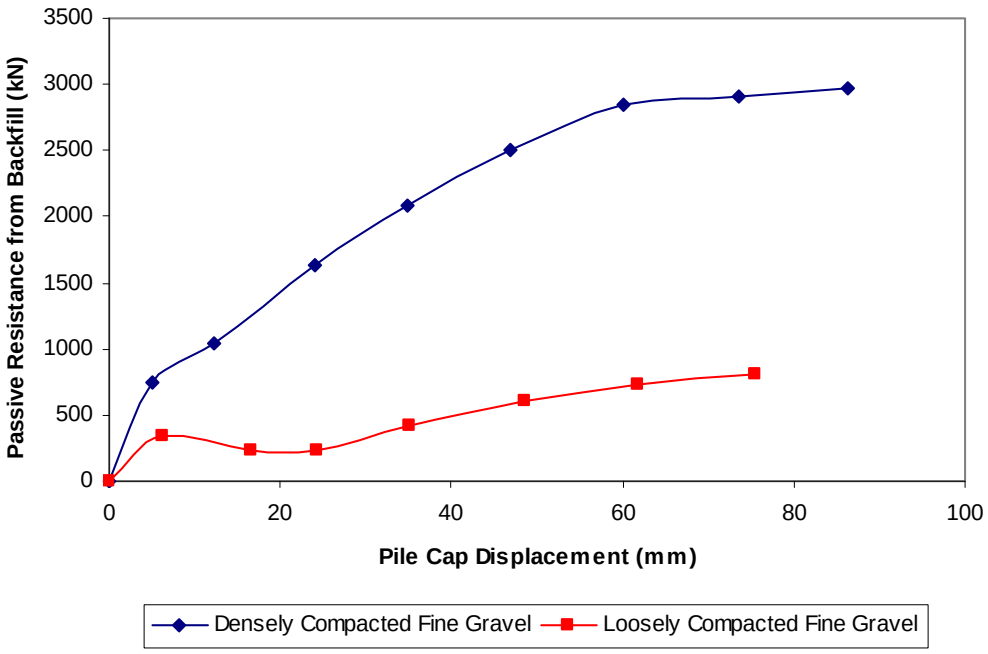

Figure 10-1 Comparison of measured passive earth force-displacement curves for densely and loosely compacted fine gravel backfill

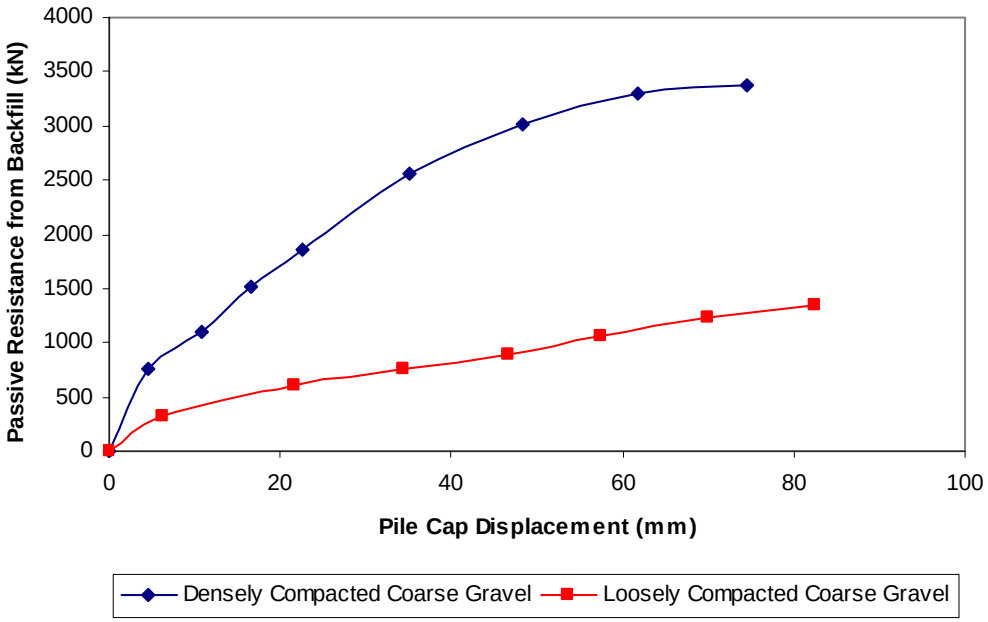

Figure 10-2 Comparison of measured passive earth force-displacement curves for densely and loosely compacted coarse gravel backfill

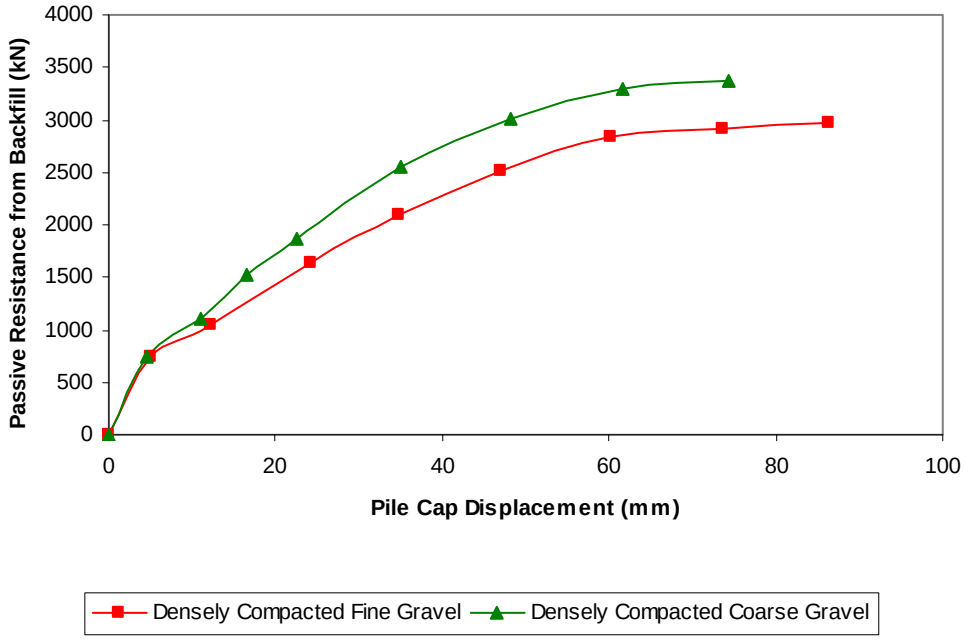

Figure 10-3 Comparison of measured earth force-displacement curves for densely compacted backfills

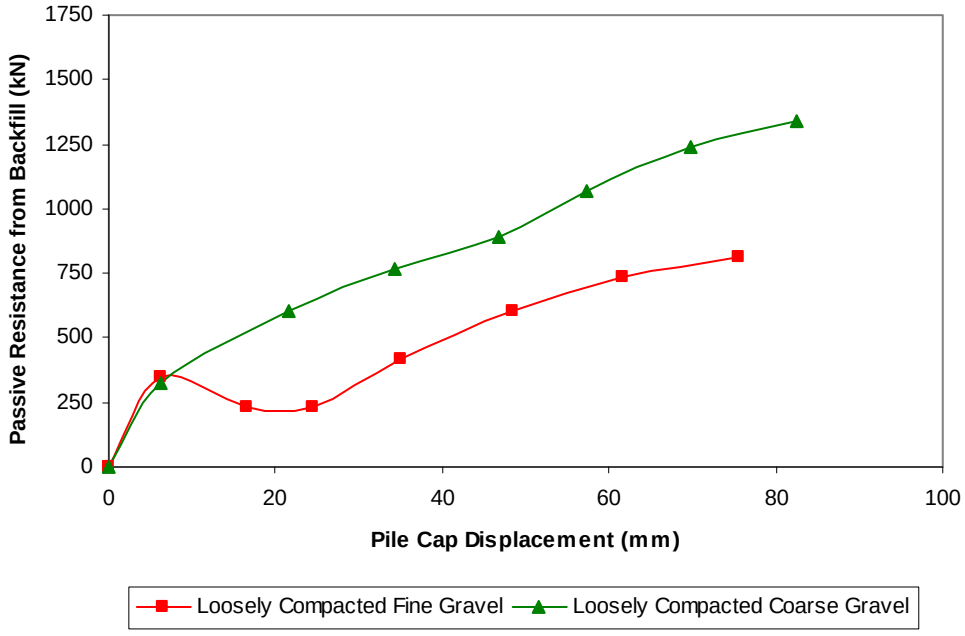

Figure 10-4 Comparison of measured earth force-displacement curves for loosely compacted backfills

limited maximum displacement levels during testing include equipment capacity limits as well as the concern of damaging the pile-to-cap connections as greater displacements were imposed on the cap. Because the loosely compacted fine and coarse gravel (see Figure 10-4) display a gradually increasing load resistance up to the maximum displacement, it may be misleading to identify this displacement as Δ_{max}; as a result, values for this parameter have not been provided in Table 10-1 for the loosely compacted backfill soils.

In general, the mobilization of passive earth force for the densely compacted fine and coarse gravel backfills occurs at a pile cap displacement-to-height ratio of about 0.04. This is relatively close to the 0.05 wall displacement-to-height ratio recently proposed for design by Shamsabadi and Yan (2008), but significantly larger than the 0.01 proposed by AASHTO (2007) for dense soils. The load-displacement curves tend to exhibit a hyperbolic shape, although the initial loading portion of the curves presented in this thesis tends to be flatter by about 50% than the slope generally associated with static, monotonic load-displacement curves. Dynamic and cyclic loading effects are suspected to play a role in the softened initial response of the backfill materials.

10.2 Calculation of Backfill Passive Forces Based on Soil Type and Compactive Effort

With field and laboratory measured values of shear strength as a starting point, load-displacement relationships were computed for each backfill soil using 1) a modified version of the spreadsheet program PYCAP, developed by Duncan and Mokwa (2001), which implements the classical log-spiral solution for passive force to generate a hyperbolic displacement curve; and 2) a computer program called ABUTMENT, which

implements the Log-Spiral Hyperbolic (LSH) method presented by Shamsabadi et al. (2007). Parameters were adjusted until a good estimate (typically within 5% of the peak observed resistance) was obtained for each method. Typically, adjustments were only made to cohesion and the interface friction angle. Emphasis was placed on comparing measured and calculated ultimate passive forces rather than initial loading stiffnesses. In general, the initial stiffnesses of the load-displacement curves from the testing presented in this thesis tend to be flatter by about 50% than the slope generally associated with static, monotonic load-displacement curves. Dynamic and cyclic loading effects seem to contribute to this behavior, although creep displacement of the cap between the time of backfill placement and the start of load testing (typically about a day) may also be a contributing factor. However, it is anticipated that the underlying piles were able to resist the at-rest earth forces resulting from backfill placement without appreciable movement of the pile cap.

A summary of the engineering parameters which provide the best match with the measured backfill response as calculated using the PYCAP spreadsheet and the ABUTMENT program is provided in Table 10-2. The load-displacement curves corresponding to the given parameters are shown in preceding chapters for each backfill type. In contrast to Table 10-2, Table 10-3 summarizes the engineering parameters believed to best represent field conditions and have not been optimized to obtain a "best fit" between measured and calculated ultimate passive earth pressures. The corresponding load-displacement curves are presented in Figure 10-5 and Figure 10-6, which include the curves for the clean sand material presented in Cummins (2009).

Table 10-2 "Best fit" engineering parameters used to calculate passive earth forces for backfills

Backfill Type	$\gamma_{m,avg}$ (kN/m^3)	ϕ (°)	PYCAP		ABUTMENT	
			c (kPa)	δ (°)	c (kPa)	δ (°)
Densely Compacted Fine Gravel	21.7	44.0	4.0	27.0	4.0	27.0
Loosely Compacted Fine Gravel	19.2	43.0	0.0	4.0	0.0	4.0
Densely Compacted Coarse Gravel	21.8	41.0	13.7	26.0	13.7	30.8
Loosely Compacted Coarse Gravel	20.1	50.0	0.0	4.2	0.0	4.2

Table 10-3 "Most-representative" engineering parameters used to calculate passive earth forces for backfills

Backfill Type	$\gamma_{m,avg}$ (kN/m^3)	ϕ (°)	c (kPa)	δ (°)	Calculated and Measured Force Difference (%)
Densely Compacted Fine Gravel	21.7	44.0	4.0*	27.0	+5*
Loosely Compacted Fine Gravel	19.2	43.0	0.0	0.0	-16
Densely Compacted Coarse Gravel	21.8	41.0	13.7	24.6	-4
Loosely Compacted Coarse Gravel	20.1	40.0	0.0	24.0	+15

* Cohesion reduced to a nominal value; with c=19.6 kPa from in-situ test, the resulting difference is +76%

Passive earth pressure calculations using both PYCAP and ABUTMENT (LSH) generally matched well against the measured data for the densely compacted soils without significant adjustment to the strength parameters, provided that in-situ field test parameters were used. It was observed that the addition of a small amount of cohesion (about 4 kPa) in the ABUTMENT model was occasionally required to obtain agreement between the two models.

In contrast, judicial manipulation of the strength parameters was required to match model-based response to the measured data for the loosely compacted soils. The interface friction generally had to be reduced and the displacement required to mobilize the ultimate passive force was typically assumed to be double that required for the densely compacted soil (thereby setting the displacement to failure beyond the displacement range in the test). The reduction or elimination of the interface friction (thereby creating conditions corresponding to Rankine earth pressure conditions) dramatically reduces the computed earth pressure coefficient and typically produces better matches with field data for the loosely compacted soils. The reduction in interface friction also seems consistent with the settlement observed near the pile cap face when loosely compacted backfill was used.

Given the belief that the failure of the loosely compacted backfills deform primarily due to punching rather than general shear failure, another approach to modeling the response of the loosely compacted backfills was also used. Rather than reducing the interface friction, the frictional strength of the backfill soil was reduced by an iteratively determined factor. This approach is similar to the one-third strength reduction method suggested by Terzaghi and Peck (1967) for dealing with local shear effects for the bearing capacity of loose to medium sands. The shear strength parameters used for each of the loosely compacted materials examined (including the loosely compacted clean sand presented in Cummins (2009)) were the laboratory-determined ultimate friction angle for the clean sand (no field test data is presented in Cummins), the friction angle from in-situ testing (the nominal cohesion was neglected) for the loosely compacted fine gravel, and the friction angle from in-situ testing (there was no cohesion) for the loosely

compacted coarse gravel. The reduced friction angle was obtained by taking the inverse tangent of the tangent of the original friction angle multiplied by 0.60, 0.65, and 0.85 for the clean sand, fine gravel, and coarse gravel, respectively. These reduced parameters were used with the log-spiral method implemented in the spreadsheet program PYCAP. Figure 10-7 gives a summary of the matches obtained from the log-spiral computations for the reduced parameters. The 0.6 and 0.65 factors for the clean sand and fine gravel are quite consistent with the 0.67 factor suggested by Terzaghi and Peck for bearing capacity with a localized punching failure mode. The previously discussed Rankine solution also produces a reasonably accurate match for both the loosely compacted clean sand material analyzed by Cummins (2009) and the loosely compacted fine gravel in this study (although the resulting failure surfaces are different); however, the loosely compacted coarse gravel is not well represented by Rankine passive earth theory. With respect to the coarse gravel and the 0.85 factor, this higher factor could stem from the intermediate relative density of the loosely compacted coarse gravel and a failure mode which may be between pure punching and pure general shear.

10.3 Response of Pile Cap and Backfill to Cyclic Actuator and Dynamic Shaker Loadings

Another area of interest in this research was quantifying the variations in the pile cap response with different backfill soil types subject to cyclic and dynamic loadings. Table 10-4 summarizes the reloading stiffness and damping ratio for the pile cap with each backfill condition due to slowly applied, cyclic actuator loadings while Table 10-5 summarizes the damped natural frequency, reloading stiffness, and damping ratio for the

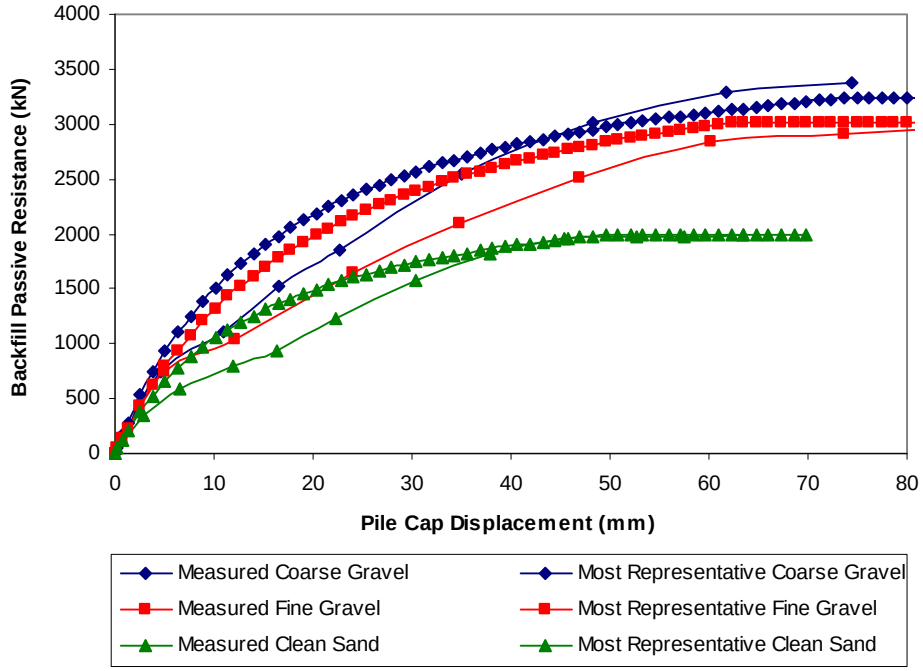

Figure 10-5 Summary of measured versus calculated load-displacement curves for densely compacted backfill materials using "most-representative" parameters

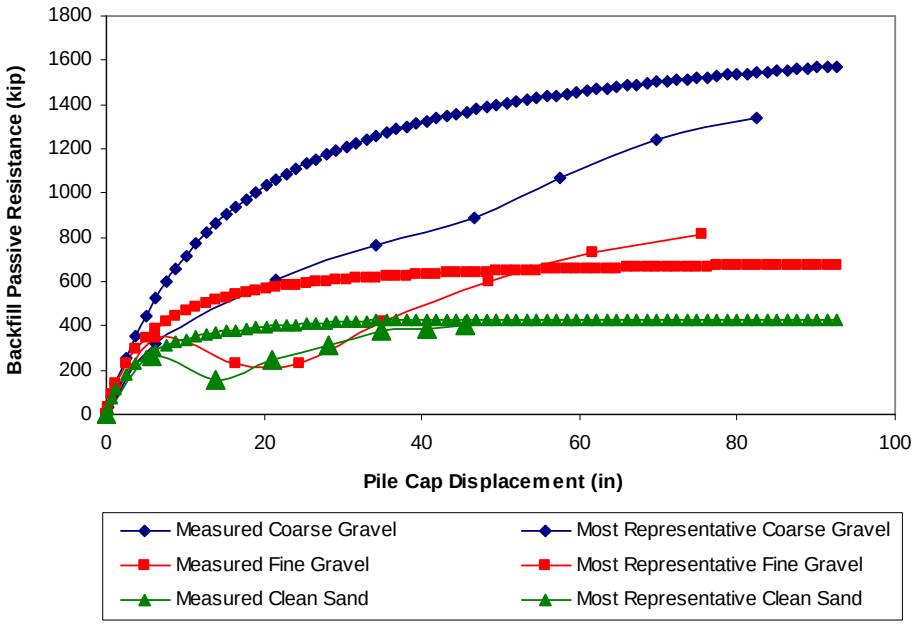

Figure 10-6 Summary of measured versus calculated load-displacement curves for loosely compacted backfill materials using "most-representative" parameters

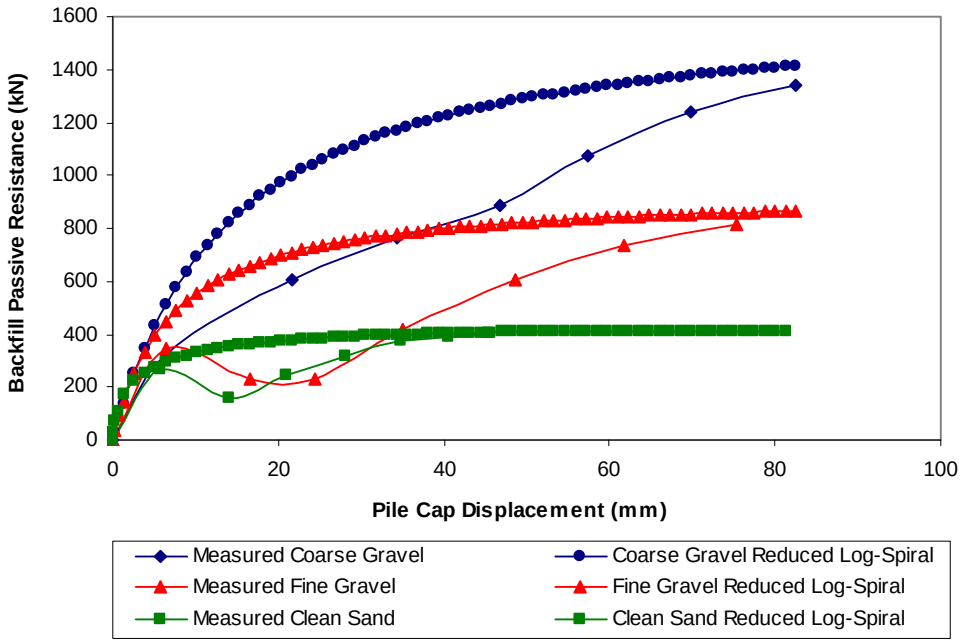

Figure 10-7 Summary of reduced shear strength parameters for use in the log-spiral approach for various loosely compacted backfill materials

pile cap with each backfill condition subject to dynamic shaker loadings in the frequency range from 4 to 10 Hz.

In Table 10-4 (response to cyclic actuator loadings), it is seen that the presence of backfill material significantly increases the reloading stiffness of the pile cap system, particularly when the backfill is densely compacted. The range of reloading stiffness for each backfill condition reflects increasing stiffness with increasing static displacement of the pile cap for each test. Reloading stiffness of the pile cap typically doubles when densely compacted backfill is used instead of loosely compacted backfill. The average damping ratio of the pile cap without backfill is approximately 26% and changes little with the placement of loosely compacted backfill. However, the damping ratio decreases to about 19 or 20% with densely compacted backfill in place.

Table 10-4 Summary of pile cap with backfill response due to cyclic actuator loadings

Pile Cap with Backfill Condition	Displacement Amplitude (mm)	Reloading Stiffness (kN/mm)	Damping Ratio (%)
No Backfill (Baseline Response)	2.4 to 2.6	40 to 115	15 to 38
Densely Compacted Fine Gravel	1.3 to 2.3	180 to 530	15 to 23
Loosely Compacted Fine Gravel	1.4 to 1.8	90 to 270	20 to 30
Densely Compacted Coarse Gravel	1.1 to 1.8	240 to 630	17 to 22
Loosely Compacted Coarse Gravel	1.9 to 2.5	120 to 270	16 to 28

The response of the pile cap is somewhat different for dynamic shaker loadings as shown in Table 10-5. However, comparisons between actuator- and shaker-based loadings are qualified by similarities in loop displacement amplitude for the two types of loadings (displacements from the shaker range from near 0 to 1 or 2 mm and actuator cycle displacements range from 1 to 2.5 mm) as well as the static displacement level of the pile cap. Damping ratios determined using the half-power bandwidth method are generally in the same range as, but with median values somewhat lower than, damping ratios measured from the actuator-based load displacement loops (on the order of 15 to 25% with loosely compacted backfill in place). Reloading stiffness and damping determined from the shaker-based load-displacement loops vary widely with frequency and displacement, but when displacement amplitudes from the shaker- and actuator-based load-displacement loops are similar (as with loosely compacted fine gravel backfill (see Figure 7-7)), stiffness and damping are generally comparable. The stiffness and damping of the test foundation system vary significantly with forcing frequency because the

backfill moves in and out of phase with the pile cap, which makes it difficult to quantify dynamic parameters.

Table 10-5 Summary of pile cap with backfill response due to dynamic shaker loadings

Pile Cap with Backfill Condition	Natural Freq. (Hz)	Max. Disp. Amp (mm)	Reloading Stiffness (kN/mm)	Damping Ratio (%)	
				Half-power Bandwidth	Load-Disp. Loops
No Backfill (Baseline Response)	5.0 to 6.5	2.3	100 to 200	8 to 18	1 to 52
Densely Compacted Fine Gravel	7.5 to 8.0	0.9	400 to 1000	--	1 to 46
Loosely Compacted Fine Gravel	6.5 to 7.0	1.5	200 to 350	23 to 25	2 to 37
Densely Compacted Coarse Gravel	7.5	0.7	400 to 1000	--	1 to 40
Loosely Compacted Coarse Gravel	7	1.5	300 to 500	23	1 to 60

10.4 Cracking, Vertical Movement, and Horizontal Movement of Backfill

In with the case of the loosely compacted coarse gravel backfill material (and the loose sand as reported by Cummins (2009)), the maps of backfill surface cracking suggest much less movement than the heave contours. The poorly graded nature and the relatively open matrix between particles in the coarse gravel made distinctions between individual cracks and natural gaps in particle-to-particle contacts difficult to make. In some cases, a thin veneer of fine-grained material was placed over the backfill to help highlight the occurrence of cracking in the underlying soil. This is the reason that the crack mapping for the densely compacted coarse gravel is so much more detailed than the crack map for the loosely compacted coarse gravel.

In general, cracking in the loosely compacted soils tended to be poorly defined. What cracks were visible appear to manifest a punching interface tapering from the edges of the pile cap to the center of the backfill, as in the case of the loosely compacted fine gravel. Contrastingly, cracking in the densely compacted materials generally appears to radiate out from the edge of the cap out to the edges of the backfill. The loosely and densely compacted soils also displayed distinctly different behavior with respect to elevation change. The loosely compacted soil backfills, especially the coarse gravel, experienced a significant amount of settlement near the pile cap face which decreased with increasing distance from the pile cap. On the other hand, the densely compacted soil backfills generally heaved near the cap face, with the heave tapering off as the distance from the cap increased. For example, for the fine gravel backfill, the loosely compacted soil experienced up to 20 mm of settlement immediately adjacent to the pile cap face whereas the densely compacted soil experienced approximately 30 mm of heave at a distance of 1.8 m from the pile cap face. The type of elevation change in the backfill, be it heave or settlement, appears to correlate strongly with the magnitude of horizontal resistance developed as the cap pushes into the backfill. Passive resistance analyses demonstrated that the loosely compacted soils fail to mobilize a large amount of their theoretical passive pressure in the range of displacements tested.

With respect to horizontal movement and compressive strain in the backfill, compressive strains on the order of 0.05 to 0.1 were experienced near the pile cap face when loosely compacted soils were present. For the densely compacted soils, the compressive strains were lower, with a range of 0.02 to 0.25 in the same vicinity. Strains were more evenly distributed in the densely compacted backfills than in the loosely

compacted backfills. Horizontal strain distributions and elevation change patterns appear to correspond well with each other as presented in the cracking and vertical movement and horizontal movement and strain sections for each backfill condition.

11 Conclusion

11.1 Summary

This thesis presents results from lateral load tests performed on a full-scale pile cap with five different backfill conditions. The results from each condition are presented in the following order: no backfill present (baseline response), densely compacted fine gravel, loosely compacted fine gravel, densely compacted coarse gravel, and loosely compacted coarse gravel. Static load-induced displacement was accompanied by low frequency small amplitude loading cycles and higher frequency small amplitude dynamic loading cycles. Analysis and interpretation of the results are presented for each backfill condition, and comparisons are made between backfill conditions.

11.2 Conclusions

Based on the data, analyses, and interpretations presented in this thesis, the following conclusions and recommendations have been developed:

11.2.1 Fine Gravel Backfill

- Passive resistance from the backfill dramatically improved the lateral load capacity of the pile cap. At the fully mobilized passive earth pressure, the

densely compacted fine gravel contributes about 70% of the total lateral load capacity of the test foundation. The loosely compacted fine gravel contributes about 37% of the total lateral load capacity of the test foundation for the maximum displacement reached during testing. In other words, the resistance offered by the densely compacted fine gravel was about 2.4 times the resistance offered by the loosely compacted fine gravel.

- At a displacement of about 62 mm (corresponding to a displacement-to-cap height ratio of about 0.037), the passive resistance of the densely compacted fine gravel appears to be fully mobilized, and placement of the densely compacted fine gravel produced a 235% increase in capacity over the pile cap acting alone. In contrast, the capacity observed with the loosely compacted fine gravel backfill test was about 60% greater than the pile cap acting by itself. The dramatic increase in resistance offered by the densely compacted backfill compared to that offered by the loosely compacted backfill demonstrates the importance of adequate backfill compaction.
- The log-spiral methods presented in PYCAP and in the LSH method are sensitive to variation in interface friction parameters and can produce a wide range of predictions of the ultimate passive force. Due to constraints presented by oversized aggregates in laboratory tests and potential shortcomings with staged in-situ tests, it is difficult to assess the shear strength parameters for the gravel materials. Log-spiral methods can

provide reasonable predictions of passive resistance as long as input parameters are judiciously selected. Recommendations for computing passive earth forces for gravelly soils are presented at the end of this chapter. In-situ shear strength parameters appeared to provide the best matches to the measured resistance curve. The Rankine passive earth approach appears to provide a good match to the measured ultimate resistance for the loosely compacted fine gravel. Reducing the shear strength parameters to 65% of their original values and setting the interface friction angle equal to the soil friction angle (similar to the approach Terzaghi and Peck (1967) took regarding the bearing capacity of loose to medium granular soils) also provides a reasonable estimate of the ultimate passive resistance of the loosely compacted soil. The CALTRANS simplified bilinear method performed poorly in the prediction of the ultimate resistance of the backfill for either density state of the fine gravel.

- The fine gravel backfill material increases the stiffness of the test foundation under slowly applied cyclic loadings. The presence of the loosely compacted fine gravel roughly doubled the stiffness of the pile cap system, compared to the no backfill case. With densely compacted fine gravel present, the stiffness of the test foundation more than quadrupled in comparison to the test with no backfill present.
- Under low frequency cyclic loadings, the median damping ratio of the pile cap with densely compacted fine gravel is approximately 19%, while the

median damping ratio of the loosely compacted fine gravel is about 24%. This represents a decrease in damping ratio with increasing cap displacement and increasing backfill stiffness

- Fine gravel backfill increased the dynamic stiffness of the test foundation when the cap was subjected to higher frequency cyclic loading (up to 10 Hz). Loosely compacted fine gravel approximately doubled the stiffness of the test foundation with no backfill. Densely compacted fine gravel roughly quadrupled the stiffness of the pile cap relative to the no backfill case. The densely compacted backfill also offers a proportionally larger range of stiffness than that obtained with no backfill behind the pile cap, as illustrated in Table 10-4.
- Damping ratio appears to vary with frequency when the pile cap system is subjected to higher frequency cyclic loading. This variation applies to all the backfill conditions tested and can be described as a wave-like pattern of high and low values as the frequency increases; however, specific values vary from one backfill condition to another. The densely compacted fine gravel backfill appeared to provide slightly more dynamic damping, in a broader range, than the loosely compacted fine gravel.
- A comparison of damping values at similar displacement amplitudes for the loosely compacted fine gravel appeared to result in reasonable agreement between low frequency (~0.75 Hz) and higher frequency (4 to 10 Hz) loadings. Similar damping for different frequency ranges suggests

that higher frequency loadings do not appreciably increase the apparent resistance of the pile cap compared to slowly applied cyclic loadings.

- Comparable stiffness between the two cyclic loading types was found at similar loop displacement amplitudes for the loosely compacted fine gravel.
- Earth pressure distributions compiled from earth pressure cell data generally showed an increase with depth and with increasing pile cap displacement. The loosely compacted fine gravel pressure distribution displayed unusual behavior in that the measured pressure appeared to be negligible near the bottom of the pile cap. Pressure distributions were used to compute passive force vs. displacement curves. These were systematically lower than the actuator-derived curves, so a multiplier was applied to adjust for three dimensional and other effects, which enhanced the similarity between the two curves.
- Vertical movement, horizontal strain, and surface cracking patterns seem to relate well with each other. For the densely compacted fine gravel, these patterns also appeared to correlate well with the computed log-spiral failure surface. The movement and surface cracking patterns manifest in the loosely compacted fine gravel appear to suggest the development of resistance due to progressive densification of the backfill, or perhaps a punching shear failure mechanism, as the pile cap displaced instead of coinciding with a well-defined log-spiral failure surface as with the densely compacted fine gravel.

11.2.2 Coarse Gravel Backfill

- Passive resistance from the backfill dramatically improved the lateral load capacity of the pile cap. At fully mobilized passive earth pressure, the densely compacted coarse gravel contributes about 68% of the total lateral load capacity of the test foundation. In contrast, the loosely compacted coarse gravel contributed about 43% of the total lateral load capacity of the test foundation for the maximum displacement reached during testing.
- At a displacement of about 74 mm (corresponding to a displacement-to-cap-height ratio of about 0.044), the passive resistance of the densely compacted coarse gravel appears to be fully mobilized, and the placement of the densely compacted coarse gravel produced a 217% increase in capacity over the pile cap acting alone. In contrast, the loosely compacted coarse gravel increased the total capacity of the pile cap system by 82% relative to the pile cap without backfill. The dramatic increase in resistance offered by the densely compacted backfill compared to that offered by the loosely compacted backfill demonstrates the importance of adequate backfill compaction.
- The log-spiral methods presented in PYCAP and in the LSH method are sensitive to variation in interface friction parameters and can produce a wide range of predictions of the ultimate passive force. Due to constraints presented by oversized aggregates in laboratory tests and potential shortcomings with staged in-situ tests, it is difficult to assess the shear strength parameters for the gravel materials. Log-spiral methods can

provide reasonable predictions of passive resistance as long as input parameters are carefully chosen. In-situ shear strength parameters appeared to provide the best match to the measured response with the least amount of manipulation for the densely compacted coarse gravel, whereas the correlation-based friction angle with a significantly discounted interface friction angle was found to provide a good match for the loosely compacted coarse gravel. However, the use of Duncan's engineering correlation can produce friction angles not in the range commonly used by designers. Reducing the shear strength parameters to 85% of their original value and setting the interface friction angle equal to the soil friction angle (similar to the approach Terzaghi and Peck (1967) took regarding the bearing capacity of loose to medium granular soils) also provides a reasonable estimate of the ultimate passive resistance of the loosely compacted soil. The CALTRANS simplified bilinear method provided a good prediction for loosely compacted coarse gravel, but severely underestimated the densely compacted coarse gravel.

- The coarse gravel backfill material increases the stiffness of the test foundation under slowly applied cyclic loadings. The presence of loosely compacted coarse gravel roughly doubled the stiffness of the test foundation acting with no backfill. The densely compacted coarse gravel provided nearly 6 times the stiffness offered by the pile cap with no backfill present.

- Under low frequency cyclic loadings, the median damping ratio of the pile cap with densely compacted coarse gravel is approximately 18%, while the median damping ratio for the loosely compacted coarse gravel test is 21%.
- Coarse gravel backfill increased the dynamic stiffness of the test foundation when the cap was subjected to higher frequency cyclic loading (up to 10 Hz). Loosely compacted coarse gravel nearly tripled the stiffness offered by the test foundation with no backfill. Densely compacted coarse gravel provided over four times the stiffness of the pile cap acting without backfill.
- Damping ratio appears to vary with frequency when the pile cap system is subjected to higher frequency loading. This variation applies to all the backfill conditions tested and can be described as a wave-like pattern of high and low values as the frequency increases; however, specific values vary from one backfill condition to the next. Significantly more damping, in a wider range of values, was observed in the loosely compacted coarse gravel test than in the densely compacted coarse gravel test.
- Neither compaction state of the coarse gravel yielded comparable loop displacement amplitudes between the slowly applied (~0.75 Hz) and the higher frequency (up to 9 or 10 Hz) loadings. The shaker was not able to produce enough force to displace the backfill adequately for such a comparison to be possible.

- Earth pressure distributions compiled from earth pressure cell data generally showed an increase with depth and with increasing pile cap displacement. The loosely compacted coarse gravel pressure distribution exhibited unusual behavior when the measured pressure fell to negligible levels after the first push, then rose incrementally with increasing cap displacement for the pressure cell nearest the bottom of the pile cap. Even with the incremental increase in pressure following the drop, the final observed pressure for the bottom cell was well below the observed pressure from the cell above after the final cap displacement. Pressure distributions were used to compute passive force vs. displacement curves. These were systematically lower than the actuator-derived curves, so a multiplier was applied to adjust for three dimensional and other effects, which enhanced the similarity between the two curves.
- Vertical movement, horizontal strain, and surface cracking patterns seem to relate well with each other. For the densely compacted coarse gravel, these patterns also appeared to correlate well with the computed log-spiral failure surface. The movement and surface cracking patterns manifest in the loosely compacted coarse gravel appear to suggest the development of resistance due to progressive densification of the backfill, or perhaps a punching shear failure mechanism, as the pile cap displaced instead of correlating with a well-defined log-spiral failure surface as with the densely compacted coarse gravel.

11.3 Recommendations for Implementation

- Given the dramatically different load-displacement response of loosely and densely compacted soils, engineering professionals should take significant measures to assure that backfill compaction requirements are met and that those requirements result in a high relative density if significant passive earth force is needed.
- For the design of concrete foundations and abutments backfilled with well-compacted granular materials, say on the order of 95% modified Proctor density or 75% relative density, the log-spiral approach can be used with a soil friction angle of 40° and a δ/ϕ ratio of 0.6 to 0.75 to determine the passive earth force. These parameters should give a lower-bound solution to the passive response of backfill subjected to static, cyclic, and dynamic loadings. The designer who has performed field shear strength testing and is confident in the resulting parameters can use them in determining a larger passive earth force, noting that calculated passive earth coefficients increase 10 to 15% for each 1° increase in ϕ beyond 40°.
- In the case of loosely compacted granular fills, say on the order of 85 to 90% modified Proctor or 35% relative density, Rankine passive earth theory may be used to determine the passive earth force. However, the Rankine method may underestimate the capacity of granular backfill soil as the failure mode transitions from punching to general shear. Alternatively, shear strengths can be reduced by a factor ranging from 0.6

to 0.85 (perhaps increasing with relative density) when using the log-spiral method to compute the passive earth force. This approach is similar to that suggested by Terzaghi and Peck (1967) for the bearing capacity of loose to medium dense granular soils.

- For densely compacted granular backfills, the load-displacement response can be modeled as a hyperbolic curve and the ultimate passive force is realized at a displacement-to-height ratio of approximately 4%.
- Under cyclic and dynamic loadings, the passive earth force acting on the face of a pile cap or abutment can contribute a significant portion of the overall resistance and stiffness. The response of pile cap structures subject to variable frequency loadings can be quantified using an average damping ratio of at least 15%, but the precise ratio will vary as inertial and total earth forces act in and out of phase. Consideration should be given to changes in structural period due to changes in dynamic stiffness and damping ratio with forcing frequency and displacement amplitude.

References

AASHTO (2007). *AASHTO LRFD Bridge Design Specifications, 4th Ed*. American Association of State Highway and Transportation Officials, Washington, D.C.

Ashour, M., Norris, G., and Pilling, P. (1998). "Lateral loading of a pile in layered soil using the strain wedge model." *Journal of Geotechnical and Geoenvironmental Engineering*, ASCE Vol. 124(4), 303–315.

Borowicka, H. (1938). "Distribution of pressure under a uniformly loaded elastic strip resisting on elastic-isotropic ground." *2nd Cong. Int. Assoc. Bridge Struct. Engrg*. Vol. 8 (3).

Brinch-Hansen, J. (1966). "Resistance of a rectangular anchor slab." *Bulletin No. 21,* Danish Geotechnical Institute, Copenhagen, 12–13.

Caltrans. (2004). *Seismic Design Criteria*. Caltrans, Sacramento, CA. Section 7-Design, 28-30.

Christensen, D. S. (2006). "Full scale static lateral load test of a 9 pile group in sand," *M.S. Thesis*, Department of Civil and Environmental Engineering, Brigham Young University, Provo.

Clough, G.W. and Duncan, J.M. (1991). Earth retaining structures, *In Foundation engineering handbook*. 2nd Ed. H.Y. Fang, Ed. Van Nostrand Reinholdt, New York.

Cole, R. T. (2003). "Full-scale effects of passive earth pressure on the lateral resistance of pile caps," *Ph.D. Dissertation*, Department of Civil and Environmental Engineering, Brigham Young University, Provo, Utah.

Cole, R. T., and Rollins, K. M. (2006). "Passive earth pressure mobilization during cyclic loading." *Journal of Geotechnical and Geoenvironmental Engineering*, ASCE Vol. 132(9), 1154-1164.

Cummins, C. R. (2009). "Behavior of a full scale pile cap with loosely and densely compacted clean sand backfill under cyclic and dynamic loadings." *M.S. Thesis*, Department of Civil and Environmental Engineering, Brigham Young University, Provo, Utah.

Douglas, D. J. and Davis, E. H. (1964). “The movements of buried footings due to moment and horizontal load and the movement of anchor plates.” *Geotechnique*, London, 14(2), 115–132.

Duncan, J. M. (2004). "Friction angles for sand, gravel and rockfill." Kenneth L. Lee Memorial Seminar, Long Beach, CA, April, 2007.

Duncan, J. M., and Mokwa, R. L. (2001). "Passive earth pressures: theories and tests." *Journal of Geotechnical and Geoenvironmental Engineering*, ASCE Vol. 127(3), 248-257.

Fang, Y.-S., Chen, T.-J., and Wu, B.-F. (1994). "Passive earth pressures with various wall movements." *Journal of Geotechnical Engineering*, ASCE Vol. 120(8), 1307-1323.

Filz, G. M., and Brandon, T. L. (1994). "Static and dynamic measurements using embedded earth pressure cells." *Transportation Research Record 1432*, Transportation Research Board, 86-95.

Filz, G. M., and Duncan, J. M. (1993). "Drift of flush-mounted pressure cell readings." *Geotechnical Testing Journal*, ASTM Vol. 16(4), 432-441.

Gadre, A., and Dobry, R. (1998). "Lateral cyclic loading centrifuge tests on square embedded footing." *Journal of Geotechnical and Geoenvironmental Engineering*, ASCE Vol. 124(11), 1128-1138.

Goel, R. K., and Chopra, A. K. (1997). "Evaluation of bridge abutment capacity and stiffness during earthquakes." *Earthquake Spectra*, Vol. 13(1).

Johnson, S.R. (2003). “Static lateral load testing a full-scale pile group spaced at 5.65 pile diameters.” *MS Thesis*, Department of Civil and Environmental Engineering, Brigham Young University, Provo, Utah.

Lee, K.L. and Singh, A. (1971). “Relative density and relative compaction.” *Journal of the Soil Mechanics and Foundations Division,* ASCE Vol. 97(7), 1049-1052.

Maroney, B. H. (1994). "Large scale bridge abutment tests to determine stiffness and ultimate strength under seismic loading," *Ph.D. Dissertation*, University of California at Davis, Davis.

Mokwa, R. L., and Duncan, J. M. (2001). "Experimental evaluation of lateral-load resistance of pile caps." *Journal of Geotechnical and Geoenvironmental Engineering*, ASCE Vol. 127(2), 185-192.

Ovesen, N. K., and Stromann, H. "Design method for vertical anchor slabs in sand." *Procs. Spclty. Conf. on Performance of Earth and Earth-Supported Structures*, Vol. 1(2), ASCE, New York, 1481-1500.

Rollins, K. M. and Cole, R. T. (2006). "Cyclic lateral load behavior of a pile cap and backfill." *Journal of Geotechnical and Geoenvironmental Engineering*, ASCE Vol. 132(9), 11.

Rollins, K.M., King, R., Snyder, J.L., and Johnson, S.R. (2005b). "Full-scale lateral load tests of pile groups and drilled shafts in clay." *Procs. Intl. Conf. on Soil-Structure Interaction, Calculation Methods and Engineering Practice*, Vol. 1, Ulitsky, V.M., Ed., ASV Publishers, Moscow: 287-292.

Rollins, K. M., Snyder, J. L., and Broderick, R. D. (2005a). "Static and dynamic lateral response of a 15 pile group." *Procs. 16th Intl. Conf. on Soil Mechanics and Geotechnical Engineering*, Vol. 4, Millpress, Rotterdam, Netherlands: 2035-2040.

Rollins, K. M., and Sparks, A. (2002). "Lateral resistance of full-scale pile cap with gravel backfill." *Journal of Geotechnical and Geoenvironmental Engineering*, ASCE Vol. 128(9), 711-723.

Rollins, K. M., Sparks, A. E., and Peterson, K. T. (2000). "Lateral load capacity and passive resistance of full-scale pile group and cap." Transportation Research Record 1736, *Paper No. 00-1411*, Transportation Research Board, 24-32.

Romstad, K., Kutter, B., Maroney, B., Vanderbilt, E., Griggs, M., and Chai, Y. H. (1996). "Longitudinal strength and stiffness behavior of bridge abutments." Report No. UCD-STR-96-1, California Department of Transportation, Sacramento, CA.

Runnels, I. K. (2007). "Cyclic and dynamic full-scale testing of a pile cap with loose silty sand backfill," *M.S. Thesis*, Department of Civil and Environmental Engineering, Brigham Young University, Provo, Utah.

Shamsabadi, A., Ashour, M., and Norris, G. (2005). "Bridge abutment nonlinear force-displacement-capacity prediction for seismic design." *Journal of Geotechnical and Geoenvironmental Engineering*, ASCE Vol. 131(2), 151-161.

Shamsabadi, A., Rollins, K. M., and Kapuskar, M. (2007). "Nonlinear soil-abutment-bridge structure interaction for seismic performance-based design." *Journal of Geotechnical and Geoenvironmental Engineering*, ASCE Vol. 133(6), 707-720.

Shamsabadi, A. and Yan, L. (2008). "Closed-form force-displacement backbone curves for bridge abutment-backfill systems." *Procs. Conf. of Geotechnical Earthquake Engineering and Soil Dynamics IV*, ASCE, 2008.

Snyder, J. L. (2004). "Full-scale lateral-load tests of a 3x5 pile group in soft clays and silts," *M.S. Thesis*, Department of Civil and Environmental Engineering, Brigham Young University, Provo.

Soubra, A.-H. and Regenass, P. (2000). "Three-dimensional passive earth pressures by kinematical approach." *Journal of Geotechnical and Geoenvironmental Engineering*, ASCE Vol. 126(11), 969-978.

Taylor, A. J. (2006). "Full-scale-lateral-load test of a 1.2 m diameter drilled shaft in sand," *M.S. Thesis*, Department of Civil and Environmental Engineering, Brigham Young University Provo.

Terzaghi, K. and Peck, R. B. (1967). *Soil Mechanics in Engineering Practice*. Wiley, New York.

Tokimatsu, K., Suzuki, H., and Sato, M. (2004). "Influence of initial and kinematic components on pile response during earthquakes." *Procs. 11th Intl. Conf. on Soil Dynamics and Earthquake Engineering* and *3rd Intl. Conf. on Earthquake Geotechnical Engineering.* University of California, Berkeley. Doolin, D., Kammerer, A., Nogami, T., Seed, R.B., and Towhata, I., Eds. Vol. 1, 768-775.

Valentine, T. J. (2007). "Dynamic testing of a full-scale pile cap with dense silty sand backfill," *M.S. Thesis*, Department of Civil and Environmental Engineering, Brigham Young University, Provo, Utah.

Walsh, J. M. (2005). "Full-scale lateral load test of a 3x5 pile group in sand," *M.S. Thesis*, Department of Civil and Environmental Engineering, Brigham Young University, Provo.

Wood, J. H. (2009). "Resistance from bridge abutment passive soil pressure in earthquakes." Paper No. 45, 2009 New Zealand Society for Earthquake Engineering (NZSEE) Conference, New Zealand.